

**EXPERIMENTAL STUDIES ON THE PERFORMANCE AND
EXHAUST EMISSION CHARACTERISTICS OF DIESEL
ENGINE USING TEXTURED PISTON RING**

A Thesis submitted to the Delhi Technological University, Delhi in fulfilment of the
requirements for the award of the degree of

DOCTOR OF PHILOSOPHY

in

Mechanical Engineering

By

ROOP LAL
(2K14/PhD/ME/04)

Under the Supervision of

Dr. R. C. SINGH
(Professor)



**DEPARTMENT OF MECHANICAL ENGINEERING
DELHI TECHNOLOGICAL UNIVERSITY
SHAHBAD, DAULPUR, BAWANA ROAD, DELHI-110042, INDIA**

October, 2019

DECLARATION

I hereby declare that the thesis work entitled “**EXPERIMENTAL STUDIES ON THE PERFORMANCE AND EXHAUST EMISSION CHARACTERISTICS OF DIESEL ENGINE USING TEXTURED PISTON RING**” is an original work carried out by me under the supervision of Dr. R.C. Singh, Professor, Department of Mechanical Engineering, Delhi Technological University, Delhi. This thesis has been prepared in conformity with the rules and regulations of the Delhi Technological University, Delhi. The research work presented and reported in the thesis have not been submitted either in part or full to any other university or institute for the award of any other degree or diploma.

ROOP LAL

(Regd. No: 2K14/PhD/ME/04)

Deptt. of Mechanical Engineering

Delhi Technological University,

Delhi

Date: 16.10.2019

Place: Delhi

CERTIFICATE

This is to certify that the thesis entitled, “**EXPERIMENTAL STUDIES ON THE PERFORMANCE AND EXHAUST EMISSION CHARACTERISTICS OF DIESEL ENGINE USING TEXTURED PISTON RING**” submitted by **Mr. Roop Lal** to the Delhi Technological University, Delhi for the award of the degree of **Doctor of Philosophy in Mechanical Engineering** is a bona fide record of original research work carried out by him under my supervision in accordance with the rules and regulations of the university. The results presented in this thesis have not been submitted, in part or full, to any University or Institute for the award of any degree or diploma.

Dr. Ramesh Chandra Singh
Professor,
Department of Mechanical Engineering
Delhi Technological University,
Delhi, India

Dedicated
to
My Parents,
My Wife,
Son(s) and
Daughter in Law

ACKNOWLEDGMENTS

I would like to express my deep gratitude, sincere thanks and appreciation to my supervisor Prof. Ramesh Chandra Singh for his valuable guidance during my Ph.D. work. I am thankful from bottom of my heart for all the help, encouragement, and support he generously extended to me.

I would like to express, a sincere gratitude to Prof. R.S. Mishra, Chairman, DRC, Mechanical Engineering Department and Prof. Vipin, Head of the Department, Mechanical Engineering, Delhi Technological University, for their valuable help, motivation and extending all the necessary processing and experimental facilities during my research work.

Thanks, are also due to Prof. L.M. Das, Prof. Harish Hirani, Prof. Raj Kumar Singh and Prof. Naokant Deo, for serving my SRC committee and many critical helps without which I would not be able to complete my thesis in time.

I am also grateful to Prof. Naveen Kumar for all the motivation and their teachings, without that I would not be able to finish my thesis work. My sincere thanks to all the faculty and staff members of Department of Mechanical Engineering (DTU), who supported me during my entire course work and research work. I am grateful to Mr. Rajesh Bohra, Mr. Tekchand, Mr. Manmohan and Mr. Ashok Dangi (MAIT) for their technical support.

I would like to express my sincere thanks to Dr. Vipin Kumar Sharma, Assistant Professor, MAIT, and Mr. Sidharth, Assistant Professor, MAIT for their support and encouragement throughout this period.

I am unable to express my sincere gratitude in words for the affection, encouragement and support by my wife Mrs. Veena Devi during the entire research work, without her support I could not have completed my work. She happily permitted me to focus all my attention on my research work and continuously provided me the encouragement to complete my Ph.D. Finally, I dedicate this Ph.D. thesis to my elder son Mr. Ramakant Rana, Daughter in Law Mrs. Sakshi Raghuvanshi and my younger son Mr. Sri Kant Rana, for their love and care.

Last but not the least; I thank the Spiritual Master and Almighty for giving me strength to complete this work in all respects.

(Roop Lal)

Place: New Delhi

October, 2019

ABSTRACT

Petroleum and automotive industries are facing tough time across the globe due to steep rise in petroleum-based fuels' prices and ever-increasing governments regulations related to improving the fuel economy and lower emissions from the fuel and lubricant system of IC engines. Therefore, worldwide substantial efforts in the design of reciprocating internal combustion (IC) engines are being made by the researchers for improving the fuel economy and reducing the exhaust emissions. Nowadays, great attention is being given on the reduction of friction at the various interfaces formed between the mating components of the IC engines. Effective lubrication at the interfaces of cylinder liner/piston rings, piston/piston rings, and piston skirt/cylinder liner play vital role in achieving high power efficiency, ensuring long operational life of the interfaces, limiting the consumptions of lubricating oil and fuel, providing a good dynamic sealing at various interfaces. Thus, efficient design of contacts formed between piston rings and counter surfaces in piston assembly is a great desirable task in the emerging scenario.

For improving the performance of the IC engines several attempts were made. The utilisations of the surface coating and designing techniques were used. For wear and friction properties of piston rings materials were evaluated using the pin on disc method. Apart from wear and friction the vibration amplitude and noise level during the experiments were also evaluated.

Similar experiments were performed by considering the surface textures. Laser techniques used to produce the textures. From the pin on disc tests it is reported that coating and texturing both helped in improving the tribological properties. Lastly, the selected textures were fabricated on the actual piston rings and engine performance were evaluated using the IC engines.

Using textured piston rings, experiments have been carried out on a commercial diesel engine fuelled with diesel and biodiesel at various loads. Textures on piston ring has made impact on engine's brake thermal efficiency (BTE), brake specific fuel consumption (BSFC), and emissions, irrespective of fuels used. BTE of engine increased with textured piston ring in comparison to standard (conventional) piston ring with both the fuels. Moreover, significant reductions in exhaust emissions were also recorded with textured face profile on compression piston rings.

List of Publications

International Journals

1. **Roop Lal** and R C Singh, “Experimental comparative study of chrome steel pin with and without chrome plated cast iron disc in situ fully flooded interface lubrication”, Surface Topography: Metrology and Properties, IOP Publishing, Vol. 6, 2018, 035001. **(SCI Indexed, Impact Factor: 2.074)**
2. **Roop Lal** and R C Singh, “Investigations of tribodynamic characteristics of chrome steel pin against plain and textured surface cast iron discs in lubricated conditions”, World Journal of Engineering, Vol. 16 No. 4, 2019, pp. 560-568. **(SCOPUS & ESCI Indexed, Impact Factor: 0.46)**
3. R C Singh, R K Pandey, **Roop Lal**, M S Ranganath and S Maji, “Tribological performance analysis of textured steel surfaces under lubricating conditions” Surface Topography: Metrology and Properties, IOP Publishing, Vol. 4 (2016) 034005. **(SCI Indexed, Impact Factor: 2.074)**
4. **Roop Lal** and R C Singh, “Experimental Study of Performance Parameters of Newly Commissioned I.C. Engine”, International Journal of advanced Production and Industrial Engineering. IJAPIE, ISSN: 2455-8419; ISSUE 2018, VOL. 3(4).
5. R. C. Singh, **Roop Lal**, Ranganath M S and Rajiv Chaudhary, “Failure of Piston in IC Engines: A Review”, International Journal of Modern Engineering Research (IJMER), Vol. 4, Issue 9, Sept. 2014, Page 1 -10, ISSN: 2249-6645.

International Conferences

1. **Roop Lal** and R. C. Singh, “Reduction of Specific Fuel Consumption in CI Engine by using modified surface of Piston Rings”, International Conference of Advance Research and Innovation (ICARI), New Delhi, India, 20 January 2019, ISBN 978-93-5346-324-3.
2. **Roop Lal** and R. C. Singh, “A study of Tribological behavior at point of contact of cylinder liner and piston rings in a diesel engine”, International Conference of Advance Research and Innovation (ICARI), New Delhi, India, 20 January 2019, ISBN 978-93-5346-324-3.

3. **Roop Lal** and R C Singh, “*Experimental Study of Performance Parameters of Newly Commissioned I.C. Engine*”, International Conference on Advanced Production and Industrial Engineering (ICAPIE-2018), Delhi, India, 5-6 October 2018.
4. R. C. Singh, R. K. Pandey, **Roop Lal** and S Maji, “*Experimental Studies for the Tribological Performances of Textured Steel Surfaces under Fully Flooded and Starved Lubricated Conditions*”, A Book on Automation in Manufacturing (AIM-2015), Page 51-62, TEQIP-II Sponsored Two Week Faculty Development Program, 04-15 May 2015.
5. **Roop Lal**, R C Singh, Ranganath M S, Rajiv Chaudhary, Gaurav Shukla, “*Tribological Analysis of Etched Mild Steel Surfaces*” “International Conference of Advance Research and Innovation (ICARI-2015), New Delhi, India, 31 January 2015. ISBN 978-93-5156-3280.
6. **Roop Lal**, R C Singh, Ranganath M.S., Rajiv Chaudhary, Ankit Kumar Saxena, “*Investigation of Wear Behavior of Aluminium Alloy and Comparison with Pure Aluminium*” “International Conference of Advance Research and Innovation (ICARI-2015), New Delhi, India, 31 January 2015. ISBN 978-93-5156-3280.

National Conferences

1. **Roop Lal** and R C Singh, “*A Study on Mild Steel and Chromium Coated Mild Steel Using Pin-On-Disc Method For Noise Pollution*”, National Conference on Recent Trends in Engineering, Science and Management, Shri Ram College of Engineering and Management, Palwal, Haryana, 18-19 April 2017. ISBN: 978-93-86238-21-4.

List of Contents

		Page No.
	Declaration	i
	Certificate	ii
	Acknowledgements	iv
	Abstract	vi
	List of Publication	vii
	List of Contents	ix
	List of Figures	xi
	List of Tables	xv
Chapter 1	Introduction	1-17
1.1	Overview	1
1.2	Internal Combustion Engine: Piston Assembly	4
1.3	Performance of IC Engines	7
1.3.1	Indicated Power, Brake Power and Mechanical Efficiency	7
1.3.2	Fuel Air Ratio	9
1.3.3	Volumetric Efficiency	9
1.3.4	Specific Output	9
1.3.5	Specific Fuel Consumption (S.F.C.)	10
1.3.6	Thermal Efficiency and Heat Balance	10
1.3.7	Heat Balance	10
1.3.8	Exhaust Smoke and Emissions	11
1.3.9	Indicated and Brake Mean Effective Pressure	11
1.3.10	Specific Weight	12
1.4	Surface texturing for reducing friction and wear at the contacts	13
1.4.1	High beam / electric discharge methods	13
1.4.2	Etching Techniques	13
1.4.3	Micro machining / forming techniques	14
1.5	Exhaust Pollution	14
1.5.1	Formation of oxides of nitrogen in Internal Combustion Engine	15
1.5.2	Diesel Smoke Problem	15
1.5.3	Diesel Engine Combustion and Smoke	16
1.6	Gasoline Engine Emission	16
1.6.1	Exhaust Emissions	16
1.6.2	Evaporative Emissions	17
1.6.3	Crank Case Blow	17
Chapter 2	Literature Review	18-33
	Introduction	18
2.1	Piston Ring Material	18
2.2	Texturing on Piston Ring	24
2.3	Engine Performance	28
2.4	Literature Gap	31
2.5	Objectives	33
Chapter 3	Methodology and Experiment	34-63
3.1	Pin on Disc	34
3.2	Thermal Imaging Camera	37

3.3	Vibration Measuring Device	40
3.4	Digital Sound Meter	41
3.5	Texturing Method	42
3.6	Four-Stroke Single Cylinder Diesel Engine	44
3.7	Smoke Analyser	47
3.8	Micro Hardness Test	47
3.9	Plan of Experimental Work	51
3.10	1 st Experimentation on Pin on Disc	52
3.10.1	Disc and Pin Specimens for 1st Experiment of Pin on Disc	54
3.11	2 nd Experimentation on Pin on Disc	55
3.11.1	Disc and Pin Specimens for 2nd Experiment of Pin on Disc	56
3.12	Preparation of Biodiesel	59
3.13	Design of Texturing on Piston Ring	62
3.14	Experimentation on Engine	63
Chapter 4	Results and Discussion	64-104
4.1	Characterisation	64
4.1.1	Disc Material	64
4.1.2	Pin Material	66
4.2	Plain & Chrome Plated Disc vs Steel Pin	68
4.2.1	Coefficient of Friction	69
4.2.2	Wear	71
4.2.3	Vibrations Amplitude	75
4.2.4	Temperature Rise	77
4.2.5	Sound	79
4.3	Plain & Textured Cast Iron Disc vs Steel Pin	81
4.3.1	Coefficient of Friction	82
4.3.2	Wear	84
4.3.3	Vibrations Amplitude	86
4.3.4	Temperature Rise	88
4.3.5	Sound	90
4.4	Engine	92
4.4.1	Brake Thermal Efficiency	92
4.4.2	Brake Specific Fuel Consumption	94
4.4.3	Carbon Monoxide	96
4.4.4	Hydrocarbon (HC)	98
4.4.5	Nitrogen Oxide	100
4.4.6	Smoke Opacity	102
Chapter 5	Conclusions and Future Works	105-109
5.1	Conclusions	105
5.2	Scope for Future Works	109
	References	110
	Appendix	

List of Figures

Figure No.	Title	Page No.
Figure 1.1	Chemical and mechanical energy losses in a typical IC engine	3
Figure 1.2	View of Engine and piston assembly	5
Figure 1.3	Face profiles of piston rings	6
Figure 3.1	Top view of Pin on Disc test rig	35
Figure 3.2	Front view of Pin on Disc test rig	36
Figure 3.3	Front View and Back side View of Thermal Imaging Camera (Fluke Ti400)	38
Figure 3.4	Range, Span and Total Level of the Thermal Imaging Camera (Fluke Ti450)	38
Figure 3.5	Image of Pin on “Pin on Disc” test rig taken from Thermal Imaging Camera	39
Figure 3.6	Thermal Image of Pin showing the Temperature at contact point and surroundings	39
Figure 3.7	Temperature Variation Graph for the Pin at its contact point and its surroundings	39
Figure 3.8	Top View of Vibration Measuring Device (PRÜFTECHNIK VIB Xpert ® II)	40
Figure 3.9	Vibrations produced in abscissa and ordinate along with their max values	41
Figure 3.10	Digital Sound Level (Instrument SL-1350)	42
Figure 3.11	Red light being incidental on Piston Ring for laser texturing	43
Figure 3.12	Laser beam machining on Piston Ring for texturing	44
Figure 3.13	Engine used for the experimentation [Kirloskar Diesel Engine (DAF8)]	45
Figure 3.14	Control Panel of the Engine (Kirloskar Diesel Engine-DAF8)	46
Figure 3.15	Smoke analyser used for analysing the smoke of engine	47
Figure 3.16	Image of Micro Hardness Measuring Device (Fischerscope HM2000s)	48
Figure 3.17	Loading Un-Loading graphs for the measurement of Vickers Hardness	49
Figure 3.18	Vicker Hardness Number for materials used in experimentation	50
Figure 3.19	Flowchart of the Plan of Experimental Work	51
Figure 3.20	Chrome Coated Cast Iron Disc	54
Figure 3.21	Chrome Steel Pin	55
Figure 3.22	Textured Surface Cast Iron Disc used in Experimentation	58
Figure 3.23	Chrome Steel Pin	58
Figure 3.24	Surface images of textured surface cast iron disc with 35X zoom	59
Figure 3.25	Microscopic images of plain (smooth) surface of cast iron disc	59
Figure 3.26	Flow chart of Biodiesel preparation	60
Figure 3.27	Separation of glycerine and biodiesel	61
Figure 3.28	Water washing of biodiesel	61
Figure 3.29	3D rendered image of laser textured piston ring	62
Figure 4.1	(a) SEM Image of the Disc	65
Figure 4.1	(b), (c) & (d): EDAX spectra image of Elemental Mapping of the Disc	65
Figure 4.2	EDS spectrum showing the elements of C, Fe and Si presence in the Disc	65
Figure 4.3	SEM image of Pin Material	66
Figure 4.4	(b, c, d): EDAX Spectra Image of element mapping of the Pin Material	67
Figure 4.4	(e, f): EDAX Spectra Image of element mapping of the Pin Material	67

Figure 4.5	EDS spectrum showing the elements of C, O, Si, Cr and Fe presence in the Pin	68
Figure 4.6	Coefficient of friction (μ) of cast iron and chromium plated cast iron against steel pin at a constant speed of 2m/s	69
Figure 4.7	Coefficient of friction (μ) of cast iron and chromium plated cast iron against steel pin at a constant speed of 6m/s	70
Figure 4.8	Coefficient of friction (μ) of cast iron and chromium plated cast iron against steel pin at a constant speed of 10m/s	70
Figure 4.9	Wear of cast iron and chromium plated cast iron against steel pin at a constant speed of 2m/s	71
Figure 4.10	Wear of cast iron and chromium plated cast iron against steel pin at a constant speed of 6m/s	73
Figure 4.11	Wear of cast iron and chromium plated cast iron against steel pin at a constant speed of 10m/s	73
Figure 4.12	(a) Microscopic view of worn surface of pin and (b) Microscopic view of worn surface of cast iron disc.	74
Figure 4.13	Dimensional details and extended view of worn surface tracks on disc	74
Figure 4.14	Vibration amplitude of cast iron and chromium plated cast iron against steel pin at constant speed of 2m/s	75
Figure 4.15	Vibration amplitude of cast iron and chromium plated cast iron against steel pin at constant speed of 6m/s	76
Figure 4.16	Vibration amplitude of cast iron and chromium plated cast iron against steel pin at constant speed of 10m/s	76
Figure 4.17	Temperature rise of cast iron and chromium plated cast iron against steel pin at constant speed of 2m/s	77
Figure 4.18	Temperature rise of cast iron and chromium plated cast iron against steel pin at constant speed of 6m/s	78
Figure 4.19	Temperature rise of cast iron and chromium plated cast iron against steel pin at constant speed of 10m/s	78
Figure 4.20	Sound of cast iron and chromium plated cast iron against steel pin at constant speed of 2m/s	79
Figure 4.21	Sound of cast iron and chromium plated cast iron against steel pin at constant speed of 6m/s	80
Figure 4.22	Sound of cast iron and chromium plated cast iron against steel pin at constant speed of 10m/s	80
Figure 4.23	Coefficient of friction (μ) of plain cast iron and textured cast iron against steel pin at constant speed of 2m/s	82
Figure 4.24	Coefficient of friction (μ) of plain cast iron and textured cast iron against steel pin at constant speed of 6m/s	83
Figure 4.25	Coefficient of friction (μ) of plain cast iron and textured cast iron against steel pin at constant speed of 10m/s	83
Figure 4.26	Wear of plain cast iron and textured cast iron against steel pin at constant speed of 2m/s	84

Figure 4.27	Wear of plain cast iron and textured cast iron against steel pin at constant speed of 6m/s	85
Figure 4.28	Wear of plain cast iron and textured cast iron against steel pin at constant speed of 10m/s	85
Figure 4.29	Vibration amplitude of plain cast iron and textured cast iron against steel pin at constant speed of 2m/s	86
Figure 4.30	Vibration amplitude of plain cast iron and textured cast iron against steel pin at constant speed of 6m/s	87
Figure 4.31	Vibration amplitude of plain cast iron and textured cast iron against steel pin at constant speed of 10m/s	87
Figure 4.32	Temperature rise of plain cast iron and textured cast iron against steel pin at constant speed of 2m/s	88
Figure 4.33	Temperature rise of plain cast iron and textured cast iron against steel pin at constant speed of 6m/s	89
Figure 4.34	Temperature rise of plain cast iron and textured cast iron against steel pin at constant speed of 10m/s	89
Figure 4.35	Sound of plain cast iron and textured cast iron against steel pin at constant speed of 2m/s	90
Figure 4.36	Sound of plain cast iron and textured cast iron against steel pin at constant speed of 6m/s	91
Figure 4.37	Sound of plain cast iron and textured cast iron against steel pin at constant speed of 10m/s	91
Figure 4.38	Variation of Brake Thermal Efficiency of Diesel as fuel with Textured and Non-textured Piston Ring	92
Figure 4.39	Variation of Brake Thermal Efficiency of Biodiesel as fuel with Textured and Non-textured Piston Ring	93
Figure 4.40	Combined variation of Brake Thermal Efficiency of both Diesel and Biodiesel as fuel with Textured and Non-textured Piston Ring	94
Figure 4.41	Variation of Brake Specific Fuel Consumption of Diesel as fuel with Textured and Non-textured Piston Ring	95
Figure 4.42	Variation of Brake Specific Fuel Consumption of Biodiesel as fuel with Textured and Non-textured Piston Ring	95
Figure 4.43	Combined variation of Brake Specific Fuel Consumption of both Diesel and Biodiesel as fuel with Textured and Non-textured Piston Ring	96
Figure 4.44	Variation of Carbon Monoxide emissions of Diesel as fuel with Textured and Non-textured Piston Ring	97
Figure 4.45	Variation of Carbon Monoxide emissions of Biodiesel as fuel with Textured and Non-textured Piston Ring	97
Figure 4.46	Combined variation of Carbon Monoxide emissions for both Diesel and Biodiesel as fuel with Textured and Non-textured Piston Ring	98
Figure 4.47	Variation of Hydrocarbon emissions for Diesel as fuel with Textured and Non-textured Piston Ring	99

Figure 4.48	Variation of Hydrocarbon emissions for Biodiesel as fuel with Textured and Non-textured Piston Ring	99
Figure 4.49	Combined variation of Hydrocarbon emissions for both Diesel and Biodiesel as fuel with Textured and Non-textured Piston Ring	100
Figure 4.50	Variation of NOx emissions for Diesel as fuel with Textured and Non-textured Piston Ring	101
Figure 4.51	Variation of NOx emissions for Biodiesel as fuel with Textured and Non-textured Piston Ring	101
Figure 4.52	Combined variation of NOx emissions for both Diesel and Biodiesel as fuel with Textured and Non-textured Piston Ring	102
Figure 4.53	Combined variation of Smoke Opacity emissions for Diesel as fuel with Textured and Non-textured Piston Ring	103
Figure 4.54	Combined variation of Smoke Opacity emissions for Biodiesel as fuel with Textured and Non-textured Piston Ring	103
Figure 4.55	Combined variation of Smoke Opacity emissions for both Diesel and Biodiesel as fuel with Textured and Non-textured Piston Ring	104

List of Tables

Table No.	Title	Page No.
Table 3.1	Details of the thermal image of Pin taken by Thermal Imaging Camera	40
Table 3.2	Specifications of the Engine	46
Table 3.3	Vickers hardness values for prepared specimens	50
Table 3.4	Properties of Diesel and Biodiesel	61
Table 4.1	The chemical stoichiometric of the individual elements of Disc Material	66
Table 4.2	The chemical stoichiometric of the individual elements of Pin Material	68

Chapter 1

Introduction

1.1.Overview

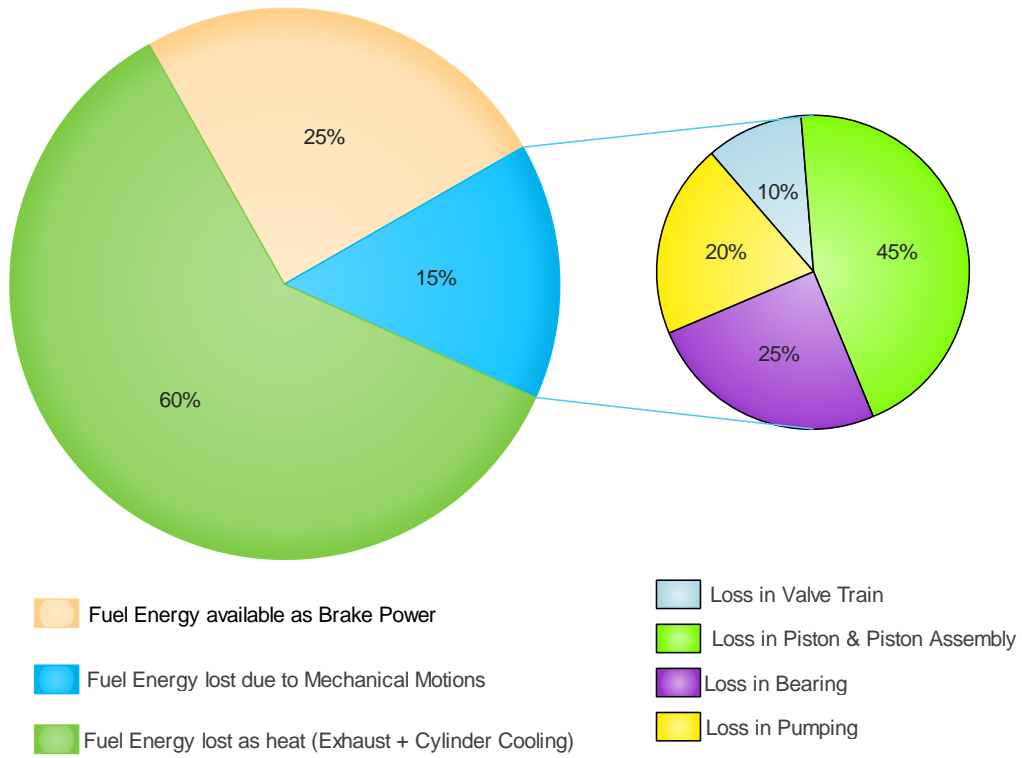
Environmental law continues to drive the optimization of combustion engines in the automotive industry. It is an effort to reduce harmful emissions by developing more efficient and compact engines. Significant frictional losses occur at the interface of the ring pack and cylinder liner. There is need of research to reduce friction at the ring liner interface. Also, the exhaust has impact on environment that is one of the causes of global warming. Friction loss in an internal combustion engine has been a determining factor in evaluating engine's performance and its fuel consumption. Approximately 20-30% of the friction losses in a compression-ignition engine are due to the piston/cylinder system, much of which is due to the piston rings (Etsion and Sher, 2009).

The purpose of internal combustion engines is to generate mechanical energy from the chemical energy of the fuel. In internal combustion engines, unlike external combustion engines, this energy is released by burning or oxidizing the fuel in the engine. The mixture of air and fuel before combustion and burned after combustion products are the actual working fluids. Diesel combustion, which is basically an unstable and unstable turbulent combustion, is essentially controlled by the mixing of fuel with the air in the combustion chamber. It focuses on the mixing process and the formation of pollutants in the combustion chamber and offers features and emission characteristics. Work transfers that provide the desired performance are made directly between these working fluids and the mechanical components of the engine. IC engines, due to their simplicity, ruggedness and high power-to-weight ratio, have

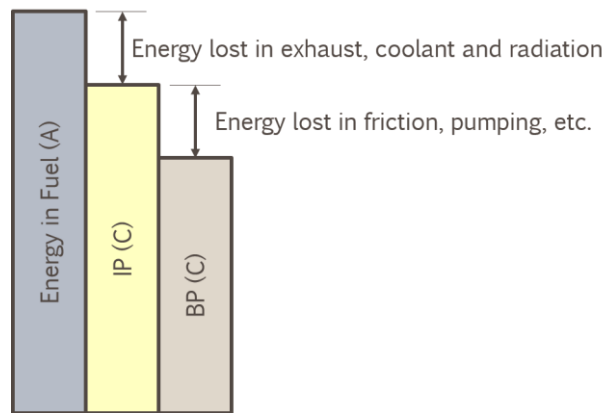
found wide application in transportation and power generation. There are two types of IC engines, the gasoline engine and the diesel engine. Both engines burn fuel in the engine cylinder. The combustion chamber design and operating characteristics differ significantly from those of other engine types.

The internal combustion engine is the most important mechanical invention of man, which played an important role in the industrialization of the world after the Second World War. With the rapid depletion of conventional fuel resources and growing environmental problems, there is an unstoppable global pressure on researchers to develop more efficient and compact combustion engines with fewer environmental issues. Over the past two decades, numerous studies have been conducted on friction testing at various interfaces in integrated circuit motors to identify the critical interfaces of the engine components and minimize the associated friction losses at the interfaces. It is worth noting here that most of the fuel energy (i.e., chemical energy) is used as waste in the form of heat. A significant portion of the chemical energy released by the combustion of the precious fuel is consumed in the frictional resistance of the various interfaces of the mobile engine components. Figure 1.1 (a) and (b) show the percentage of chemical energy removed in different ways in a typical IC engine. It can be seen that the fraction of chemical energy consumed by friction during mechanical movements in a typical internal combustion engine is considerably large.

Reductions of fuel consumption and emission in an internal combustion engine are largely a function of improved lubrication. Therefore, a recent investigation of the interfaces between engine and combustion chamber is to be carried out. The development of engines for intelligent and the correct use of engines for combustion and economic saving of millions of dollars in an industrialized country.



(a)



(b)

Figure 1.1: Chemical and mechanical energy losses in a typical IC engine

This is an indication that improvements improve the performance of IC interfaces.

1. Reduced fuel consumption
2. Increase the engine power
3. Reduced oil consumption

4. A reduction in harmful exhaust emissions
5. Improved durability, reliability and engine life
6. Reduced maintenance requirements and longer service intervals

With large numbers of IC engines in use across the globe, even a fraction of improvements in engine efficiency and emission level can have a major influence on the world fuel economy and the environment in a long term. Singh et al. evaluated the influence of piston segments on the fuel consumption and the composition of the event gas of a pressure generator. The dynamic tests were performed on a Ford Transit Moteur of 2500 cc with natural aspiration in a wide range of engine speeds load conditions. The study found that the LST piston segments have a fuel economy rate with a 4% breach, a change in gas composition, or smoke emissions (Singh, Pandey and Maji, 2016).

1.2.Internal Combustion Engine: Piston Assembly

It must be said that the heart of the internal combustion engine is the piston unit. Figure 1.2 shows a line diagram of a single-cylinder vertical reciprocating internal combustion engine. The piston rings of the piston group form a labyrinth seal. This function is achieved by Piston rings in closely joining its grooves in the piston and interacting with the cylinder wall. The piston and the piston rings form a critical unit that converts the energy of the fuel into useful kinetic energy. The piston ring pack includes the piston rings, which is a series of compression rings and oil ring. The main role of the compression piston ring is to maintain an effective gas seal between the combustion chamber and the housing.

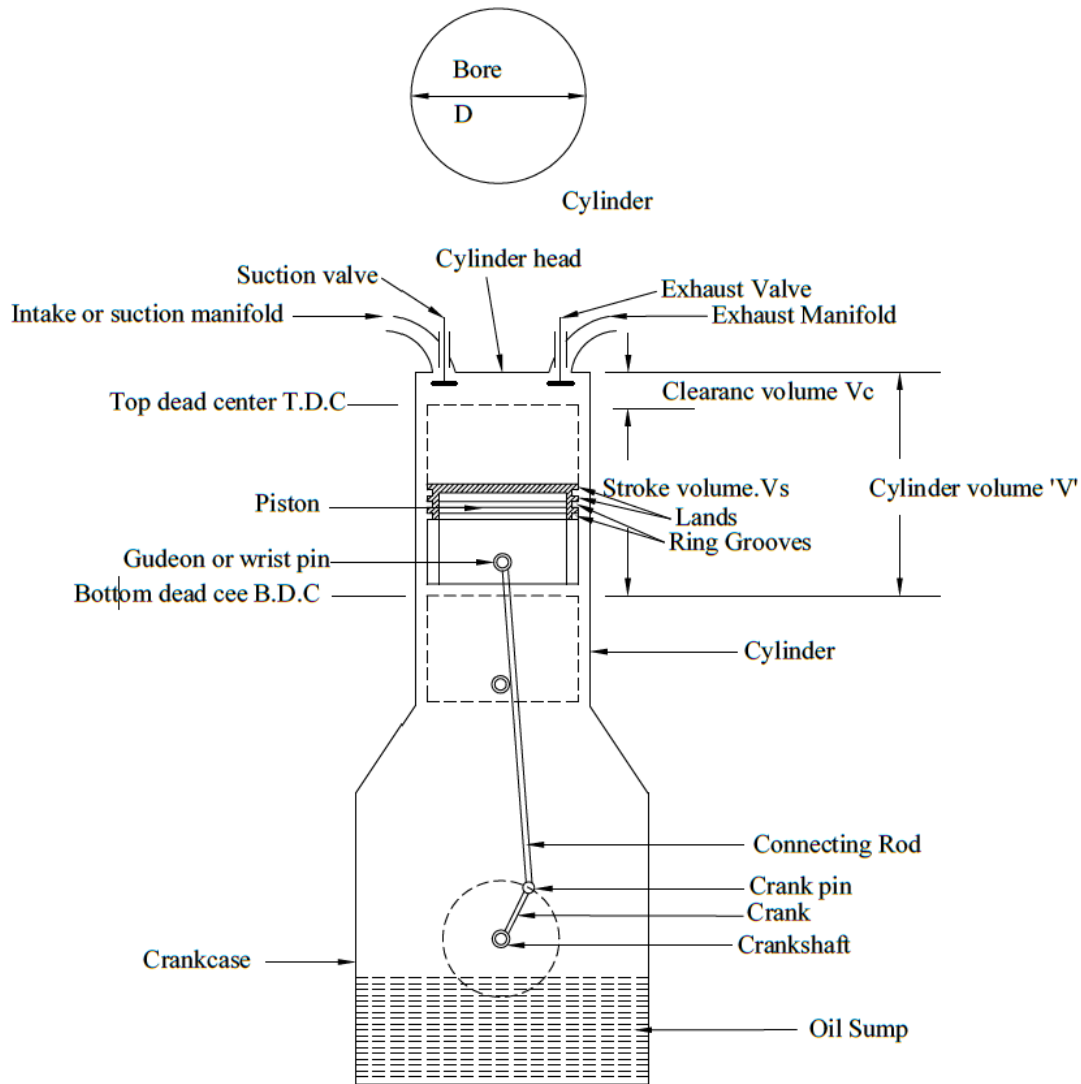


Figure 1.2: View of Engine and piston assembly

The additional function of the piston rings is to transfer heat from the piston to the cylinder wall and limit the amount of lubricating oil carried by the crankcase to the combustion chamber. This flow path is perhaps the most important contribution to the consumption of engine oil and causes an increase in harmful exhaust emissions when the lubricating oil mixes and reacts with other components present in the combustion chamber.

Two top piston rings are compression rings. The pressure generated during combustion pushes the piston rings radially outward, causing the entire surface of the

piston rings to engage the cylinder wall. This process helps keep gas sealing. The second compression ring, called the scraper ring, is designed to help limit the upward flow of the oil in addition to providing a secondary gas seal.

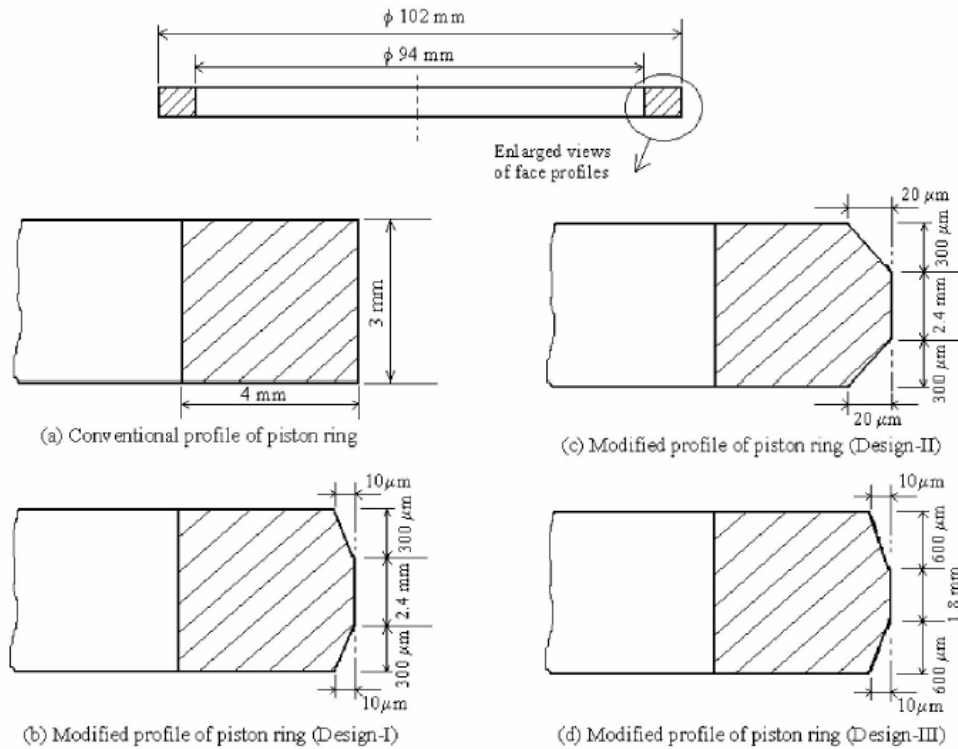


Figure 1.3: Face profiles of piston rings

Figure 1.3 (b) illustrates the excess oil scraped from the wall of the cylinder from the second compression ring of the piston. For the scraping function, the second compression ring has a conical front profile. The lower segment of the piston assembly is known as an oil control segment, which has two running faces (or lands) and a spring element to improve the radial load. The purpose of this ring is to limit the quantity of oil transported from the crankcase to the combustion chamber. The piston ring is the most complex tribological element of the internal combustion engine that must be analyzed due to the large variations in load, speed, temperature and availability of lubricant. In one stroke of the piston, the segment interface with the wall of the cylinder lining it is possible to experience boundary, mixing and fluid film lubrication. During

the engine cycle, the piston itself has a complex movement, ie a transverse movement, an axial movement and a secondary movement. These movements involve a hydrodynamic / mixed lubrication at the different interfaces of the piston group. In case of insufficient lubrication in the piston sleeve and in the cylinder wall, noise may occur due to the piston stroke.

1.3.Performance of IC Engines

The primary aim of the development engineer is to reduce the cost of production, improve the efficiency and power output of the engine which in turn reduce the capital and running cost of the engine. In order to achieve the above, development engineer to develop and take measurements of performance parameters, compare them with performance parameters of existing engines. There so many performance parameters are different in nature so it becomes difficult to take care of all of them during engine design. Hence it becomes necessary to conduct the test on the engine and determine the measures which should be taken care of to improve the engine performance. Engine performance is an indication of the degree of success with which the chemical energy of the fuel converted into useful mechanical work. The basic performance parameters are enlisted and discussed below:

1.3.1. Indicated Power, Brake Power and Mechanical Efficiency

The total power developed in the engine cylinder by combustion of fuel in the combustion chamber is known as Indicated Horse Power and is designated as IP. It is always more than brake power. The IP of an engine at a particular running condition is obtained from the indicator diagram. The indicator diagram is the $p-v$ diagram for one cycle at that load drawn with the help of indicator fitted on the engine. The construction and use of mechanical

indicator for obtaining $p-v$ diagram is already explained. While calculating the Mechanical efficiency, Indicated Horse Power (IP) is considered and is given by,

$$\text{Indicated Power (IP)} = \frac{P_m L A N k}{60} \text{ Watts or } = \frac{P_m V k}{60} \dots\dots\dots (1)$$

Where:

P_m = is the mean pressure,

V = is the displacement volume of the piston

k = is the number of cylinders

An IC engine converts chemical energy produced by combustion of fuel into the mechanical power. Here Power is referred to the rate of doing work. It is expressed as the product of force and linear velocity or product of torque and angular velocity. In order to measure power one needs to measure torque or force and speed. The force or it converts power developed by an engine and measured at the output shaft is called the brake power (BP) and is given by,

$$\text{Brake Power (BP)} = \frac{2\pi NT}{60 \times 1000} \text{ kWatts} \dots\dots\dots (2)$$

Therefore, the difference between IP and BP indicates the power loss in the mechanical components of the engine (due to friction). So, the mechanical efficiency is defined as ratio of brake Horse power to the indicated horse power.

$$\text{Mechanical Efficiency} = \eta = \frac{BP}{IP} \text{ or } \frac{BP}{BP+FP} \dots\dots\dots (3)$$

FP = Friction Horse Power is defined as the difference between the indicated horse power and the brake horse power.

$$FP = IP - BP \dots\dots\dots (4)$$

1.3.2. Fuel Air Ratio

It is the ratio of the mass of fuel to the mass of air in the fuel air mixture. Relative fuel air ratio is defined as the ratio of the actual fuel – air ratio to that of stoichiometric fuel – air ratio required to burn the fuel supplied.

a)
$$\frac{\text{Brake Specific Fuel Consumption}}{\text{Brake Power}}$$

$$\text{Brake Power} = \frac{V \times I}{0.9} \text{ W} \quad \text{Unit} - \text{gm/Sec KW} \quad \dots (6)$$

Where, P = Power of the engine in Watts,
 V = Voltages developed,
 I = Current in Ampere,
 0.9 is power factor of generator

b)
$$\frac{\text{Specific Fuel Consumption}}{\text{Mass Flow Rate}} = \frac{\text{Volume in ml} \times \text{Density of fuel}}{\text{Time in sec}} = \frac{\text{mass}}{\text{time}} \frac{\text{gm}}{\text{sec}} \dots (5)$$

1.3.3. Volumetric Efficiency

Defined as the ratio of actual volume reduced to N.T.P. of the charge drawn in during the suction stroke to the swept volume of the piston. The average value of volumetric efficiency is 70 to 80% but in case of supercharged engine it may be more than 100%, if air at about atmospheric pressure is forced into the cylinder at a pressure greater than that of air surrounding the engine.

1.3.4. Specific Output

Defined as the brake output per unit of piston displacement, given by

$$\text{Specific Output} = \frac{B.P.}{A \times L} = \text{Constant} \times P_{mb} \times \text{r. p. m.} \dots (7)$$

Note: That for the same piston displacement and brake mean effective pressure an engine running at higher speed will give more output.

1.3.5. Specific Fuel Consumption (S.F.C.)

May be defined as the mass of the fuel consumed per kW developed per hour and is a criterion of economic power production

$$\text{S.F.C.} = \frac{m_f}{B.P.} \text{ kg/kWh.} \dots\dots\dots (8)$$

1.3.6. Thermal Efficiency and Heat Balance

Thermal Efficiency is the ratio of indicated work done to the energy supplied by the fuel.

$$\text{Indicated thermal efficiency} = \eta_{th. (I)} = \frac{I.P.}{m_f \times C} \dots (9)$$

$$\text{Brake thermal efficiency} = \eta_{th. (B)} = \frac{B.P.}{m_f \times C} \dots (10)$$

$$\text{Brake Thermal Efficiency} = \frac{\text{Brake Power}}{\text{Mass} \times \text{Calorific Value}} = \% \text{ Approx.} \dots (11)$$

1.3.7. Heat Balance

The performance of an engine is given by heat balance sheet. To draw a heat balance sheet for I. C. engine, it is run at constant load. The indicated diagram is obtained with the help of an indicator. The quantity of fuel used in a given time and its calorific value, the amount, inlet and outlet temperature of cooling water and the weight of exhaust gases are recorded. After calculating I. P. and B. P. the heat in different items is found as follows:

For the gas engine, heat supplied = V × C,

Where V = volume at N. T. P. (M³/Min)

C = lower calorific value of gas

(i) Heat absorbed in I. P.:

$$\text{Heat equivalent of I.P. (per Minute)} = \text{I.P.} \times 60 \text{ kJ}$$

(ii) Heat taken away by cooling water:

$$Q_{\text{water}} = m_w \times c_w \times (t_2 - t_1)$$

(iii) Heat taken away by exhaust gases:

$$Q_{\text{exhaust gases}} = m_e \times c_{pg} \times (t_e - t_r)$$

Note: The mass of exhaust gases can be obtained by adding the mass of fuel supplied and mass of air supplied.

Heat Balance Sheet:

Sl. No.	Item	kJ	Per centd
	Heat Supplied by Fuel		100%
(i)	Heat absorbed in I. P.		
(ii)	Heat Taken away by cooling water		
(iii)	Heat Taken away by exhaust ed		
(iv)	Heat Unaccounted for		
	Total		

1.3.8. Exhaust Smoke and Emissions

Smoke is an indication of incomplete combustion. It limits the output of an engine if air pollution control is the consideration. Exhaust emissions have lately become a matter of grave concern and with the enforcement of legislation on air pollution in many countries, it has become necessary to view them as performance parameters.

1.3.9. Indicated and Brake Mean Effective Pressure

Mean effective pressure is defined as hypothetical pressure which is thought to be acting on the piston throughout the power stroke. If it is based on I. P. it is

called Indicated mean effective pressure ($I_{m.e.p.}$ or p_{mi}). If it is based on B. P. it is called Brake mean effective pressure ($B_{m.e.p.}$ or p_{mb}). Friction mean effective pressure ($F_{m.e.p.}$ or p_{mf}) may be defined as:

$$F_{m.e.p.} = I_{m.e.p.} - B_{m.e.p.}$$

Power of an engine depends upon its size and speed, therefore it is not possible to compare engine on the basis of either power or torque. mean effective pressure is the true indication of the relative performance of different engines.

1.3.10. Specific Weight

It is the weight of the engine in kg for each B. P. developed. It is an indication of the engine bulk Power developed in the engine cylinder is greater than that at the crankshaft due to engine losses. Thus,

$$I.P. = B. P. + \text{Engine losses}$$

Indicated power is usually determined with the help of a P–V diagram taken with the help of an indicator. In case indicated power cannot be measured directly, it is made possible by measuring the brake power and also engine losses. If the indicated diagram is available, the indicated power may be computed by measuring the area of the diagram, either with a planimeter or by ordinate method and dividing by the stroke measurement in order to obtain the mean effective pressure (m. e. p)

$$P_{mi} = \frac{\text{Net area of diagram in mm}^2}{\text{Length of diagra in mm}} \times \text{Spring Constant}$$

Where, P_{mi} is in bar

(The spring Constant is given in bar per mm of vertical movement of the indicator stylus.)

The main types of engine indicators are:

1. Piston indicator.
2. Balanced diaphragm type indicator:
3. Electrical indicators
4. Optical indicator

Calculation of Indicated Power

$$I.P. = P_{mi} \times A \times 10^5 \times L \quad N - m$$

- Work done per second

= Work done per stroke \times Number of working strokes per second

$$= P_{mi} \times L \times A \times 10^5 \times \frac{N}{60} \times k \quad N-m \text{ or } J/s$$

$$= \frac{P_{mi} \times L \times A \times N \times k \times 10^5}{60 \times 1000} \text{ kW}$$

If n is the number of cylinders, then = $\frac{n \times P_{mi} \times L \times A \times N \times k \times 10^5}{60 \times 1000} \text{ kW}$

1.4.Surface texturing for reducing friction and wear at the contacts

This comes under modification of surface topography. The three types of surface texturing methods:

1.4.1. High beam / electric discharge methods:

Laser texturing and pulsed air arc treatment

1.4.2. Etching Techniques:

Electro polishing, photochemical machining and maskless electro chemical texturing etc.

1.4.3. Micro machining / forming techniques:

Vibro - rolling, abrasive jet machining, diamond embossing, shot blasting and photolithography, mechanical indentation, shot peening micro CNC texturing.

Among all above surface texturing methods, laser beam texturing technique is one of the most widely used thermal energy base, noncontact type advanced method. This micro machining method can be employed for surface texturing on almost all type of materials. In laser texturing, laser beam melts and vaporises the material to form dimples.

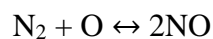
1.5.Exhaust Pollution

Flue gases, emissions from refineries and factories; exhaust from automobiles etc., are the major sources of air pollution. The internal combustion engine exhaust contains sever pollutants in the form of oxides of nitrogen NO_x which are toxic. If the concentration exceeds 100 ppm in closed space, it may even cause death. Photochemical smog is formed when oxides of nitrogen and hydrocarbon react in the presence of sunlight. Chemical smog has bad effects like crop damage, eye irritation, objectionable odour, decrease of visibility, cracking in rubber, etc. Whenever there is combustion inside I. C. engine, NO_x is formed. It may be from petrol, diesel engines and gas turbines. Emission of NO_x from petrol engine is much more compared with the diesel engine and gas turbine. The combustion temperature in petrol engines is in the order of 6000°C and is ideal for the formation of oxides of nitrogen. At this high temperature, atmospheric nitrogen present in the charge gets oxidised to NO and NO_2 .

About 90% of the oxides of nitrogen are in the form of NO. Later it gets oxidized to NO₂ in the atmosphere. These oxides when react with hydrocarbon in the presence of sun light. It forms photochemical smog.

1.5.1. Formation of oxides of nitrogen in Internal Combustion Engine

On the basis of thermodynamic format of NO from its elements begins at 800°C and is significant above 2220°C.



At around 4400°C reverse reaction is possible. Here one should note that temperature alone is responsible for the formation of NO_x.

1.5.2. Diesel Smoke Problem

The diesel engine has always been a preferred prime mover for transportation of heavy loads due to fuel economy. During last decay there is a rapid increase in the number of diesel vehicles. Diesel engines rated above 100 BHP are used in buses and trucks. Well maintained and normal rated engine emits negligible amount of carbon monoxide and hydrocarbon, though considerable amount of nitrogen oxides are emitted. The diesel engines smoke has following objections:

- i. It causes a reduction in visibility.
- ii. It has an unpleasant odour due to the presence of certain aldehydes, ketones and oxygenated compounds.
- iii. Soot particles in the exhaust gases settle down on building and trees, etc, in turn, spoil the appearance of building.
- iv. It is dangerous for health and causes breathing problems.

1.5.3. Diesel Engine Combustion and Smoke

In a diesel engine, air is compressed inside the cylinder and fuel is injected in it. Complete mixing of fuel and air is not possible as it has to take place inside the combustion chamber. Hence there is hardly complete combustion. Also load requirements are met through variation in quantity of injected fuel. Air fuel mixture ratio varies within wide limits, about 20:1 to 80:1. Local over rich zones thus exist within the combustion chamber and the high pressure and temperature generated due to combustion make the condition favourable for some fuel molecules to undergo thermal decomposition and dehydrogenation resulting in soot formation due to lack of oxygen in these over rich zones. If the amount of soot generated is large, the exhaust smoke density high. **Black smoke** is suspension of soot particles in the exhaust gases and results from incomplete combustion of fuel. The **white smoke** is due to too low operating temperature or too long delay between the start of fuel injection and beginning of combustion. **Blue smoke** is usually due to excessive lubricating oil consumption and its emission indicates a very poor condition of the engine.

1.6. Gasoline Engine Emission

There are following sources of air pollution in gasoline engine:

1.6.1. Exhaust Emissions

It contains substances which contribute the air pollution—hydrocarbon (HC), Carbon monoxide (CO) and Oxides of nitrogen (NO_x). Hydrocarbon is the unburned fuel vapour coming out with the engine exhaust due to incomplete combustion. Carbon monoxide occurs only in engine exhaust. It is the product

of incomplete combustion due to insufficient amount of air in the air – fuel mixture or insufficient time for combustion. Oxides of nitrogen (NO_x) are the combination of nitric oxide (NO) and nitrogen dioxide (NO_2) and occurs in engine exhaust. High temperature and availability of oxygen are the two main reasons for the formation of NO_x , because nitrogen and oxygen react at high temperature. Combination of NO_x and HC in the presence of sun light and certain atmospheric conditions produce photochemical smog.

1.6.2. Evaporative Emissions

These emissions are from the fuel supply system. About 30% of total hydrocarbon emissions occur from the fuel tank, fuel line and carburettor due to high temperature and fuel volatility.

1.6.3. Crank Case Blow

Crank Case Blow means the leakage past the piston and piston rings from the cylinder to the crankcase. It is about 20% of the total HC emission from the engine and maybe 30% if piston rings are worn.

Name:	Chemical Formulas
Gasoline:	C_8H_{18}
CNG:	CH_4
LPG:	$\text{C}_3\text{H}_8\text{C}_4\text{H}_{10}$

Chapter 2

Literature Review

Introduction

This chapter presents the research findings in the field of performance improvement of the internal combustion engine. The whole chapter is divided into three parts. The first part presents the works of the researchers in the area of the piston ring material. The second part includes research work on texturing on the piston ring. The third part has recent works related to the performance of engine. After reviewing the research articles the possible gaps in the literature were discussed.

Based on the literature gaps and discussions with the experts from the field of the internal combustion engines tribology, objectives of the present work were selected.

2.1. Piston Ring Material

Improvement in the mechanical efficiency of internal combustion engines can be achieved by decreasing the frictional losses occurring in cylinder and piston assembly. Wear measurements had been carried out and analysed in cylinder and piston ring during their mating with each other when the automotive engine was operated under artificially created dusty environmental conditions (Wakuri *et al.*, 1992), (Nautiyal, Singhal and Sharma, 1983) & (Pawlus, 1993). Tests were conducted on pin-on-disc test apparatus with boundary-lubricated cast iron materials and the values of specific wear rates were observed to be between 10^{-13} and 10^{-10} mm³/mm/N (Childs and Sabbagh, 1989). Based on the Newton-Raphson-Murty algorithm, the

nonlinear finite-element method was used to analyse the piston rings problems based on the theories of elasto hydrodynamic and hydrodynamic lubrication (Chu-Jung and Cheng-I, 1991).

The understanding of theoretical concepts and use of a methodology for estimating the service life of an I.C. engine, based on the law of adhesive wear and experimental evidence, were explained extensively (Picken and Hassaan, 1983). The study and experimental research were conducted on materials, metallurgical aspects of piston ring scuffing, piston ring lubrication in a two-stroke diesel engine and the film thickness between the cylinder liner and piston rings (Scott *et al.*, 1975), (Moore, 1981). Experiments were also performed on a reciprocating test rig having the supply of lubricant into the contact patch and measuring the friction force between specimen and counter-specimen. Tribological behaviours of cylinder liner with and without oil pockets were examined and compared (Grabon, Pawlus and Sep, 2010), (Grabon *et al.*, 2013). A test method was developed for evaluation of the friction and wear of piston rings and cylinder liner used in heavy-duty diesel engines. These works focussed on the conditions of the lubricating oil and its effect (Truhan, Qu and Blau, 2005b), (Michalski and Woś, 2011). At Volvo, technology had been updated for better evaluation of the friction between different combinations of materials. The elements under considerations were the piston rings and the cylinder liner which were analysed for friction, wear, and change in surface morphology during the running conditions (Johansson *et al.*, 2011). The Olander *et al.* investigated the role of sulfur for the high performance of the current tribo system. The field worn samples were examined to conclude that no tribo film containing sulphur existed under the tribological conditions set up for the piston rings and cylinder liner in the reciprocating test rig (Olander, Hollman and Jacobson, 2013). A similar work was carried out using the mathematical

model to solve the Reynolds equation (Mezghani *et al.*, 2012). A non-firing engine simulator was developed which operated at same linear speed, load and stroke as that of an actual engine. Except firing pressures, all engine operating conditions were simulated (Srivastava, Agarwal and Kumar, 2007). Experimental investigation was carried out to study the characteristics of the cylinder liner-piston ring tribopair. The process parameters selected for the experiment were sliding velocity, applied load and type of lubricating oil. A mathematical model was developed using L16 Taguchi orthogonal design to optimize the reciprocating wear for minimum weight loss and friction (Kapsiz, Durat and Ficici, 2011). Gara *et al.* performed an experimental study of single cylinder diesel engine operating at steady state to measure wear and surface roughness of cylinder liner by a WYKONT 1100 optical surface profile meter at various locations on the surface of cylinder liner before and after each test. It was observed that surface roughness decreased with time following which it experienced a steep decrease in rate during the run-in period. The results obtained in terms of volume of wear were reasonable and within the tolerance limits (Gara *et al.*, 2010). An investigation of temperature effect on wear and friction was carried out when steel to steel contacts was unlubricated, in various aerobic gaseous atmospheres and at a high temperature of about 200 °C. The inference was drawn considering the current results compared to previously published results (Velkavrh *et al.*, 2016). A ring segment was tested in Laboratory to evaluate wear and friction behaviour of piston ring on a flat specimen of grey cast iron representing cylinder liners in real engine. Various lubricants including mineral oil, Jet aviation fuel, fully formulated 15W40, category of heavy-duty oil, were used to evaluate the condition of lubricant. During the test the temperatures were maintained from 25 to 100 °C. An incremental load procedure was used to evaluate friction behaviour which showed boundary lubrication for all

lubricants at 100 °C. Wear tests were performed at 240 N for 6 h at a constant temperature of 100 °C with new ring segments following which weight loss method was used to measure the wear. A geometric model was designed for wear volume and wear depth to take into account the compound curvatures before and after testing (Truhan, Qu and Blau, 2005a). Carbon fabric was treated with gamma irradiation technique with varying doses (100–300 kGy) to develop composites with polyetherimide (PEI) matrix which was characterized for inter-laminar shear strength (ILSS) and adhesive wear studies. FTIR and SEM indicated presence of carbonyl functional group and roughening of surface inferred improved fiber–matrix interface (Tiwari, Bijwe and Panier, 2011). Investigation was carried out to develop and analyse the material properties of a Polybenzimidazole (PBI)-Polyetherketone (PEK) blend-based composite and composites containing solid lubricants (SLs), short fibers of glass and carbon. It was inferred from the experimental work that the SLs or fibers together showed excellent tribo-properties in accordance to the composite based on PBI–PEEK blend (Bijwe *et al.*, 2015). Experimentation was carried out for two diesel fuels i.e. EN590 and GDK650 as lubricants in the pin-on-disc model during the testing of wear behaviour of hydrogenated diamond like carbon (DLC) coating in DLC/steel. It was concluded that anti-wear additives were harmful to DLC influencing its wear rate while steel remains unaffected by pressure, temperature, speed and type of lubricant used (Djoufack *et al.*, 2015). The investigation was conducted to analyse the tribological properties of ground, lapped and textured lapped discs against polished pins for reciprocating motions. Various output parameters were analysed among which coefficient of friction showed 30% reduction and vibrations between contact points of textured surface-balls interface showed a prominent dip at the resonance frequency in comparison to interface of polished surface-balls (Sudeep, Pandey and Tandon, 2013).

This work laid down the tribological analysis carried out for the dimpled piston rings. In order to curb the fuel consumption, research is being conducted to reduce the friction between cylinder liner and the piston rings. The experimental work yielded the result in favour of the dimpled piston rings as it helped saved considerable amount of fuel and lubricating medium. The tribological parameters, coefficient of friction and wear had been studied in this research work under full lubricating conditions for smooth/textured surfaces of steel discs and smooth surface of steel pins. Reduction in considered tribological parameters had been recorded in textured steel disc for fully flooded and starved conditions (Pandey, Tandon and Singh, 2013). Another work investigated the mechanical properties of synthesised Mg_2Si co-doped with Bi and Sb through in situ spark plasma reaction sintering.

Muthiah *et al.* displayed the synthesis of a process to enhance the mechanical properties such as hardness $\sim 5.4 \pm 0.2$ GPa and an elastic modulus $\sim 142.5 \pm 6$ GPa with a fracture toughness of $\sim 1.71 \pm 0.1$ MPa/m, t as thermal shock resistance as ~ 300 W/m. It promised the sustainability of their thermoelectric modules under all circumstances (Muthiah *et al.*, 2017). An investigation was carried out on the stir casted aluminium based composite reinforced with 2–4–6% weight flyash. The pin-on-disc test rig was used to conduct the experiment for the smooth surfaces of cast iron disc and smooth MMC pin tribo-pair for the study of tribological parameters i.e. friction force and wear. The experimental work concluded that MMC with 6% flyash wears less while MMC with 4% flyash provides low coefficient of friction or friction force (Sharma, Singh and Chaudhary, 2017).

Michalski and Woś considered a reciprocating tribometer for the evaluation of frictional behaviour for different materials and their combinations. The piston assembly is a source of frictional losses, consumer of lubricating oil and contributor of

particulate emissions (PM). After the experimental research of wear, friction and surface topology, it was said that surface roughness is a vital output parameter irrespective of properties of materials (Michalski and Woś, 2011).

Wakuri et al. stated that improving the wear resistance of the cylinders working surfaces is the most typical problem. The work surfaces of cylinders are subjected to wear which reduces performance characteristics of the engine. Wear resistance of the cylinder block could be reduced by 6 six copper inserts, forming a layer of low shearing resistance metal on its working surface. Considering that the width of each insert was 1.5 mm, inclination angle of the insert to the diametric plane was 17.2° . Reduction in friction was the greatest at inclination angles from 15° to 25° (Wakuri et al., 1992).

Scott et al. conducted a study on the arc PVD method of coating of molybdenum nitride (MoN) on the piston surface in a diesel engine. An analysis was carried out in terms of microhardness, SEM, X-ray diffraction and surface roughness and an increment in hardness were recorded to 2000 ± 400 HV for coated piston against uncoated piston (123 HV) (Scott et al., 1975).

Tan and Ripin, reviewed literature conducted on the materials and metallurgical properties of piston ring with respect to scuffing of I.C. engines and gas compressors. A discussion was carried out on the scuffing mechanisms and outlined the role of material properties, etc on the scuffing of I.C. engines (Tan and Ripin, 2011).

Shinkarenko et al. conducted tribological tests for grey cast iron and carbidic cast iron which is used as piston rings under boundary-lubrication with a light medicinal paraffin oil and zinc dialkyl dithio phosphate (ZDDP) (1% by weight) added paraffin. Wear mechanisms were examined for visual evidence of metal fatigue, direct metallic and chemical reaction film wear (Shinkarenko, Kligerman and Etsion, 2009).

2.2. Texturing on Piston Ring

Researchers investigated aspects such as the effect of hybrid texturing, laser texturing on steel surface filled with poly phenylene sulphide (PPS) powder, ball-on-disk sliding tests performed under dry lubrication conditions and pin-on-disc model with two diesel fuels, concluding that hybrid texturing protects metal surfaces with the formation of a polymer transfer layer. The dependency of the surface texture parameters on the friction coefficient to redefine surface topography of a product after the surface finishing processes were investigated, which reported a dip in friction coefficient with an increase in load (Cho, 2016), (Kuilenburg et al., 2012; Djoufack et al., 2015).

Various researchers evaluated the dependency of partial laser surface texturing (LST) on the reduction of friction in piston rings and concluded that partial LST cylindrical piston rings for variable engine speeds under near-half-load conditions reduce friction by 25 per cent in comparison to non-textured convention rings, vibrations, fuel and lubricating oil consumption (Etsion and Sher, 2009; Ryk and Etsion, 2006; Sudeep et al., 2013; Pandey et al., 2013). Researchers also studied the tribological performance of micro dimples, which formed the base of frictional tests, laser peen textured copper surface in starved lubrication and multi-shape textured surface produced by laser ablation; they concluded that combination of geometric pattern surface helped in reducing friction significantly in both dry and lubricated conditions (Kim et al., 2014; Li et al., 2014; Zenebe Segu and Hwang, 2015). Investigation of the effect of machining environment on the quality of machining under dry and wet conditions yield a reduction in friction and wear values at higher sliding speed and heavy loads (Hu and Xu, 2016).

Wear behavior of textured surfaces specimen, brake disc material with groove textured, and un-textured counter specimen, both specimen textured and un-textured with varying spacing under dry condition, simultaneous variations in dimple densities for unidirectional sliding under starved lubrication, by varying the normal loads were considered to evaluate the behaviour at room and elevated the temperature. The results showed reduced values of friction and wear indicating the small texture spacing helps in achieving the highest friction coefficient and the shallowest wear depth, which are actually the combined effect of increased surface roughness and the micro-cutting effect by the texture edges which reduced real contact area, and led to entrapment of wear debris (Wos et al., 2017, 2018; Mo et al., 2013; Xing et al., 2017). Olofinjana et al. 2015, investigated the influence of laser surface texturing on the formation and durability of tribo chemical films. Vladescu et al. (2016) and Gachot et al. (2017) analyzed the tribological behaviour under synthetic lubrication with and without additives. The fused silica specimens with textures were studied against a convex steel pad. The fabrication techniques of surface texturing and their effect on the tribological behaviour of materials and textured gray cast iron (CI) using lubricated block-on-ring tests were studied by Silva and Costa (2017). The results showed improvement in the relative performance of the textured specimens due to the development of progressive contact into the mixed and boundary regime inmost of the cases. Many researchers used a numerical model to investigate the tribological behaviour and deduced an optimal design of a multidimpled surface. The laser fabrication technique was used for developing texture on stainless steel and low alloy carbon steel.

The influence of machining parameters and vibration modes on the tribological behaviour along with the tribological properties were investigated considering metal-

on-metal and metal on plastic contacts. Results showed extremely high static friction coefficients, reduction in dynamic friction coefficient reduced wear rate and adhesion between pin and samples surface. The dimpled specimen yielded a further reduced friction coefficients and wear rates (Wei et al., 2013; Dunn et al., 2015; Amini et al., 2016; Jones and Schmid, 2016). Textured the specimen by whirling electrical discharge texturing (WEDT). The friction tests yielded to decrease in the friction coefficient under the boundary lubrication and the mixed lubrication condition (Yamaguchi et al., 2016). The composite of PEK and PBI was studied by authors Bijwe et al. (2015). Textures formed by honing and plateau honing process on the surfaces of the cylinder liners. Specimens were cut from gray CI cylinder liners. Then experiments were performed under lubrication conditions on an oscillating wear tester. It showed excellent tribo-potential, which has a coefficient of friction of level 0.5 and the specific wear rate $10^{-16} \text{ m}^3/\text{Nm}$ (Grabon et al., 2017). Wear resistance and friction coefficient of non-smooth surfaces were investigated. Effect of massive laser shock peening (LSP) on dry sliding wear was evaluated and discussed (Luo et al., 2014). Meng et al. discussed microscale textures engraved on surfaces of carbides with the help of a laser. These textures were filled with a solid lubricant to act as coatings on the surfaces of cemented carbide. Then dry lubrication sliding tests were carried out against austenitic steel balls in the atmospheric air. The results showed lower friction in case of micro scale textured cemented carbides, which compared with un-textured cemented carbides (Meng et al., 2018). Double-layer thermal barrier coatings were formed on SS310 substrates with the help of high-velocity oxygen fuel thermal spray method. Coatings were exposed to a high-temperature corrosive environment and then tested for performance. The result reported that there was an improvement in the resistance to corrosion (Taie et al., 2018). Qu et al. presented a high temperature

method of indentation. This method was developed for the investigation of residual stress and high-temperature fracture toughness in a typical TBC. Nanostructured 8 Wt.% yttrium partially stabilized zirconia (YSZ) coating. It was observed that cracks were caused by the high-temperature indentation tests (Qu et al., 2018). Sharma et al. prepared aluminium melt fly ash particles and studied their effect on the wear (Sharma et al., 2017). This study reported the synthesis of Mg₂Si co-doped with Bi and Sb and carried out spark plasma reaction sintering, shown enhancement in mechanical properties. (Muthiah et al., 2017) Tribological performance analysis was performed of textured steel surfaces and plain CI under lubricating and dry conditions (Singh et al., 2016; Lal and Singh, 2018; Rana et al. (2018)). From the above literature review, it was found that a reduction in wear and friction in bearings is a vital task. It also found that there were few studies available for exploring the behaviours of the journal bearing in oil-lubricated conditions. Therefore, the objective of this research paper is to experimentally find out tribodynamic performances of interfaces formed by chrome steel pin with plain surface and textured surface CI discs. Also, the study aims to further explore the possibility of manufacturing of textured surface CI journal and chrome-coated bearing.

Shibata et al. during research observed that few ceramics show excellent tribological properties under water lubrication. Experimental work was conducted for surface textured Si₃N₄, whose result yielded improvement in the tribological characteristics. The experimental and analytical results inferred an enhancement in the tribological properties due to laser surface texturing (Shibata et al., 2016).

Wolski et al. developed a theoretical model to assess the potential of spherical micro-dimples generated by laser surface texturing (LST) for soft elasto-

hydrodynamic lubrication (SEHL). This model consists of mutual smooth elastomeric and LST rigid surfaces moving relative to each other under viscous lubricant conditions. The experimentation led to the identification of significant parameters to the defined problem i.e. aspect ratio and dimples area density. It was observed that LST enhance load capacity and lower down the friction in SHE (Wolski, Podsiadlo and Stachowiak, 2011).

Priest et al. considered a plateau honed surface with a cross hatch pattern of valleys for oil retention for friction and wear properties during reciprocating motion. It was used for a comparative study of lubricity of cylinder liner surfaces possessing different marks developed by plateau honing. The friction and wear results of these surfaces were compared against the results obtained from randomly ground surfaces (Priest, Dowson and Taylor, 1999).

2.3.Engine Performance

The scarceness of conventional fuels, along with increasing emissions of pollutants, and also their increasing costs have made biomass a more attractive source (Sensoz et al., 2000). Petroleum-based fossil fuels are available at very limited reserves, which are concentrated only in certain regions of the world. Those regions are reaching their peak for the production of these fuels. This scarceness of known Petroleum-based fossil fuels has made renewable sources of energy more attractive (Sheehan et al., 1998). Word “Biodiesel” was born from a Greek word “bio” which, means “life” and word “diesel” from Rudolf Diesel. Biodiesel is referred as an equivalent to diesel as, it is a processed fuel which, is derived from the available biological sources. This fuel has attracted a lot of attention worldwide as blending

component as well as direct replacement of fuel in vehicle with diesel engines (Demirbas et al., (2008).

Among all the available methods of production of biodiesel, trans esterification is a widely used method. This process lowers down the viscosity of oil. Biodiesel fuel is a renewable fuel, which is used in different ratio with petro diesel fuel to decrease exhaust emissions. Apart from being renewable, it is biodegradable, non-toxic, possess better properties against petrol diesel fuel, and is sulphur free. It is an eco-friendly fuel and is usable without modification (Hasannuddin et al., 2018).

Dhar and Agarwal carried out the experimental research in terms of engine performance and emissions for an IC engine fuelled with two bio-diesels and petroleum diesel. The blend ratio of the two bio-diesels showed a decrease in their performance as the ratio increased. This happened because of low energy content of bio-diesel than that of petroleum diesel. Hence, it is essential to experiment and validate the effect of bio-diesels before recommending on a mass scale production (Dhar and Agarwal, 2014).

Truhan et al. studied the effect of bio ethanol as a lubricant through tribological tests in terms of friction and wear at piston ring. The influence of bio ethanol was considered with the addition of ethanol combustion products and the process was operated on an artificial engine oil alteration process during the tribo tests. A major performance difference in tribological behaviour was observed (Truhan, Qu and Blau, 2005b).

Mróz et al. formulated a model consisted of two parts. The model predicted the lubrication behaviour of ring packs before and after the running periods during the first part and of top compression ring in the second part. The aim of research was to identify the tribological properties during actual running of engine (Mróz, Kucharski and Pączelt, 2018).

Xing et al. experimentally studied a single cylinder diesel engine at steady state were selected in which liner surface roughness and wear were measured by WYKONT 1100 optical surface profile meter. Different locations were considered for noting the wear values before and after each test yielding that during run-in period, with time surface roughness reduced while rate of decrease was significantly high (Xing et al., 2017).

Friction mechanisms were spotted for piston rings and piston skirt, crank and bearing system for crankshaft engine (CSE), linear electric generator for free-piston engine (FPE) and valve train system. Estimation of frictional losses in each mechanism was done and it led to the conclusion that total frictional loss in FPE is half to the frictional loss incurred in CSE (Sabeur et al., 2013).

Khusainov and Glushchenko stated that significant frictional losses occur in the piston ring cylinder liner assembly in an I C engine i.e. at the interface of top compression ring and the cylinder liner at the TDC and BDC due to existence of boundary layer lubrication. Variation in the piston speed governs the change in lubrication regime in the cylinder which directly affects the friction between the piston ring and cylinder liner during the piston stroke. Theoretical modelling of friction force

was carried out and experimental runs were conducted on the reciprocating tribometer to analyse the different tribological parameters under speed range of 300 rpm to 1500 rpm with 60 N constant load. It was inferred that the reduction in the friction force and friction coefficient was recorded when speed was increased (Khusainov and Glushchenko, 2017).

Hazar, specified that the loads, speed and temperatures are increasing on major tribopairs of the engine. This leads to decrease in oil film thicknesses between the component surfaces. The review involved the study of surface behaviours and resulted in highlighting the areas of future research (Hazar, 2010).

Cabboi and Woodhouse formulated the mathematical models for piston ring seal and lubrication on the basis of thermodynamic and hydrodynamic lubrication equations. Simulations were carried out to investigate the lubrication performances of the piston ring, and effects of the piston motion to piston ring lubrication process were compared against a conventional engine. The experimental result inferred that seal working time was longer than the conventional engine's seal for defined cycle time (Cabboi and Woodhouse, 2018).

2.4.Literature Gap

It is observed from the literature review that, limited research has been conducted for experimentally examining the performance of a diesel fuel-based engine using textured piston rings. As far as the coating materials of the piston rings are concerned, attempts have been made by several researchers to optimize the process

parameters of the engine. In this work, prime factors are considered and investigated to enhance the performance of the diesel engine.

The main points observed by studying the literature are mentioned below:

- More accurate analysis of the physics and mechanisms of piston seizure with textured piston ring to save valuable resources and time.
- The technology that can enhance the life of the piston rings and a reduction in running cost.
- Need of better understanding of the correlation between friction and surface roughness of the materials for piston ring and the cylinder liner.
- Improved knowledge of oil film with nanoparticles could lead to a better understanding of oil flow within the ring pack.
- The instantaneous hydrodynamic power loss of each ring can be predicted with considerable accuracy.
- Identification of points where blow by/blow back may occur more readily.
- The instantaneous hydrodynamic power loss of piston ring can be predicted with considerable accuracy.
- Require more thermo hydrodynamic analysis at the interface of piston ring and cylinder liner in an I.C. Engine.
- A special surface texturing is considered as the new promising technology for piston rings durability improving, for example, some recent works indicate that making pits on piston ring face can reduce friction and decrease wear rate thereby increase the life of the piston rings significantly.
- An exhaustive study required to include a full-scale validation of tribometer test and engine performance test approach.

- A better understanding of the role of additives at the interface of tribo pairs.
- More analysis of friction, wear, thermal considerations at the interface of mating pairs.
- Performance analysis of I C Engine with nanoparticles and textured piston rings fuelled with diesel and biodiesel.

2.5.Objectives

The proposed research work will incorporate the following objectives:

1. To analyze friction and wear at the contact of textured piston ring material and cylinder liner material using a special Test Rig.
 - Characterization – basis of pitch and cross-section.
2. To determine specific wear constants.
3. To determine the coefficient of friction for the particular set of textured piston ring material and cylinder liner material.
4. To design and fabrication of textured piston rings.
5. To determine the efficiency and fuel consumption of the diesel engine.
6. To examine the exhaust emissions from the diesel engine.

Chapter 3

Methodology and Experiments

For achieving the objectives of the thesis work, different experimental setups were used. The wear and friction from the piston rings material were evaluated with the help of pin on disc machine with using coated and textured disc specimens. The selected texturing was produced on the actual piston ring by using the laser texturing method and experiments with diesel and bio-diesel fuels were performed on a four-stroke engine to evaluate the effects of surface textures. This chapter describes the various equipment used in performing these experiments.

3.1. Pin on Disc

Figure 3.1 & 3.2 shows the diagram of wear and friction tester used for this experimental study according to ASTM G-99. It had a motor having different speeds depending on the position of the rheostat. Circular disc specimen was fixed at disc holder on the horizontal disc fixture. It had a sensor for speed and the probe for wear measurement. Pan having horizontal platform was used for placing different weights. A horizontal platform supports weight in the gravity direction. The applied weight/ force was transmitted to unilever via wire, pulleys and bell-crank mechanism arrangement.

A probe was fixed on the side of the bell crank lever which detected/determined force of friction. This test rig has the speed range between 200 and 2000 rpm as per its specifications and it can measure friction force up to 200 N, with 0.1 N as least count. Frictional force, Newton (N), can be measured with an accuracy of $0.1 \pm 2\%$.

Specifications of materials used in these experiments were: (i) chrome steel pin having a diameter of 8 mm; Discs: (ii) A cast iron disc with a plain surface. Diameter = 165 mm and thickness 8 mm (iii) Another cast iron disc had textured surface, Diameter = 165 mm and thickness 8 mm.

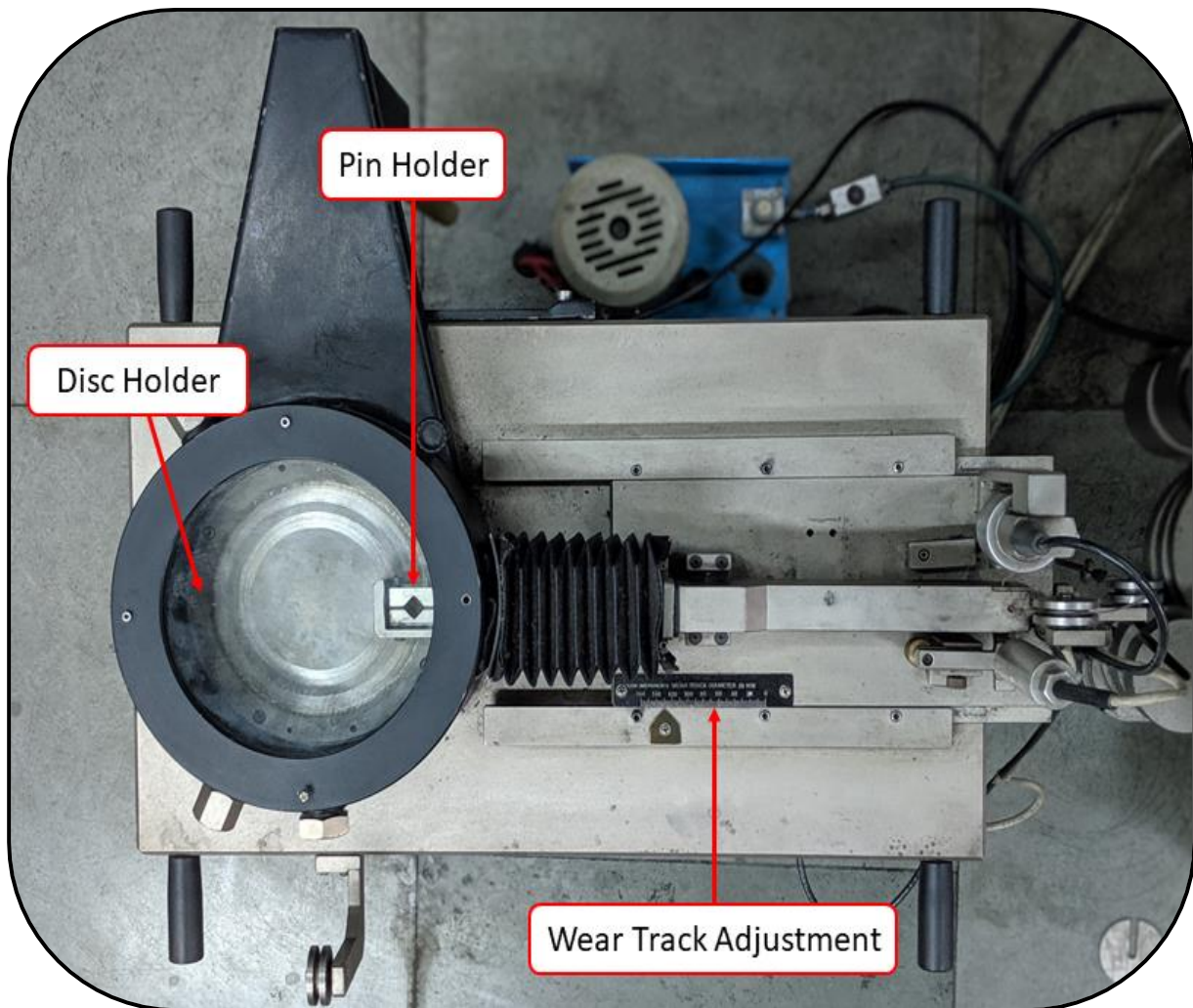


Figure 3.1: Top view of Pin on Disc test rig

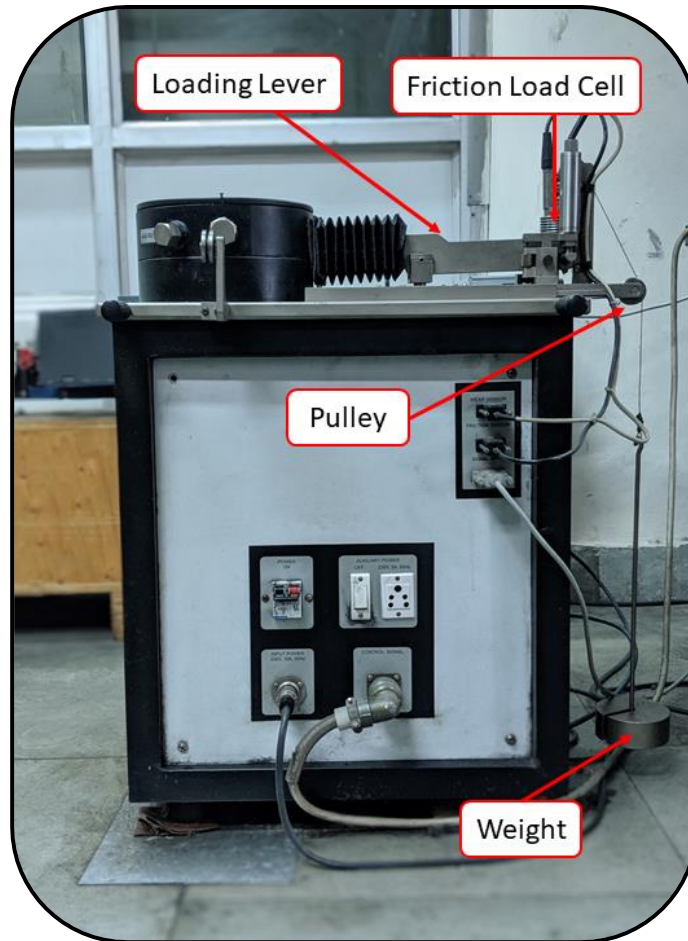


Figure 3.2: Front view of Pin on Disc test rig

Experiments were planned in such a way that each factor had been analyzed individually. The time required for experimenting was significantly reduced. This plan was very efficient for investigating the effect of individual factors as well as investigation of the effects of multiple performance factors. The experiments were conducted in Tribology Lab, Delhi Technological University, Delhi. Experiments performed on each disc were 27. The tribological performance studies were done at different loads, loads taken in terms of pressure vary from 1.95 to 3.1 MPa, sliding speeds taken between 2 to

10 m/s which is equal to 200 – 2000 r.p.m. when taken in terms of rpm. and also, distance travelled by the pin over disc was between 1000 m to 5000 m.

3.2. Thermal Imaging Camera

Figure 3.3 shows the front and back side view of Fluke Ti 400 thermal imaging camera. Fluke Ti 400 thermal imaging camera is used to capture high definition visible light images. This thermal imaging camera consists of 5-megapixel digital camera and gives 320x240 thermal images. It captures an accurate and clear image via automatic or manual focusing. This thermal imaging camera can measure the temperatures ranging from -20 °C to +1200°C.

The Figure 3.4 shows the Range, Span and Total Level of the Fluke Ti400 Thermal Imaging Camera. 1st is Range and it is the temperature level to view within the total range of temperatures. *Range* consists of the values within the temperature set in Total Range and so does the Span. 2nd is Span and it consists of the span of temperatures for viewing the temperature within the Total Level of temperature. In automatic Range/Span mode, the Imager sets Range/Span based on the temperatures set in Total Level.

Figure 3.5, 3.6 & 3.7 shows a series (sample) of image of the Pin being used on a Pin on Disc test rig. Figure 3.5 the shows the Image of Pin on “Pin on Disc” test rig taken from Fluke Ti400 Thermal Imaging Camera. Figure 3.6 shows the maximum, average and minimum temperature of the pin at the contact area and as well as of the surroundings. Whereas, Figure 3.7 shows the temperature variation graph for the contact area of pin along with its surroundings. Fluke Ti400 thermal imaging camera also gives a table of

details like background temperature, average temperature, range of temperature in whole image, camera model number image size along with IR sensor size, time at which image was taken and distanced between the camera and target, all of which can be seen in Table 3.1.

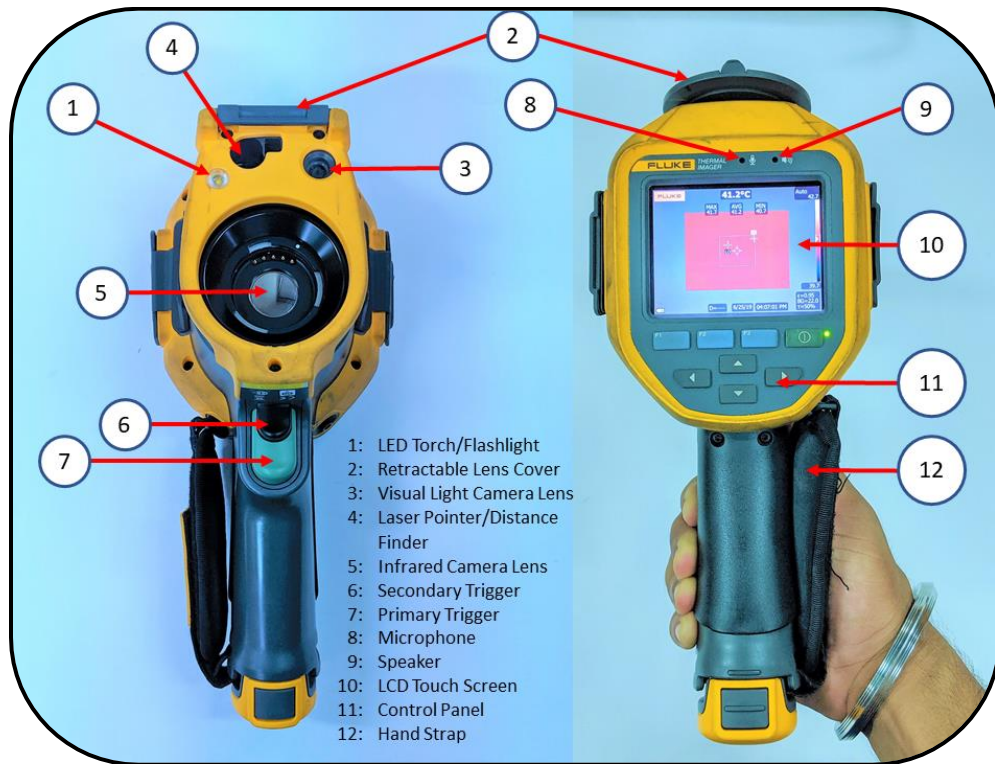


Figure 3.3: Front View and Back side View of Thermal Imaging Camera (Fluke Ti400)

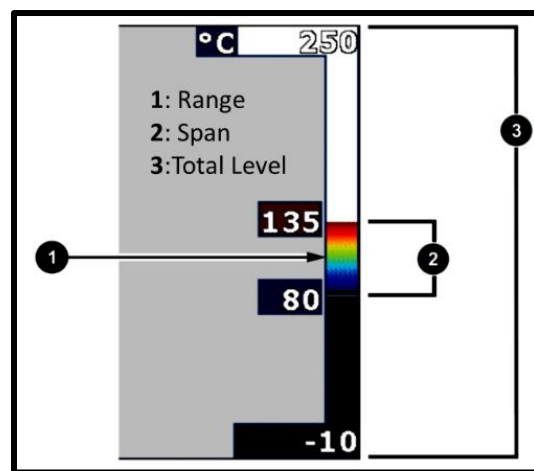


Figure 3.4: Range, Span and Total Level of the Thermal Imaging Camera (Fluke Ti400)

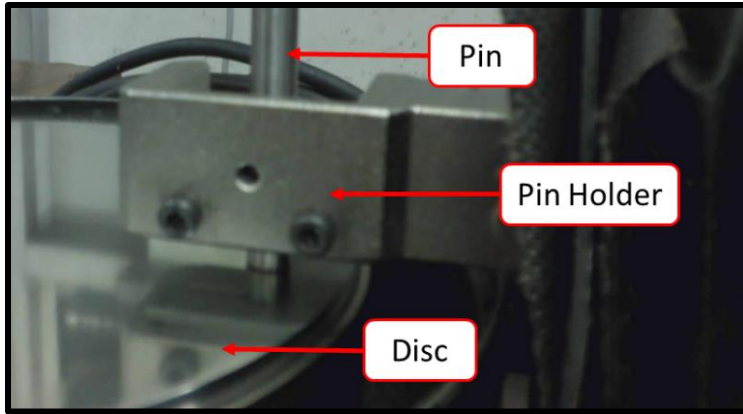


Figure 3.5: Image of Pin on “Pin on Disc” test rig taken from Thermal Imaging Camera

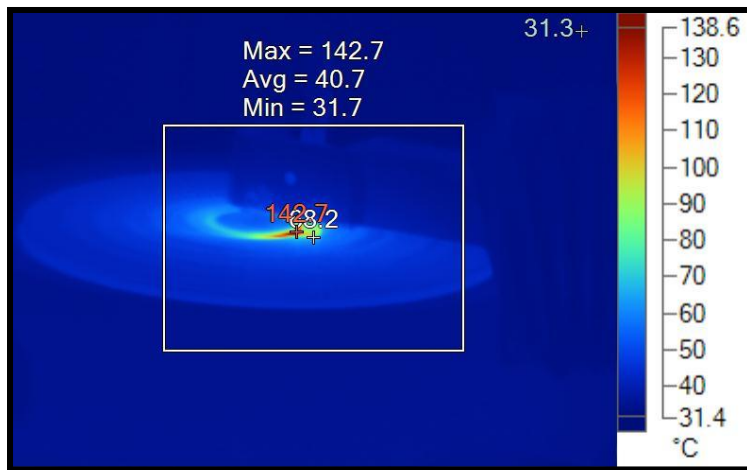


Figure 3.6: Thermal Image of Pin showing the Temperature at contact point and surroundings

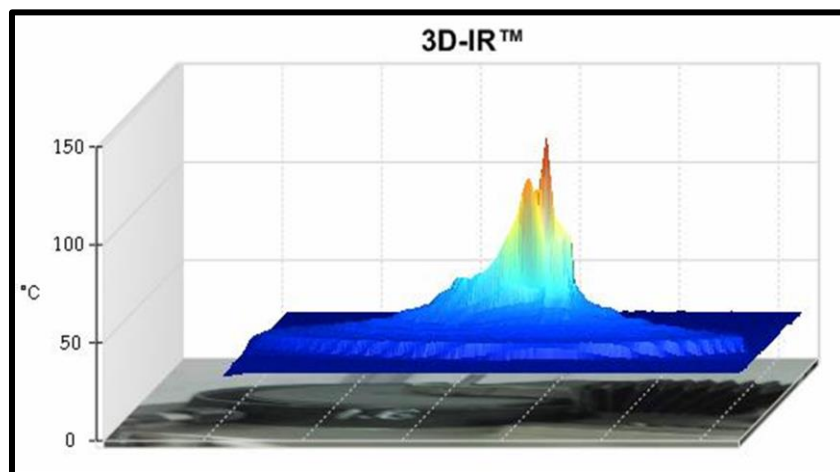


Figure 3.7: Temperature Variation Graph for the Pin at its contact point and its surroundings

Table 3.1: Details of the thermal image of Pin taken by Thermal Imaging Camera (Fluke Ti400)

Background Temperature	34.0°C
Average Temperature	35.7°C
Image Range	31.3°C to 142.7°C
Camera Model	Ti400
IR Sensor Size	320 x 240
Camera serial number	Ti400-13120004
Image Time	6/16/2016 3:25:52 PM
Distance to Target	0.96m

3.3. Vibration Measuring Device

Figure 3.8 shows the top view of PRÜFTECHNIK VIB Xpert ® II. PRÜFTECHNIK VIB Xpert ® II was used for measuring the vibrations produced at the micro-level. It is used to measure the vibrations in both abscissa and ordinate.



Figure 3.8: Top View of Vibration Measuring Device (PRÜFTECHNIK VIB Xpert ® II)

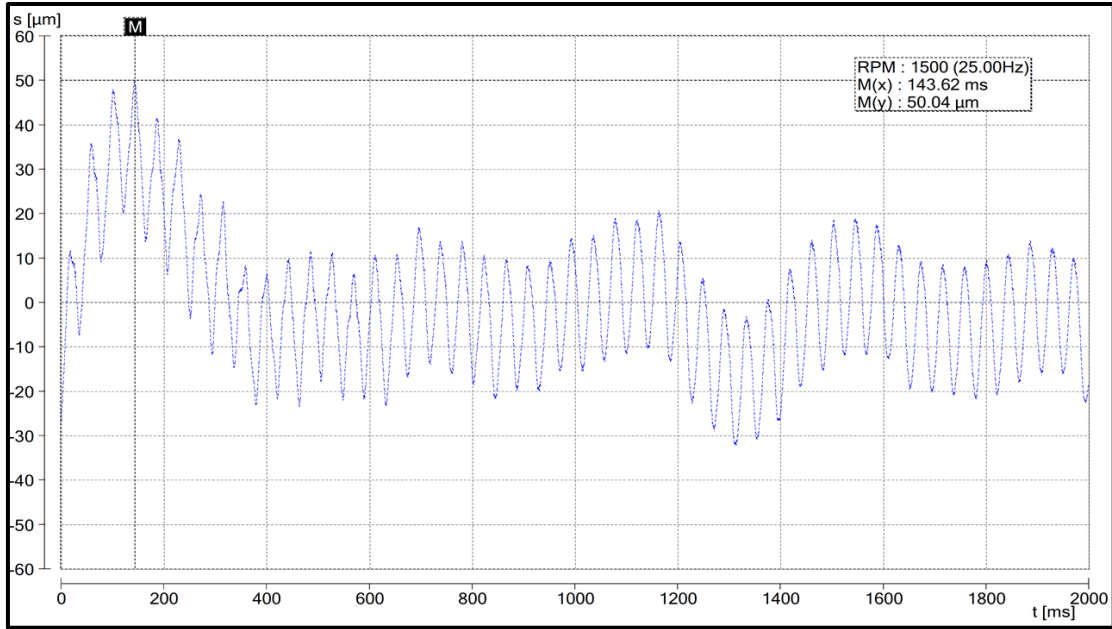


Figure 3.9: Vibrations produced in abscissa and ordinate along with their max values.

As can be seen in Figure 3.8 it consists of two magnetic probes for the measurement of vibration. The output of the combined effort of both magnetic probes is plotted and come out in the form of a graph like shown in Figure 3.9. The vibration produced by the machine vs time taken. It is plotted as a graph by the VIB Xpert ® II and is shown in Figure 3.9. hence, from Figure 3.9 we can see that the maximum value of vibration is $50.04\mu\text{m}$ which was measured for a time period of $143.62\mu\text{s}$.

3.4. Digital Sound Meter

The rules of noise pollution, 2000, had set different acceptable limits depending upon the category i.e. day and night. For industries, it is 75 dB for the day and 70 dB for the night. Similarly, for residential areas, it is 55 dB for the day and 45 dB for the night (Noise Pollution Rules, 2000).

Digital Sound Level (SL-1350) was used to measure the sound pollution caused by the friction between the sliding pairs. The device measures the sound in Decibels (dB). Frequency ranges from 31.5 Hz to 8kHz, measuring Sound from 30dB to 130dB. This digital sound level has a resolution of 0.1 dB with an accuracy of ± 1 dB.



Figure 3.10: Digital Sound Level (Instrument SL-1350)

3.5. Texturing Method

Theodore H. Maiman at Hughes Research Laboratories in 1960 built up the first laser, based on the theoretical work by Arthur Leonard Schawlow and Charles Hard Townes. An instrument which emits light through a process of optical amplification of stimulated emission of electromagnetic radiation is known as Laser. The word "Laser" sprang up as an acronym of "Light Amplification by Stimulated Emission of Radiation" (Gould, 1959).

Laser machine used in texturing the Piston ring and Disc was the "LASER P400" laser texturing machine. It is used in laser engraving, texturing, and structuring of small parts. One can use this machine for cutting tools, watches, small inserts, micromachined

workpieces, etc. It can accommodate a workpiece of up to $60 \times 40 \times 25$ cm. The laser is a standard type Nano Second Pulsed-Fibre Laser with 100 W of standard power. The speed of rapid traverse is 40 m/min for all the axis.

The piston rings were held on a motorised chuck for smooth circular movement of piston ring for laser texturing. Figure 3.11 shows the red-light being incident on the piston ring so, that one can see the texturing shape and location of the texturing. Figure 3.12 shows the laser being incident on the piston ring for texturing.



Figure 3.11: Red light being incidental on Piston Ring for laser texturing

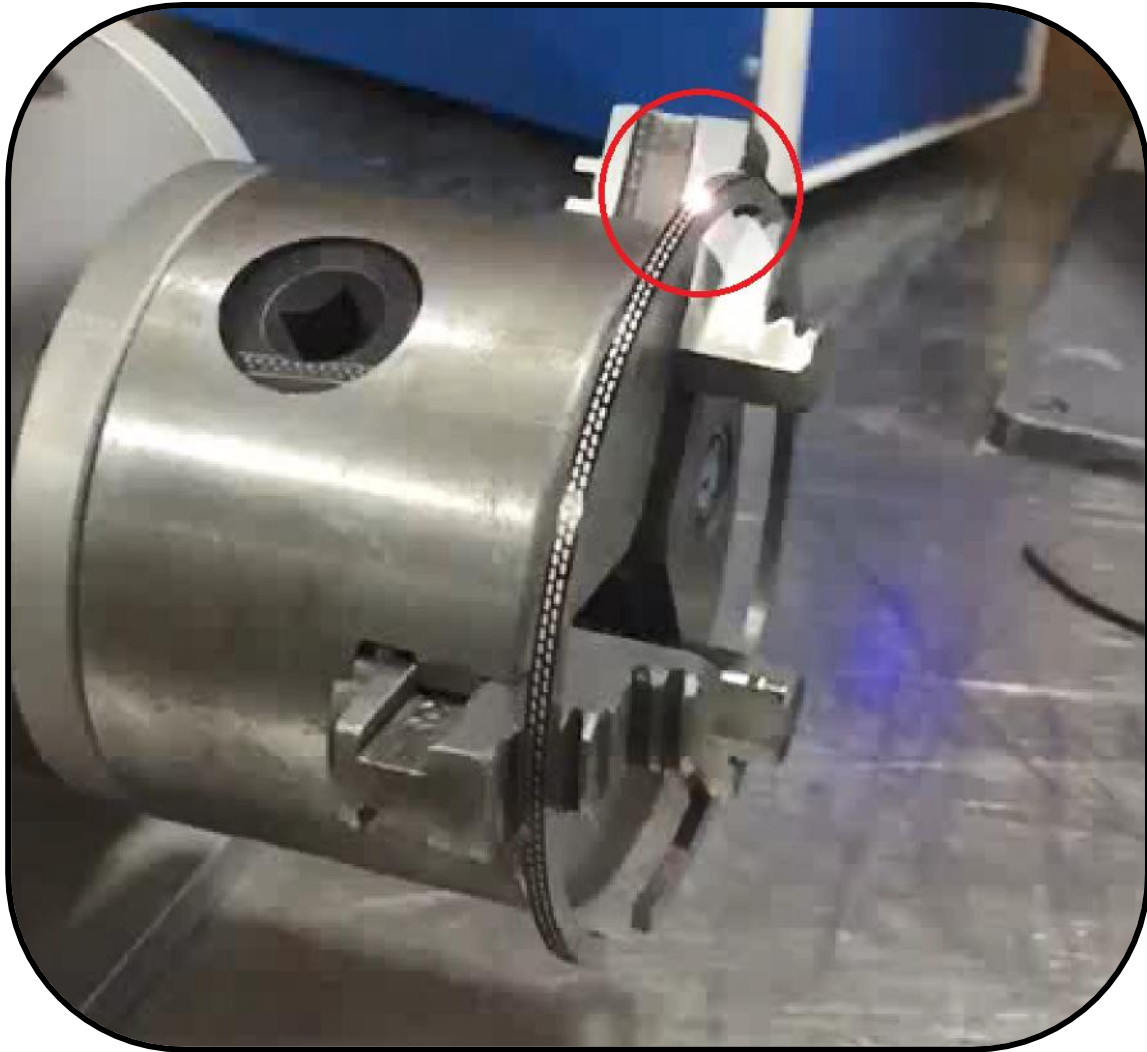


Figure 3.12: Laser beam machining on Piston Ring for texturing

3.6. Four-Stroke Single Cylinder Diesel Engine

For the evaluation of different engine performance parameters, A Kirloskar make diesel engine (DAF8) was used for the experimental research work as shown in Figure 3.13. The detailed specification of the engine is given in Table 3.2.

A provision of electrical loading has been provided in this engine. The cylinder is fitted with a hardened high-phosphorus cast iron liner and it is made up of cast iron. The

wet sump type of lubrication system is used in this engine. Various instruments like gas analyser, Smoke analyser, have to mount on the engine at the proper location on the experimental engine setup. Apart from this, a dual fuel system has been used for diesel and biodiesel, which can be seen in Figure 3.14. Figure 3.14 shows the control panel for the engine. This panel can be used to control the load on the engine in steps of 500 watt, it also consists of the ammeter, voltmeter, temperature indicator and RPM indicator.

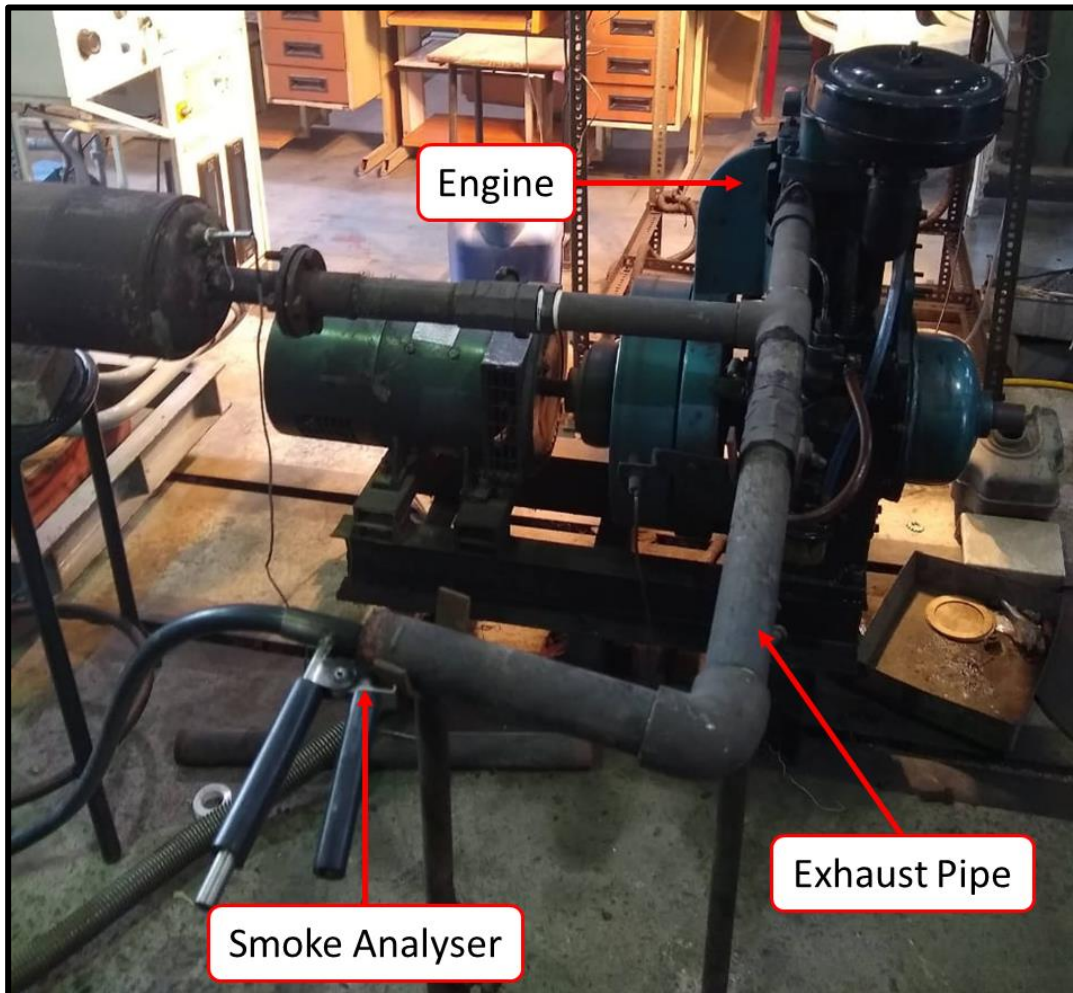


Figure 3.13: Engine used for the experimentation [Kirloskar Diesel Engine (DAF8)]

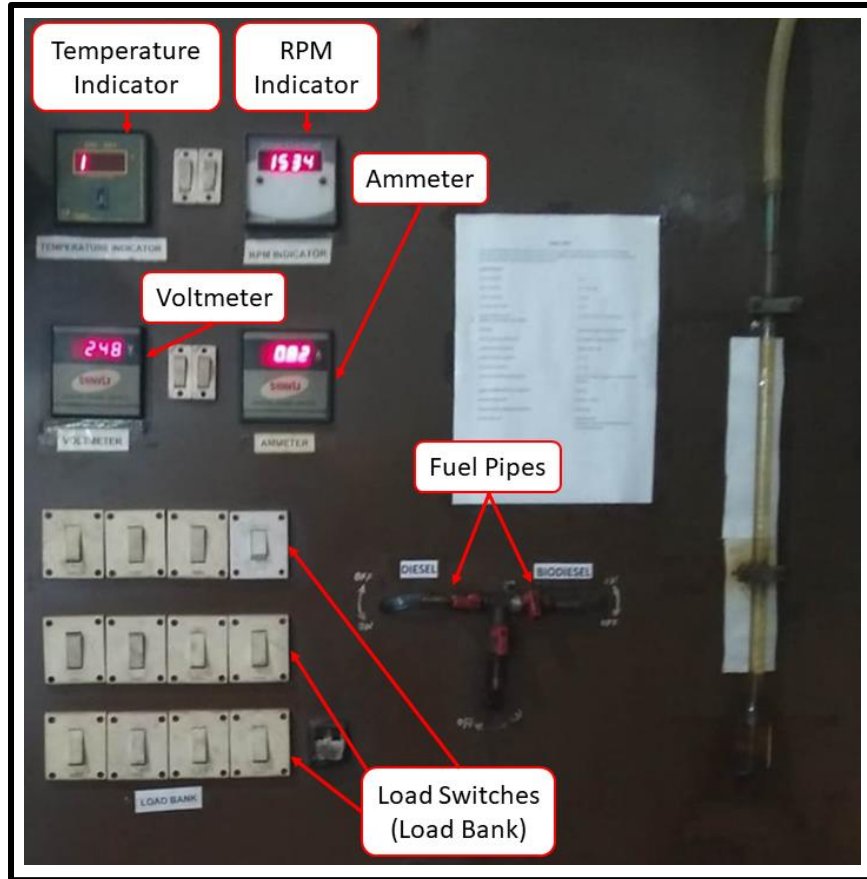


Figure 3.14: Control Panel of the Engine (Kirloskar Diesel Engine-DAF8)

Table 3.2: Specifications of the Engine

Make	Kirloskar
Model	DAF 8
Rated Brake Power (bhp/kW)	8 / 5.9
Rated Speed (rpm)	1500
Number of Cylinder	One
Bore X Stroke (mm)	87.5 x 110
Compression Ratio	17.5:1
Cooling System	Air Cooled
Lubrication System	Forced Feed
Cubic Capacity	0.78 Lit
Inlet Valve Open (Degree)	4.5 BTDC
Inlet Valve Closed (Degree)	35.5 ABDC
Exhaust Valve Open (Degree)	35.5 BBDC
Exhaust Valve Closed (Degree)	4.5 ATDC
Fuel Injection Timing (Degree)	26 BTDC

3.7. Smoke Analyser

A smoke analyser was used to measure the smoke opacity. Smoke opacity is the basis for the measurement of amount of smoke coming out from exhaust of a diesel engine. The degree to which, smoke of an engine blocks light is known as Opacity. High smoke opacity or in other words excessive smoke is increased with malfunctioned or poorly maintained engines. According to Indian Emission Regulation 2018, ARAI, smoke opacity test is only mandatory for diesel-powered vehicles. Figure 3.15 shows the smoke analyser used to analyse the smoke opacity while performing the experiments on engine.

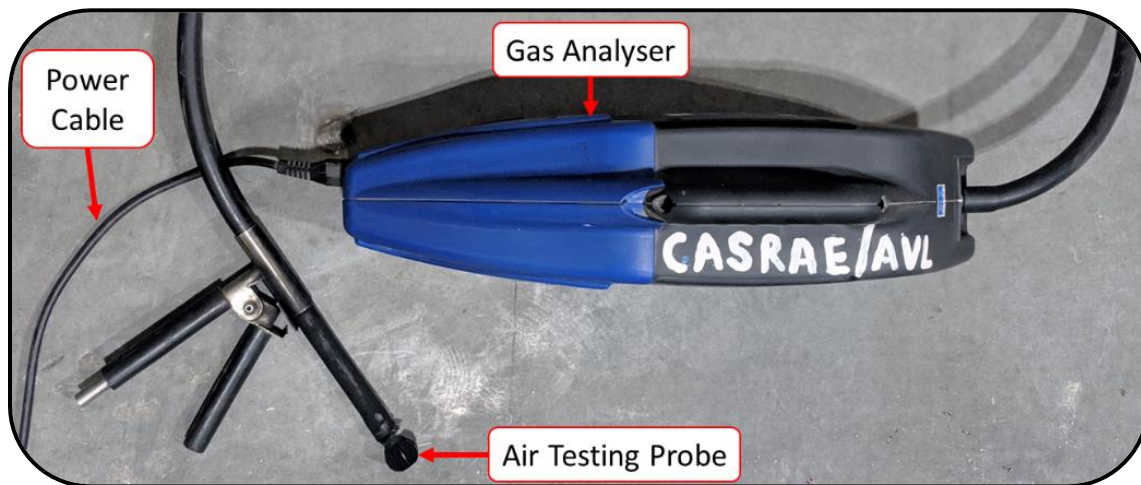


Figure 3.15: Smoke analyser used for analysing the smoke of the engine

3.8. Micro Hardness Test

Smith and Sandland in 1924 developed a hardness testing method known as the Vickers hardness test. This method calculates the hardness of material without being dependent on the size of the indenter used. Due to this, Vickers hardness test is the most versatile method for all the materials. In this hardness method, the SI unit of hardness obtained is expressed as the Vickers Pyramid Number (HV).

A Fischer made Fischerscope HM2000s was used to measure the micro hardness (Vicker Hardness Number) of various materials used in experimentation. This machine is capable of Nano indentation, which is why it was used for the measurement of the micro hardness in the experimentations.

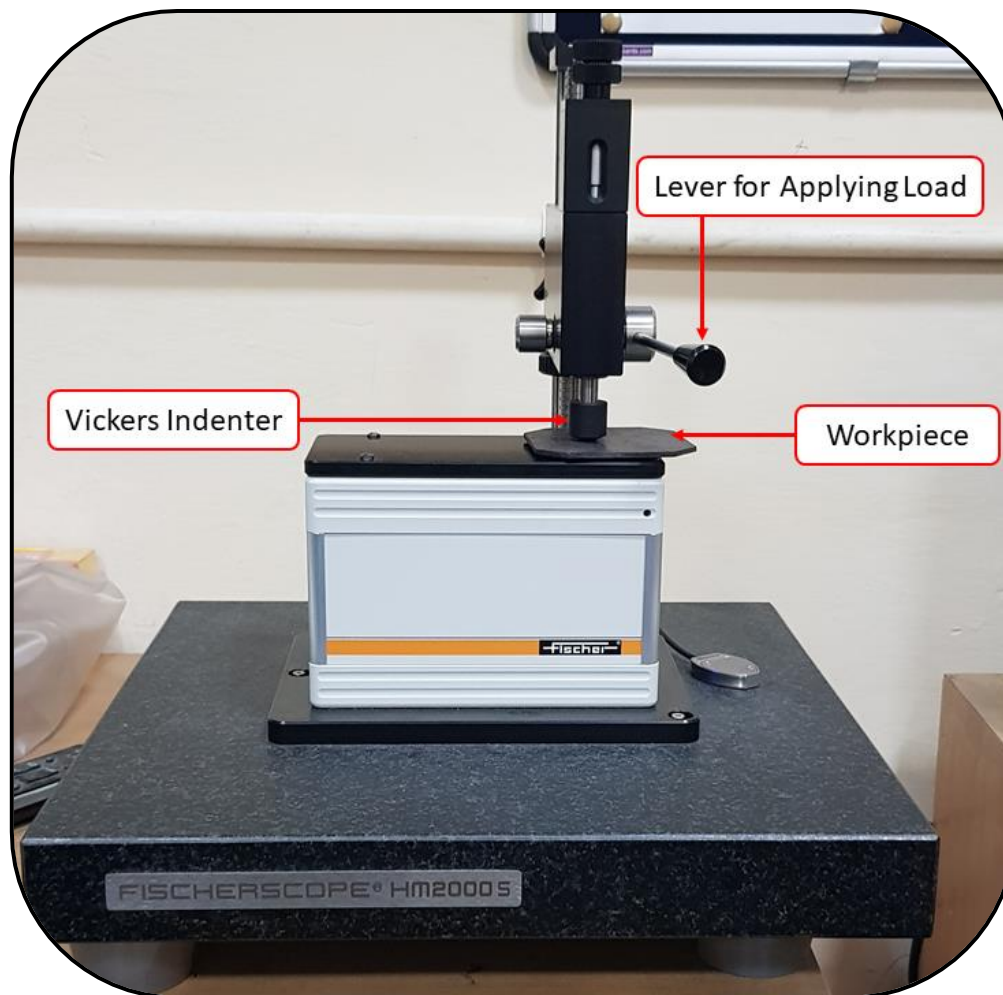


Figure 3.16: Image of Micro Hardness Measuring Device (Fischerscope HM2000s)

The ASTM E-384 standards (ASTM E-384 standards, (2017)) were followed while performing the hardness measurements on the materials used in experimentation. For the hardness test to be performed, the specimens were cleaned using acetone so that

accumulated dust particles are removed. The specimen was placed perpendicular to the indenter as can be seen in Figure 3.16. A diamond indenter of square pyramid shape was used to indent on the surface of test specimens at a load of 3000 mN for 20 seconds.

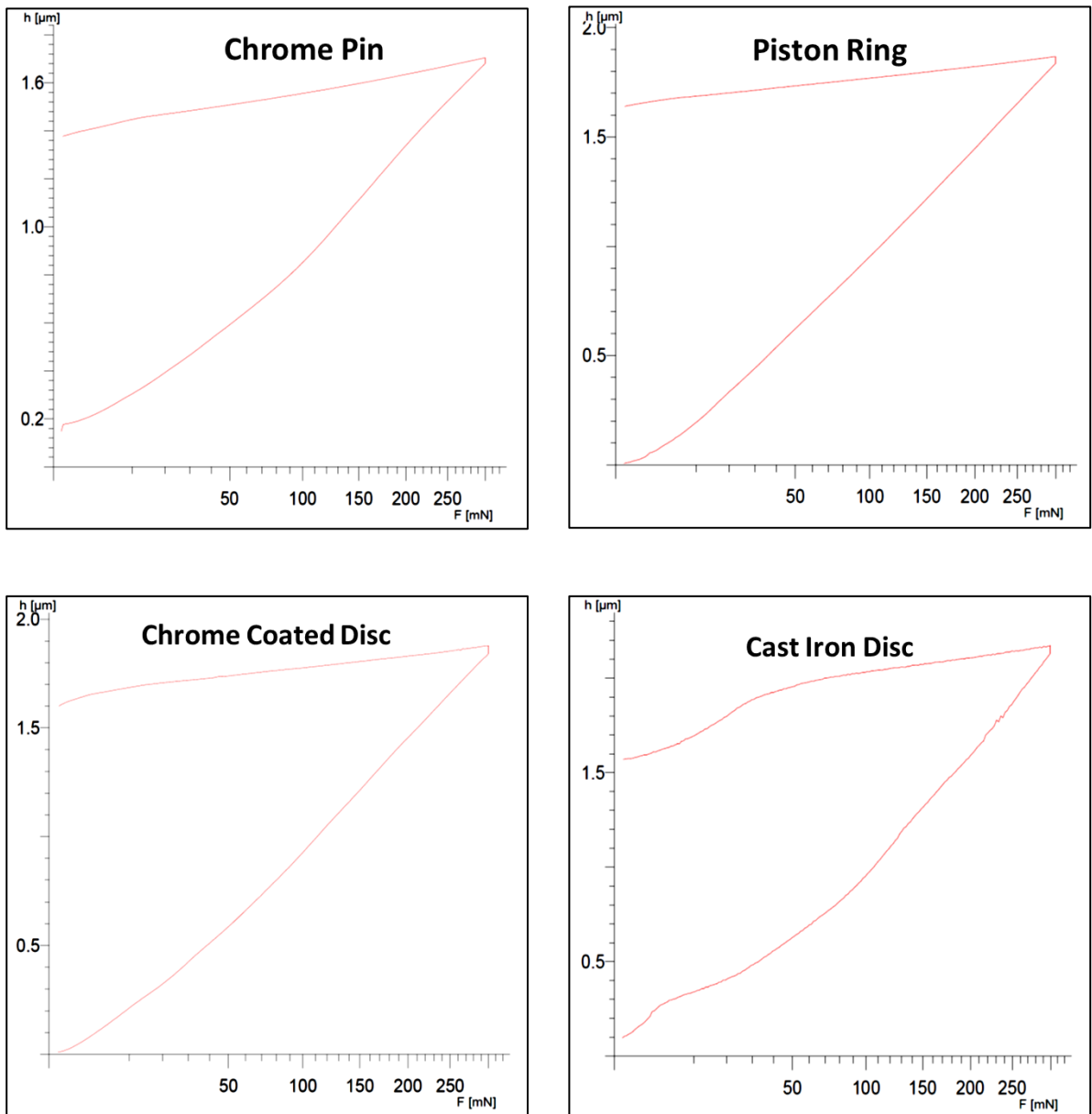


Figure 3.17: Loading Un-Loading graphs for the measurement of Vickers Hardness

In this work for the measurement of Vicker Hardness Number, each specimen was measured three times and then, the average value of the three was taken for the analysis and plotting the graphs. The average selected value of Vicker Hardness Number for Chrome Pin, Piston Ring, Chrome Coated Disc and Cast-Iron Disc is 457.15, 354.4, 351.91, and 273.82 respectively. The same has been listed in Table 3.3 and also have been plotted graphically in Figure 3.17 and Figure 3.18.

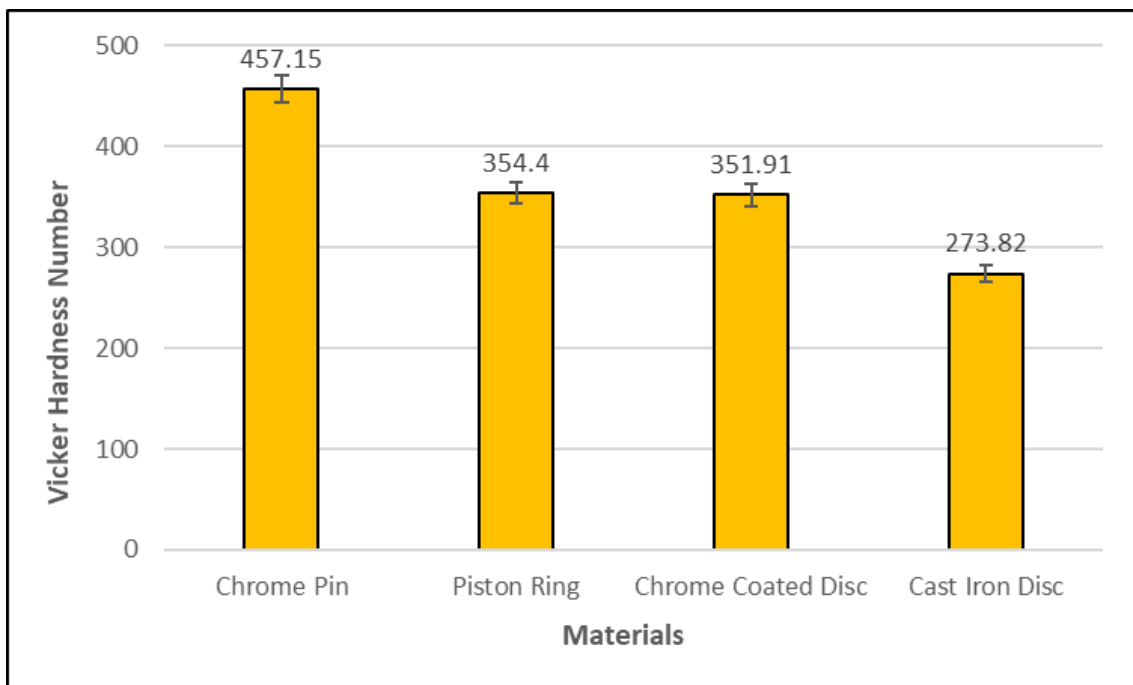


Figure 3.18: Vicker Hardness Number for materials used in experimentation

Table 3.3: Vickers hardness values for prepared specimens

Material	Hardness (HV)
Chrome Pin	457.15
Piston Ring	354.4
Chrome Coated Disc	351.91
Cast Iron Disc	273.82

3.9. Plan of Experimental Work:

The basics for experimentation work was decided after going through detailed literature review (chapter 2) from, which the parameters affecting the performances of an Engine were identified. It is noticed that friction and wear reduction in piston and piston ring system are vital task.

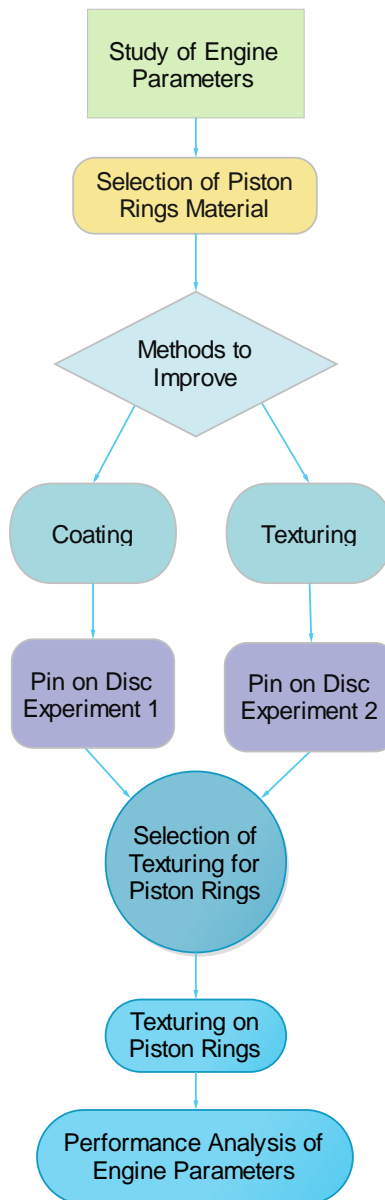


Figure 3.19: Flowchart of the Plan of Experimental Work

It was noticed that there was dearth of experimental studies toward exploring the tribo-dynamic behaviours of piston and piston ring system in situ condition under thin/mixed film lubrication. Hence, after selecting the piston ring material, two methods were selected to improve the tribological properties of piston and piston ring tribo system. Two experiments were conducted on Pin on Disc test rig, 1st with chrome coating and the 2nd with texturing. After analysing the results from both experiments textures for piston ring were selected, then the piston rings were textured using the laser. Finally, the performance of Engine is analysed using the textured piston ring. The sequence of experiments has been shown in Figure 3.19 with the help of a flow diagram.

3.10. 1st Experimentation on Pin on Disc

The specimens of the Cast Iron disc and Chromium coated Cast Iron disc of diameter 165 mm and thickness 8 mm were got manufactured as depicted in Figure 3.20, for conducting the experimental investigation. The surface finished discs attained the surface roughness level in the range 0.15 to 0.3 μm R.M.S. value. Surface roughness was measured by Telly Surf; 8 readings along the radial direction at interval of 45° and 8 readings perpendicular to it from middle of the stroke of Talysurf. A cylindrical steel pin with diameter 8 mm and length 70 mm was considered for testing the circular discs made of Cast Iron and Chromium-Coated Cast Iron. The face of the circular pin was levelled and checked by rubbing it against a soft paper for removing the debris if any. Face flatness was checked with the help of ink impression on paper. The pin was held rigidly 4 mm below the clamp for the test purpose on the disc to minimize bending and this distance was ignored while evaluating the tribological properties. Generally, the lubricating oil

(15W40) used in tropical regions was considered for the experimentation. The characteristics determined in the laboratory at 40°C and atmospheric pressure were (1) kinematic viscosity of 160.32 mm²/s as per ASTM D—445, (2) Density of 0.8744 g cm⁻³ as per ASTM D—4052 and (3) Specific gravity of 0.8752 as per ASTM D—287 (Singh et al., 2016).

The schematic diagram of friction and wear tester used in the present study is shown in Figure 3.1 and Figure 3.2. It has a motor which can rotate at varying speeds based on the rheostat position. The desired speed was selected between 200–2000 r.p.m. There is a horizontal fixture on which the specimen disc was bolted at 4 points along with the speed sensor and the probe for measurement of wear. Weights for loading were placed on the pan which has a horizontal platform to support it in the direction of gravity. Weight placed in the pan is transmitted through a bell-crank mechanism comprising uni-lever via wire and pulleys. A force detector probe attached to the side of the bell crank to measure the shear friction force. Specifications of friction and wear tester used in these experiments were: Pin diameter 8 mm of chrome steel; Disc (i) diameter 165 mm and thickness 8 mm made of cast iron and disc (ii) diameter 165 mm and thickness 8 mm made of the chrome-plated cast iron disc. According to the specifications of tribometer the range of speed varies between 200 to 2000 r.p.m and frictional force can be measured upto 200 N with the least count of 0.1 N and Accuracy of 0.1% ± 2% measured frictional force in Newton(N).

In this experimental plan, the analysis has been designed in such a manner that each factor was analysed independently. Implementation of this plan showed significant

reduction in the execution time needed for conducting the experiment. It was very efficient in investigating the effects of multiple performance factors and also to study the effect of individual factors. The experiment was performed in Tribology Lab, Delhi Technological University, Delhi. The pressure was varied between 1.95 MPa to 3.1 MPa and pin used for the same was 8 mm in diameter and 70 mm in length as shown in Figure 3.21. Parameters were selected on the basis of preliminary investigations and 27 experiments were performed on each disc. The tribological study was carried out for the loads represented by pressure varying from 1.95 MPa to 1.4 MPa, at varying sliding speeds 2-10 m s⁻¹ (equivalent to 200-2000 rpm) and distances traversed by the pin between 1000 m to 5000 m as per the experimental plan.

3.10.1. Disc and Pin Specimens for 1st Experiment of Pin on Disc



Figure 3.20: Chrome Coated Cast Iron Disc

Pin used for the experimentation was 8 mm in diameter and 70 mm in length as shown in Figures 3.21 and as mention above coated cast iron disc of diameter 165 mm and thickness 8 mm were used and can be seen in Figure 3.20.

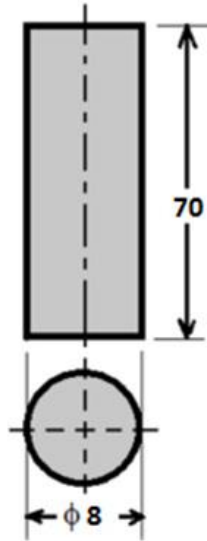


Figure 3.21: Chrome Steel Pin

3.11. 2nd Experimentation on Pin on Disc:

Based on the literature review (chapter 2), it is noticed that friction and wear reduction in piston and piston ring system are a vital task. It has also been noticed that there is dearth of experimental studies towards exploring the tribo-dynamic behaviours of piston and piston ring system in situ condition under thin/mixed film lubrication. Hence, the objective of this experimentation was to present the experimental tribodynamic findings of fully flooded contacts of chrome steel pin and cast iron/textured cast iron discs in situ condition for highlighting the possibility of manufacturing of textured piston rings.

The lubricating oil used was 15W40. This oil was considered for the experiment because it is generally used in our tropical regions. The characteristics of this lubricating oil were determined at 40°C in the laboratory. They were:

- 1) As per ASTM D – 445, kinematic viscosity = 160.32 mm²/sec
- 2) As per ASTM D – 4052, density = 0.8744 g/cm³ and
- 3) As per ASTM D – 287, Specific gravity = 0.8752

The common data for all experiments have been mentioned below along with the results and discussion:

- The varying speed ranged between 1000 r. p. m. and 5000 r. p. m. at various diameters of the disc, the value of loads applied in terms of the pressure were 1.95, 2.5 and 3.1 MPa.
- The sliding speed was taken as 2 m/s, 6 m/s and 10 m/s.
- The pin used is made of chrome steel, with the dimensions as 8 mm diameter and axis 70 mm long.
- The disc material with the specification is:
 - Plain surface cast iron disc, diameter = 165 mm and thickness = 8 mm.
 - Textured surface cast iron disc, diameter = 165 mm and thickness = 8 mm.
- The lubricating oil used is 15W40 and Weighing Machine used has a least count 0.0001gm.

3.11.1. Disc and Pin Specimens for 2nd Experiment of Pin on Disc

The specimens of a plain surface cast iron and textured surface cast iron discs having diameter 165 mm and thickness 8 mm, shown in Figure 3.22, were got

manufactured by casting process for experimentation. Surfaces of both the discs were finished with the help of belt emery paper. The surface finish was measured by a surface roughness measuring Instrument Talysurf. The measurement was taken at an interval of 45° in the radial direction, and 8 readings perpendicular to it. Obtained roughness value in terms of R.M.S. was 0.15 to 0.3 μm .

On one of the cast iron discs, the circular texture was formed by the laser texturing process. Stereo Zoom Microscope was employed for measuring the diameter of circular texture. The average diameter of circular texture was found to be 0.5965 mm \approx 0.6 mm, and it was calculated that the 65%-disc surface was textured and can be seen in Figure 3.24. Surface images of the plane surface cast iron disc taken with microscope are shown in Figure 3.25.

Descriptions Chrome Steel Pin:

A cylindrical Pin of Chrome steel, 8 mm diameter and an axis 70 mm, was used in testing on specimens of plain surface and textured surface cast iron discs, reference Figure 3.23. The face of cylindrical pin levelled and debris removed from the face of the pin by rubbing it on the soft paper. The surface plate was used to check the flatness of the pin face. The part of pin length was held rigidly in the clamp, and 4 mm length of the pin was protruding out of the fixture. This ensures that during the test part of the pin outside the clamp did not bend.

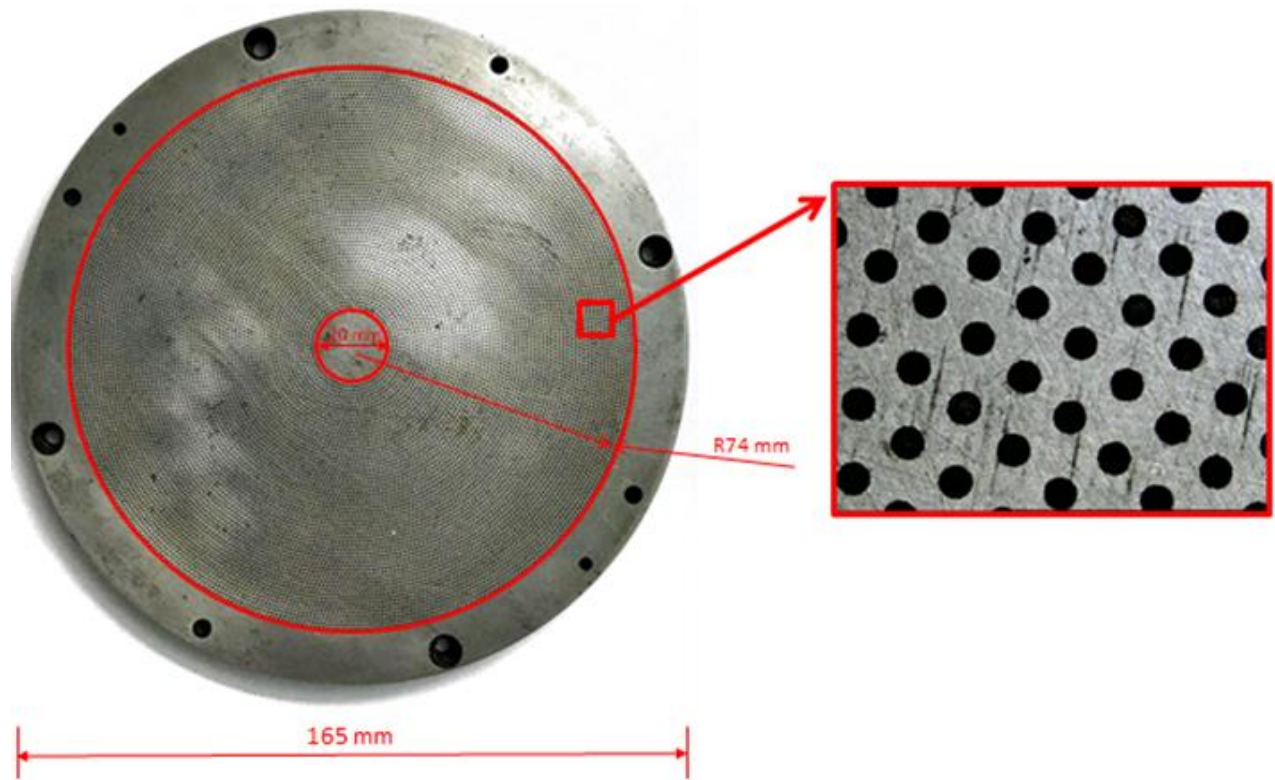


Figure 3.22: Textured Surface Cast Iron Disc used in Experimentation

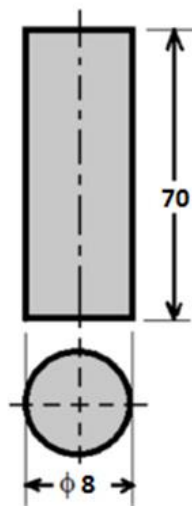


Figure 3.23: Chrome Steel Pin

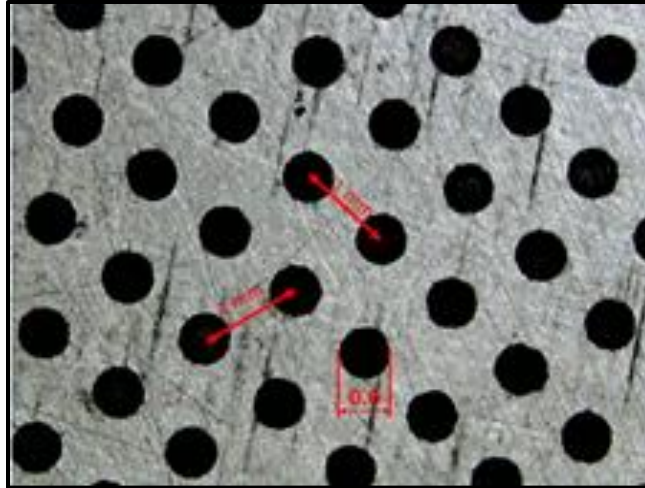


Figure 3.24: Surface images of textured surface cast iron disc with 35X zoom

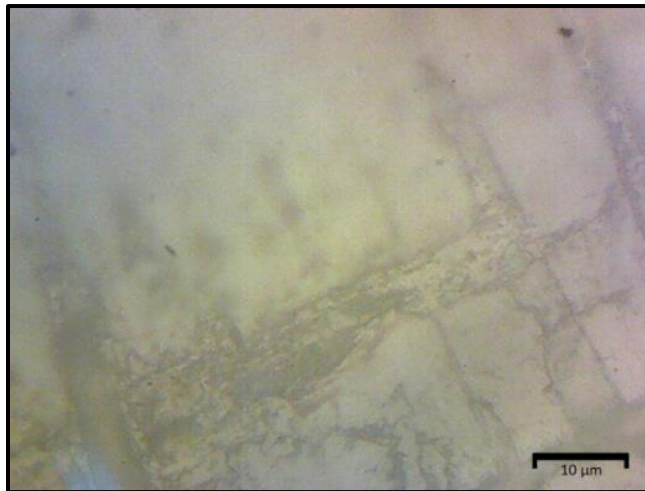


Figure 3.25: Microscopic images of the plain (smooth) surface of cast iron disc

3.12. Preparation of Biodiesel

Figure 3.26 shows all the steps involved in production of biodiesel. To prepare biodiesel, firstly the potassium hydroxide is mixed to methyl alcohol to form a solution. Then the oil is heated in a separate vessel at 100 degree Celsius to remove moisture. Then the oil is cooled to 60°C, then potassium hydroxide and methanol solution are mixed into the oil and the reaction mixture is stirred for more than one hour until separation of

glycerine starts which, can be seen in Figure 3.27. When separation of glycerol starts then stirring is stopped and the reaction mixture is transferred to a separating funnel. The reaction mixture is separated into the methyl esters in the upper layer and the glycerol in the lower layer. The methyl esters are water washed three times with warm distilled water to remove traces of unreacted chemicals. This water washing of biodiesel is shown in Figure 3.28. The final product obtained is biodiesel. Table 3.4 is depicting the properties of Diesel and Biodiesel used in the experimentations.

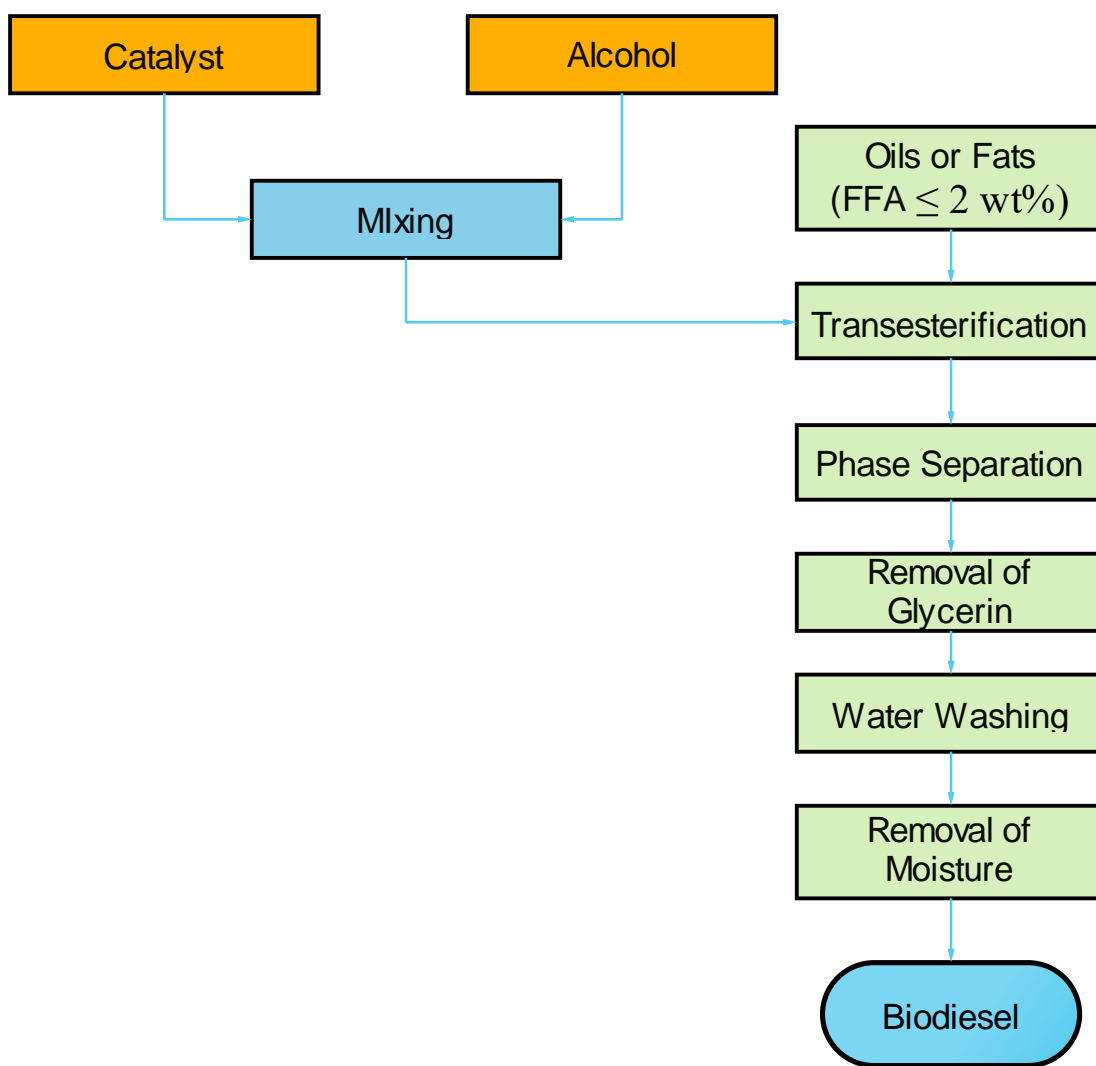


Figure 3.26: Flow chart of Biodiesel preparation



Figure 3.27: Separation of glycerine and biodiesel **Figure 3.28:** Water washing of biodiesel

Table 3.4: Properties of Diesel and Biodiesel

	Diesel	Biodiesel
Density (ρ) Diesel =	0.82215 g/cm ³	0.88634 g/cm ³
Specific Gravity =	0.8229	0.8871
Kinematic Viscosity		
Time =	108 sec	189 sec
v =	kxt	kxt
Where,		
k =	0.02672 mm ² /sec ²	0.02672 mm ² /sec ²
v =	0.02672 × 108	0.02672 × 189
=	2.88576 mm ² /sec	5.05 mm ² /sec
Calorific Value (CV)		
Weight of sample =	0.73130 gm	0.71332 gm
CV =	10961.204 cal/gm	9280.415 cal/gm
CV =	45.8178 MJ/kg	38.829 MJ/kg

3.13. Design of Texturing on Piston Ring

As discussed in section 3.5, the texturing on piston ring was done with the help of a laser machine which was also shown in Figure 3.12. Figure 3.29 shows the 3D rendered image of laser textured piston ring. The textures cover 7.91% area of piston ring. The calculations for the same have been done and shown in equation no. 3.1.



Figure 3.29: 3D rendered image of laser textured piston ring

Calculations:

$$\begin{aligned}
 \text{Pitch} &= 1 \text{ mm (average)} \\
 \text{Curved Surface Area} &= \pi Dt \\
 \text{Where,} \\
 D &= \text{Diameter of Piston Ring} \\
 t &= \text{Thickness of the Piston Ring} \\
 \\
 \text{Surface Area of Piston Ring} &= \pi Dt \\
 &= \pi \times 87 \times 2.3 \\
 &= 628.63 \text{ mm}^2 \\
 \\
 \text{No. of Dimples (n)} &= 396 \\
 \text{Average Diameter of Dimple} &= 0.4 \text{ mm} \\
 \text{textured area (total area of all the dimples)} &= n \times \left(\frac{\pi}{4} d^2\right) = 49.76 \text{ mm}^2 \\
 \\
 \% \text{ area under textures} &= \frac{49.76}{628.63} = 7.91\% \quad \dots(3.1)
 \end{aligned}$$

3.14. Experimentation on Engine

As shown in Figure 3.13 and discussed in section 3.6, a Kirloskar make diesel engine (DAF8) was used to perform the experimental research work. The engine was fitted with normal piston rings and was run with the constant RPM of 1500 along with a compression ratio of 18:1. Then, first set of experiments were performed using diesel as a fuel, experiments were performed talking load as 0KW, 0.5KW, 1KW, 1.5KW, 2.0KW, 2.5KW, 3.0KW, 3.5KW, 4KW, 4.5KW, 5KW, and 5.5KW. Figure 3.14 shows the control panel of the engine which, was used to change the load. Then, the corresponding values of voltage (V), current (I), time for 10ml fuel consumption (sec) were recorded. Also, with the help of smoke analyser smoke opacity was measured and with gas analyser quantity of Carbon Monoxide (CO), Carbon Dioxide (CO₂), Hydrocarbon (HC) and Nitrogen Oxide (NO_x) were measured. This above experiment was repeated by using biodiesel. After completion of above experiments piston rings of the engine were replaced with laser textured piston rings and the experiments were repeated with both the fuels viz. diesel and biodiesel by using same parameters.

Chapter 4

Results and Discussion

4.1. Characterisation

The prepared pins and discs were examined for the compositions and microscopic structures with the help of a scan electron microscope. The specimen surfaces were cleaned with acetone. The prepared disc surfaces were textured using laser machining process. The SEM images obtained are shown in Figures 4.1 (a) and Figure 4.3. The elemental mapping of pin and disc material are also shown. The tests for obtaining the SEM images and elemental mapping images were performed at Nano Fabrication Research facility at IIT Delhi.

4.1.1. Disc Material

Scan electron microscopic images of disc material are shown in Figure 4.1 (a) along with the EDAX Spectra Images of element mapping of the disc material in Figure 4.1(b, c & d). The EDAX spectrum of pin material shown in Figure 4.2 shows the presence of Carbon, Silicon and Iron in the disc. Table 4.1 shows the chemical stoichiometric of the individual elements of disc material.

Figure 4.1 (a, b, c & d) shows a typical microstructural image of the cast iron disc and the corresponding elemental distribution maps, employing scanning electron microscope. Figure 4.2 and Table 4.1 shows the EDS spectrum, exhibiting the individual constituent elements in the cast iron disc, and the inset confirms the chemical composition of the individual elements.

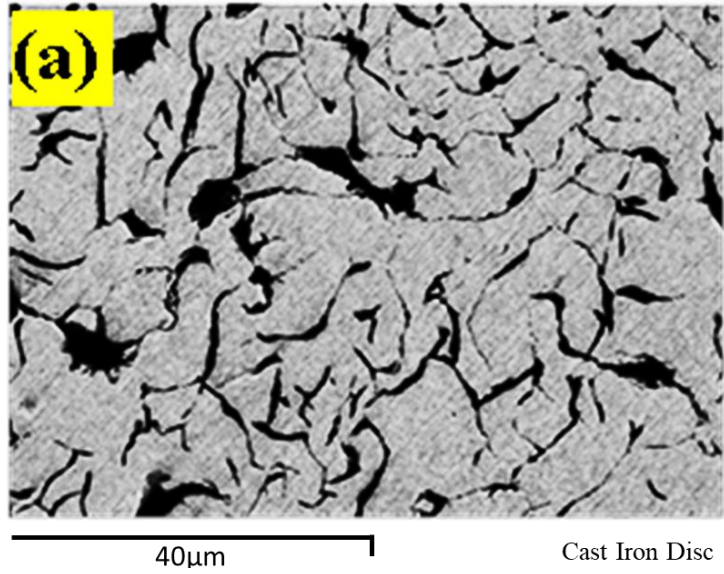


Figure 4.1 (a): SEM Image of the Disc

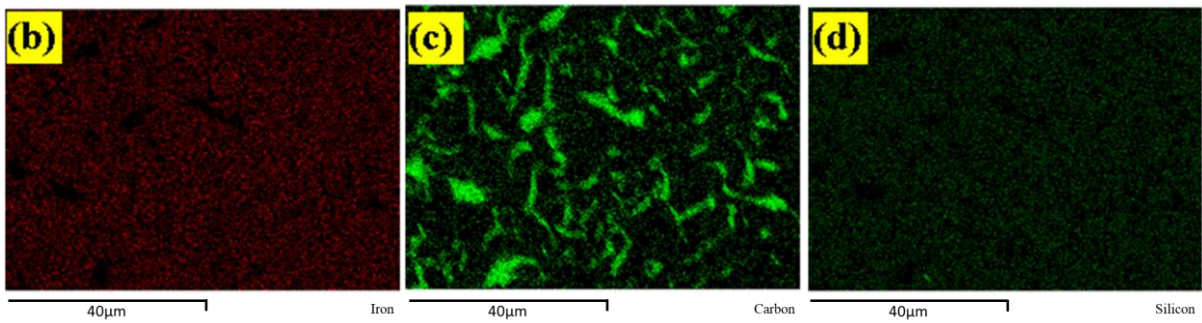


Figure 4.1 (b), (c) & (d): EDAX spectra image of Elemental Mapping of the Disc

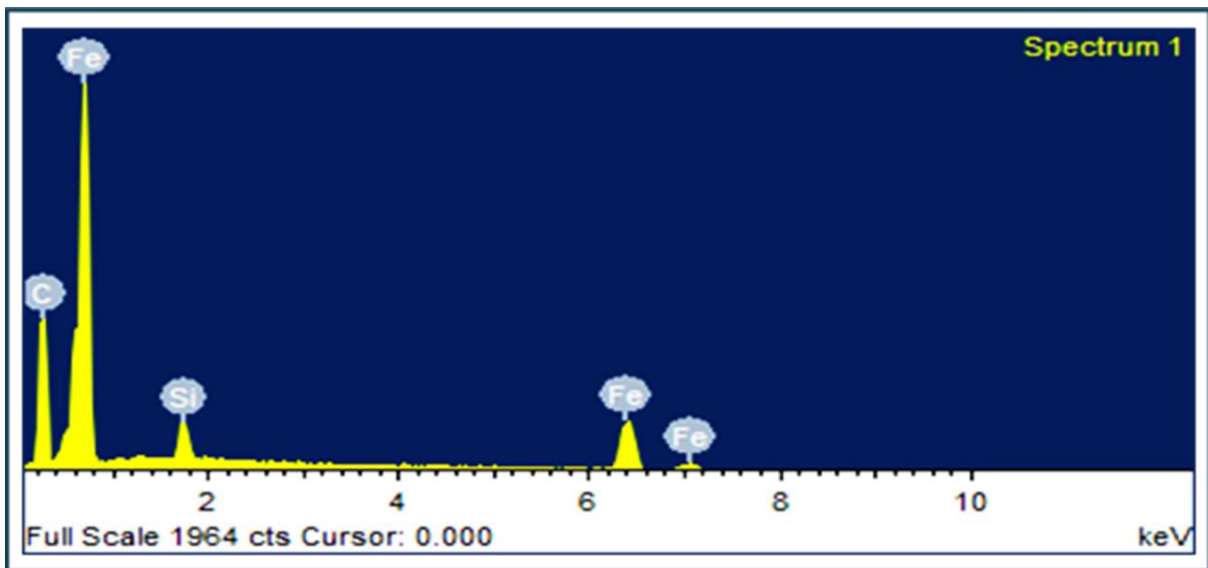


Figure 4.2: EDS spectrum showing the elements of C, Fe and Si presence in the Disc

Table 4.1: The chemical stoichiometric of the individual elements of Disc Material

Element	Weight %	Atomic %
Iron	80.42	48.35
Carbon	17.66	49.35
Silicon	1.93	2.30

4.1.2. Pin Material

Scanning electron microscopic images of pin material are shown in Figure 4.3 along with the EDAX Spectra Images of element mapping of the pin material in Figure 4.4. The EDAX spectrum of pin material shown in Figure 4.5 shows the presence of Carbon, Oxygen, Silicon, Chromium and Iron in the Pin. Table 4.2 shows the chemical stoichiometric of the individual elements of pin material.

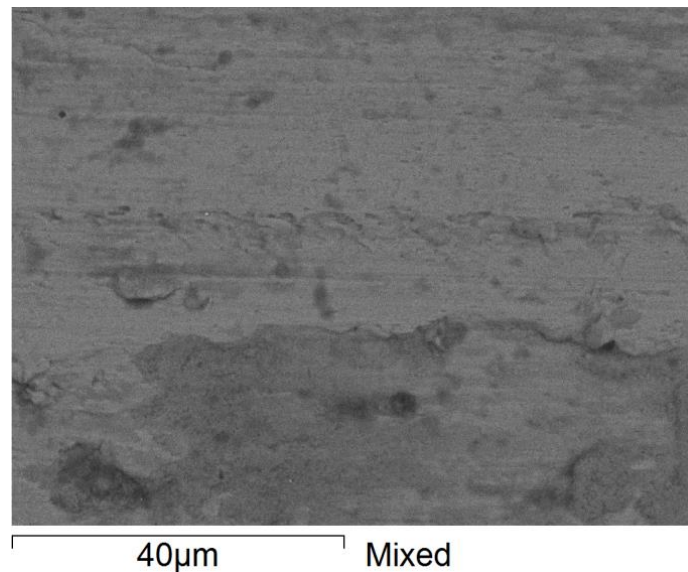


Figure 4.3: SEM image of Pin Material

Figure 4.3 and Figure 4.4 shows a microstructural image of the pin material and the corresponding elemental distribution maps, using scanning electron microscope. Figure 4.5 and Table 4.2 shows the EDS spectrum, depicting the

individual constituent elements in the pin material, and the inset confirms the chemical composition of the individual elements. The morphology and composition were analyzed for the cast iron disc-steel pin tribopair which was then subjected to tribological performance employing Pin-on-Disc Tribometer (Make: Ducom, India). The results obtained have been discussed in the following paragraphs.

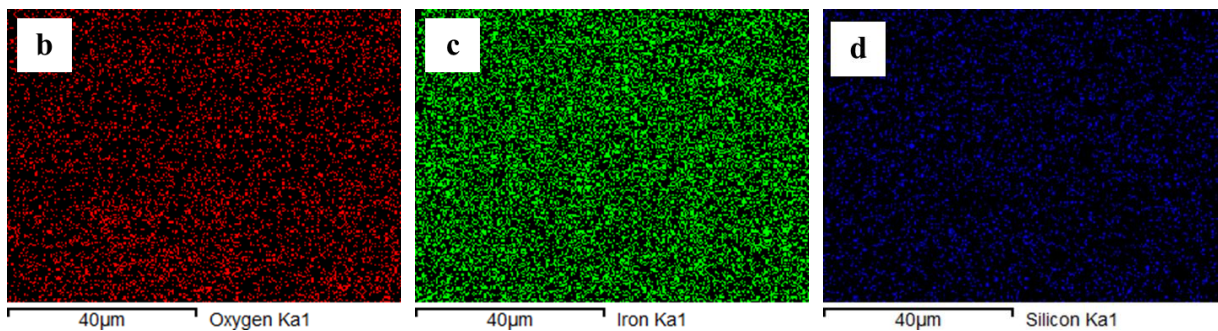


Figure 4.4 (b, c, d): EDAX Spectra Image of element mapping of the Pin Material

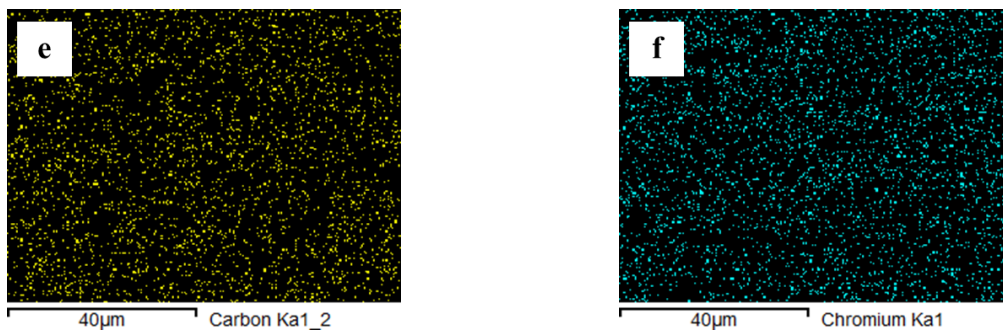


Figure 4.4 (e, f): EDAX Spectra Image of element mapping of the Pin Material

Note: SEM images & elemental maps of pin material; accumulator voltage: 15.0 kv; resolution: 256x192 pixels: resolution viewed: 100%; process time: 5; image width: 82.6 µm

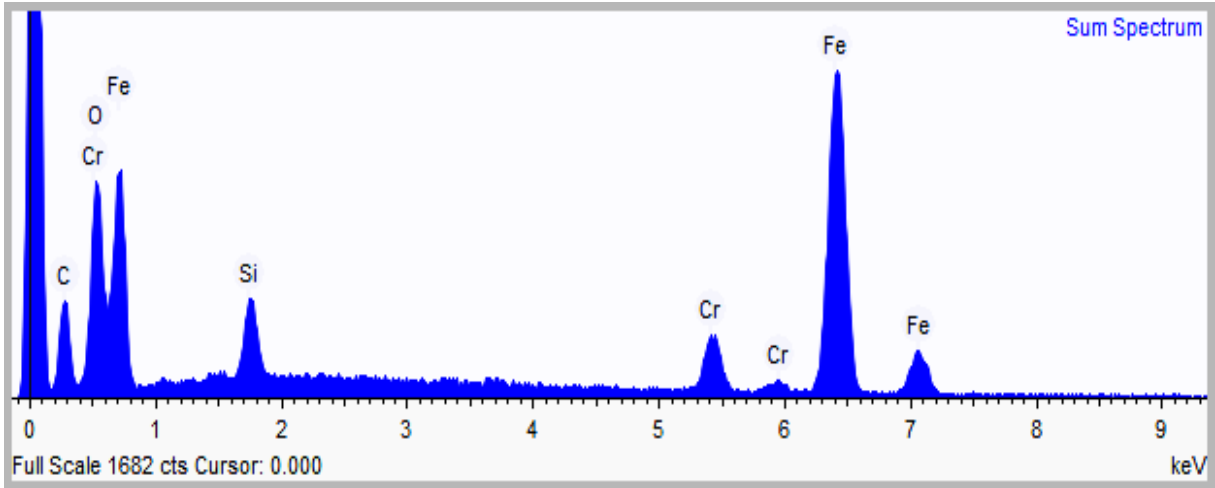


Figure 4.5: EDS spectrum showing the elements of C, O, Si, Cr and Fe presence in the Pin

Table 4.2: The chemical stoichiometric of the individual elements of Pin Material

Element	Weight %	Atomic %
Carbon	20.110	42.636
Oxygen	17.244	27.446
Silicon	2.597	2.354
Chromium	5.381	2.635
Iron	54.668	24.928

4.2. Plain & Chrome Plated Disc vs Steel Pin

The specimens of the Cast Iron disc and Chromium coated Cast Iron disc of diameter 165 mm and thickness 8 mm were manufactured as depicted in the Figure 1, for the conduction of experimental investigation. The surface finished discs attained the surface roughness level in the range 0.15 to 0.3 μm R.M.S. value. Surface roughness was measured by Talysurf; 8 readings along the radial direction at interval of 45° and 8 readings perpendicular to it from middle of the stroke of Talysurf. A cylindrical Steel pin with diameter 8 mm and length 70 mm was considered for testing

the circular discs made of Cast Iron and Chromium-Coated Cast Iron. The face of the circular pin was levelled and checked by rubbing it against a soft paper for removing the debris if any. Face flatness was checked with the help of ink impression on paper. Pin was held rigidly 4 mm below the clamp for the test purpose on the disc to minimize bending and this distance was ignored while evaluating the tribological properties. Generally, the lubricating oil (15W40) used in tropical regions was considered for the experimentation. The characteristics determine in the laboratory at 40°C and atmospheric pressure were (1) kinematic viscosity of 160.32 mm²/s as per ASTM D—445, (2) Density of 0.8744 g/cm³ as per ASTM D—4052 and (3) Specific gravity of 0.8752 as per ASTM D—287 (Singh et al., 2016).

4.2.1. Coefficient of Friction

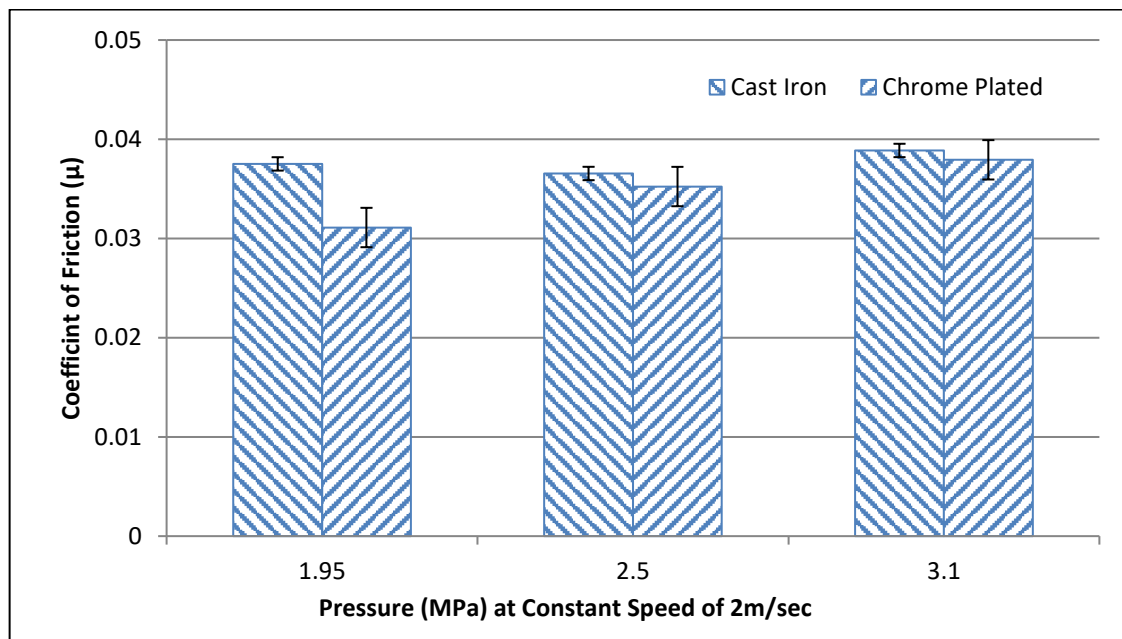


Figure 4.6: Coefficient of friction (μ) of cast iron and chromium plated cast iron against steel pin at a constant speed of 2m/s

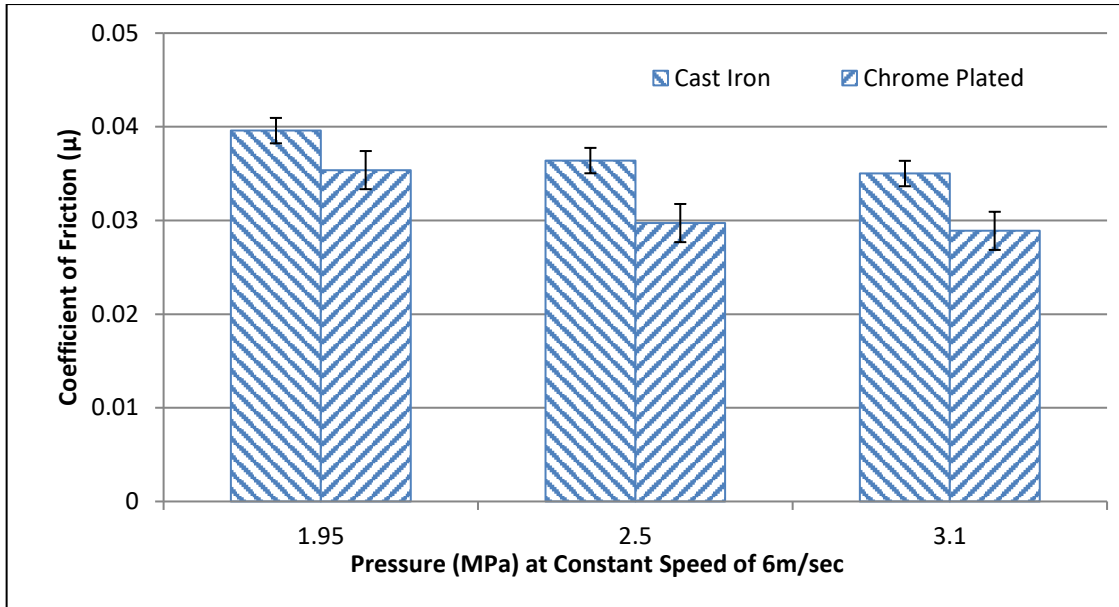


Figure 4.7: Coefficient of friction (μ) of cast iron and chromium plated cast iron against steel pin at a constant speed of 6m/s

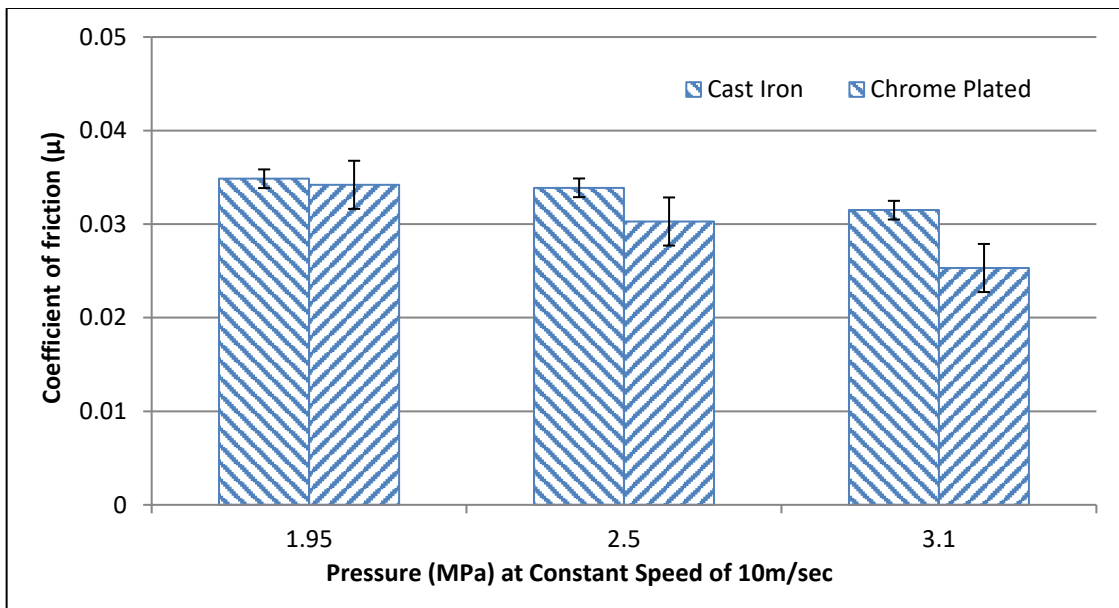


Figure 4.8: Coefficient of friction (μ) of cast iron and chromium plated cast iron against steel pin at a constant speed of 10m/s

The trend of the coefficient of friction (μ) versus pressure (MPa) considering sliding speed of 2m/s, 6m/s & 10m/s has been plotted in Figure 4.6, 4.7, 4.8

respectively for the pressure ranging between 1.95 MPa – 3.1 MPa for flooded lubrication. Chromium plated disc shows improvement in the tribological parameters immensely in comparison to the cast iron disc. Experiments were performed by varying the distance between 1000 m to 5000 m at the same pressure range and in the presence of same lubricating oil (SAE 15W40). The coefficient of friction as in Figures 4.6, 4.7 & 4.8 was observed 0.02–0.04 between the steel pin and the cast-iron disc, that the plain cast iron disc had the maximum value of the coefficient of friction i.e. 0.04. Under the same corresponding conditions, Chromium Plated cast iron disc had a coefficient of friction as 0.025–0.035. It was observed that the coefficient of friction continuously decreased with an increase in pressure and attained the least value of the coefficient of friction 0.025, at the pressure of 3.1 MPa. So, the hard surface in relative motion had a low coefficient of friction in fully flooded condition.

4.2.2. Wear

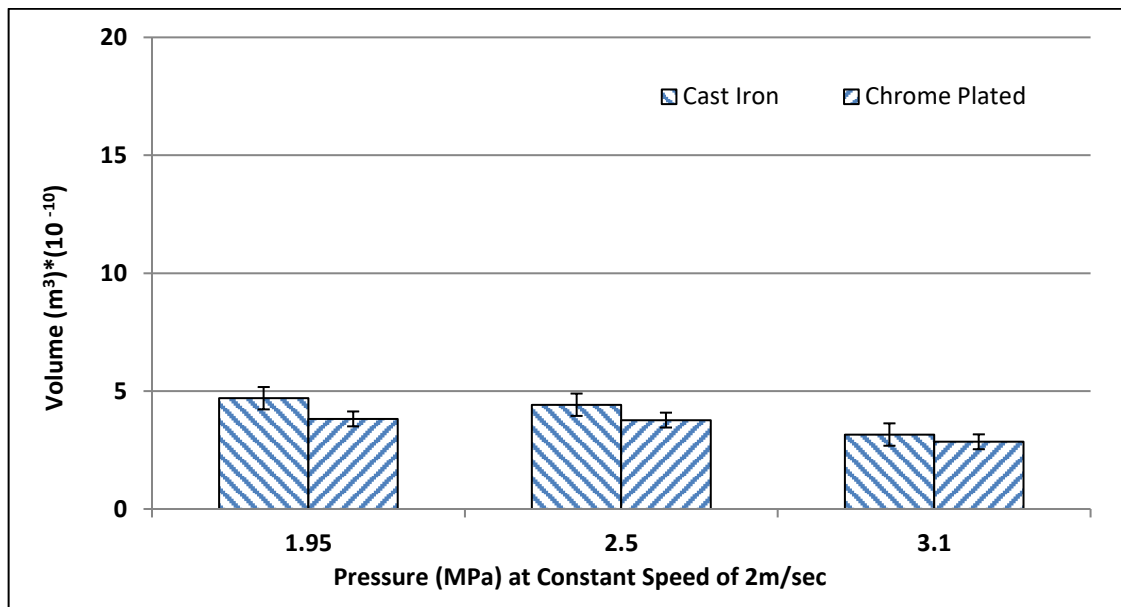


Figure 4.9: Wear of cast iron and chromium plated cast iron against steel pin at a constant speed of 2m/s

Wear characteristics are shown in Figure 4.9, 4.10 & 4.11, where initially fast growth in wear was observed at the start due to solid contact, the interlocking of asperity and as tribopair had relative motion, breaking of the asperity took place as shown in Figure 4.12. The variation of wear with different pressure values under the condition of fully flooded lubrication was displayed in Figure 4.9, 4.10 & 4.11. A decrease in wear rate was observed as the pressure increased. This phenomenon was governed by thin layer mixed and elasto hydrodynamic lubrication. Under contact stresses, a very thin film of lubricating oil formed that separate the contact surfaces. It resulted in elasto hydrodynamic lubrication. This resulted in reduction of friction and wear. Wear pattern on the pin material was shown in Figure 4.12(a). The initial increase in wear occurred due to the abrasion wear owing to the highly strained fragments in between the contact surfaces and later decrease was due to the diffusion of surface debris which was insignificant in comparison to the abrasion wear.

The decrease in wear was also due to the formation of thin layer of lubricant at the interface of the discs and pin. This resulted into thin layer mixed lubrication processes. In experiment, the various values of distances were taken from 1000–5000 μ m for the disc with predefined diameter against varying pressure values i.e. 1.95 MPa, 2.5 MPa, and 3.1 MPa. Under fully flooded lubrication, the wear increased from $1 \times 10^{-10} \text{ m}^3$ to $15 \times 10^{-10} \text{ m}^3$, was due to thin layer mixed and elasto hydrodynamic lubrication. Hence, it was inferred that the pin material wears more as the pressure is increased. Microscopic views as in Figure 4.12 and extended view as in Figure 4.13 depict the abrasive wear and ploughing took place in thin layer lubrication.

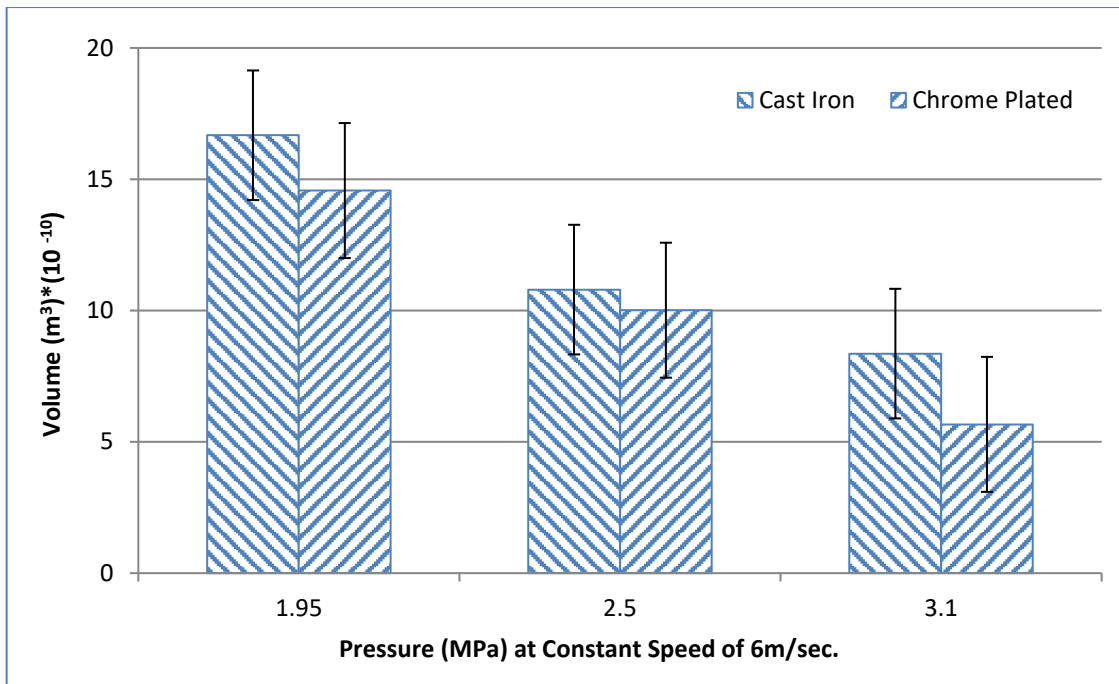


Figure 4.10: Wear of cast iron and chromium plated cast iron against steel pin at a constant speed of 6m/s

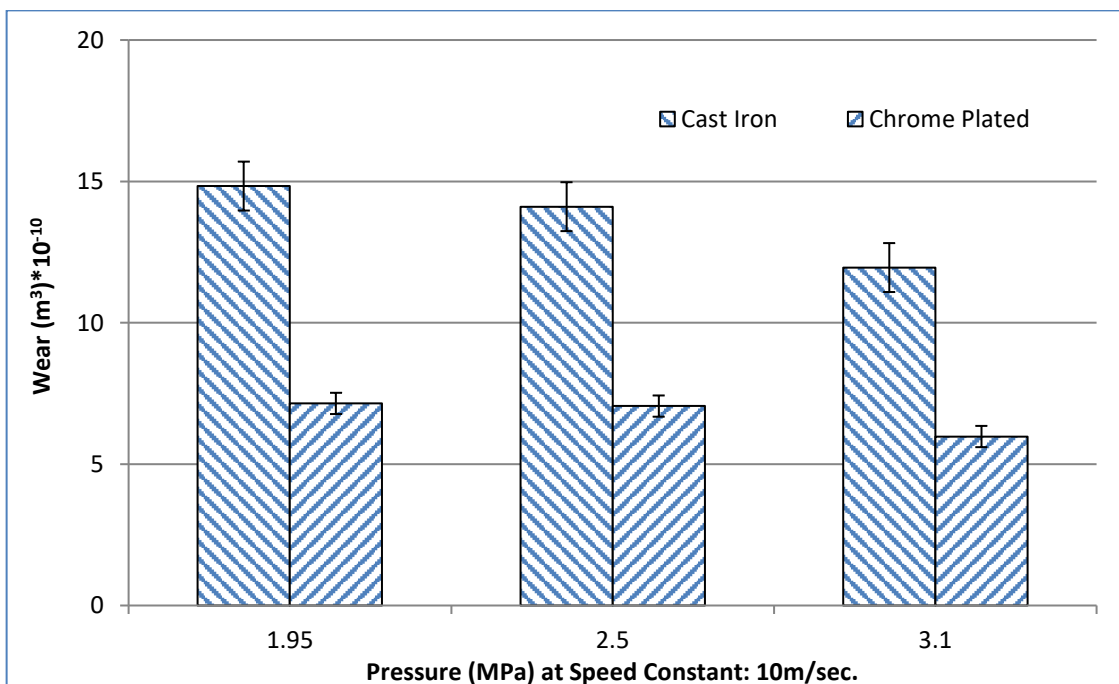


Figure 4.11: Wear of cast iron and chromium plated cast iron against steel pin at a constant speed of 10m/s

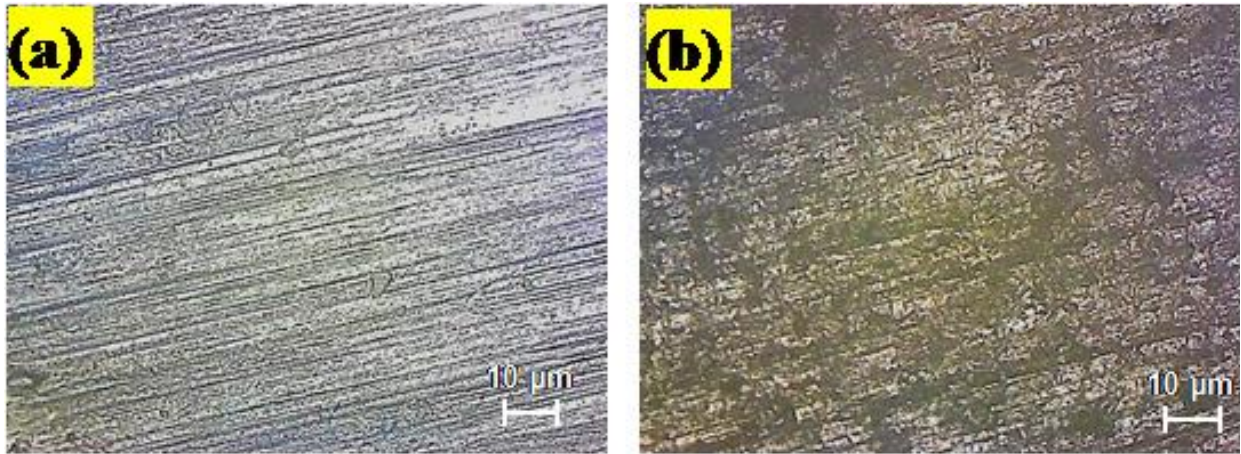


Figure 4.12: (a) Microscopic view of worn surface of pin and (b) Microscopic view of worn surface of cast iron disc.

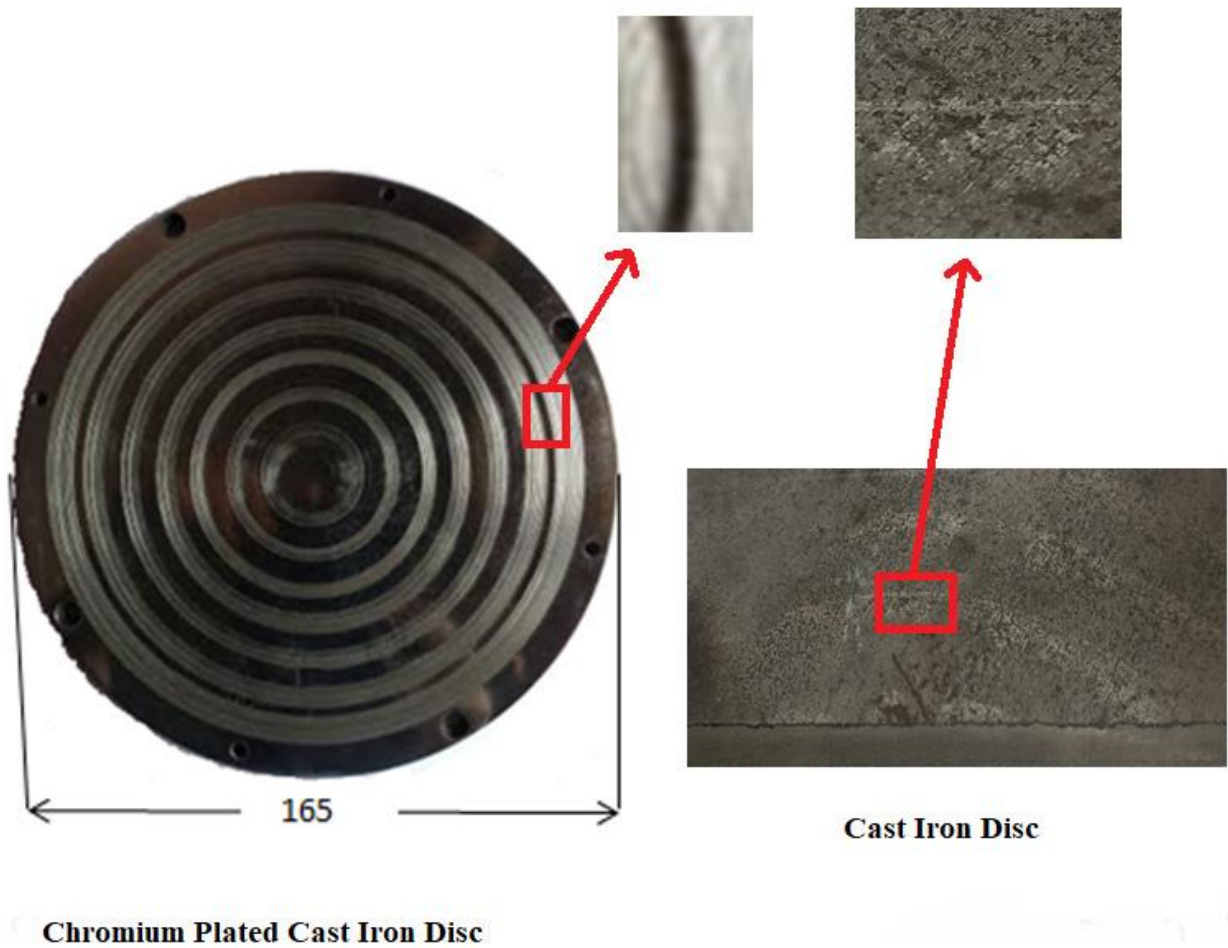


Figure 4.13: Dimensional details and extended view of worn surface tracks on disc

4.2.3. Vibrations Amplitude

Experiments were conducted taking various values of distances from 1000 m to 5000 m at different disc diameters and different pressure. It was observed that when lubrication was fully flooded, the vibration amplitude varied between 40 μm and 52 μm as shown in Figure 4.14, 4.15 & 4.16. It was due to the hydrodynamic lubrication.

As per Figure 4.14, 4.15 & 4.16, the amplitude of vibrations increases with the pressure at the considered values i.e. 1.95 MPa, 2.5 MPa, and 3.1 MPa. This was caused by excessive pressure at the interface of the tribopair. The vibrational values showed the experiment carried out was stable.

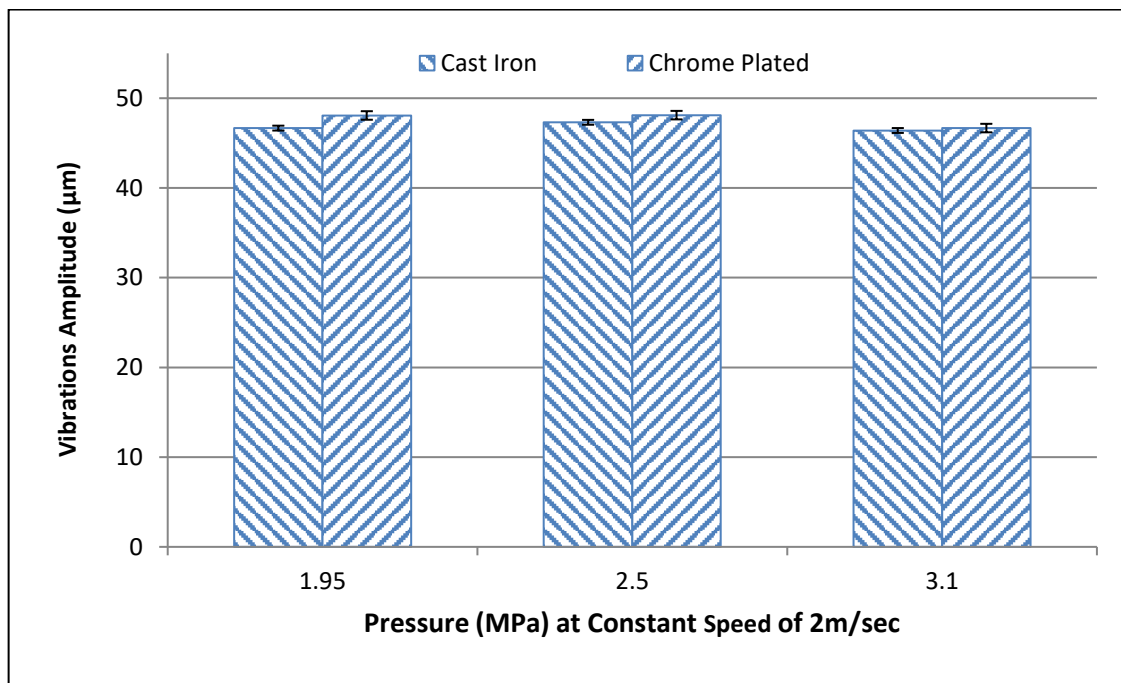


Figure 4.14: Vibration amplitude of cast iron and chromium plated cast iron against steel pin at constant speed of 2m/s

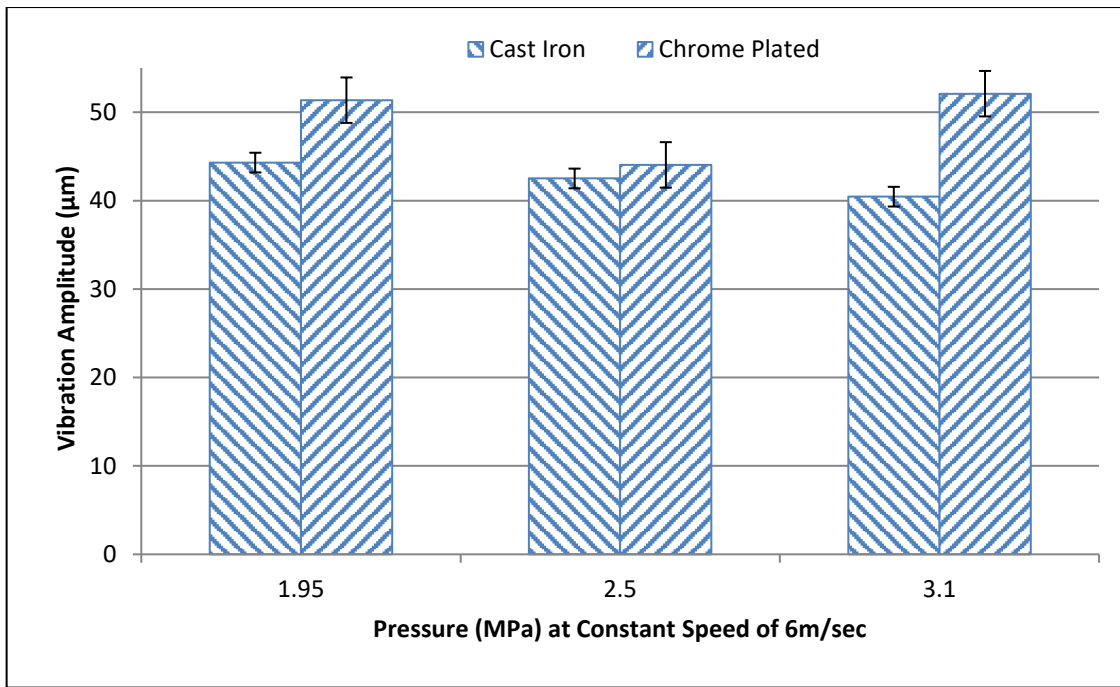


Figure 4.15: Vibration amplitude of cast iron and chromium plated cast iron against steel pin at constant speed of 6m/s

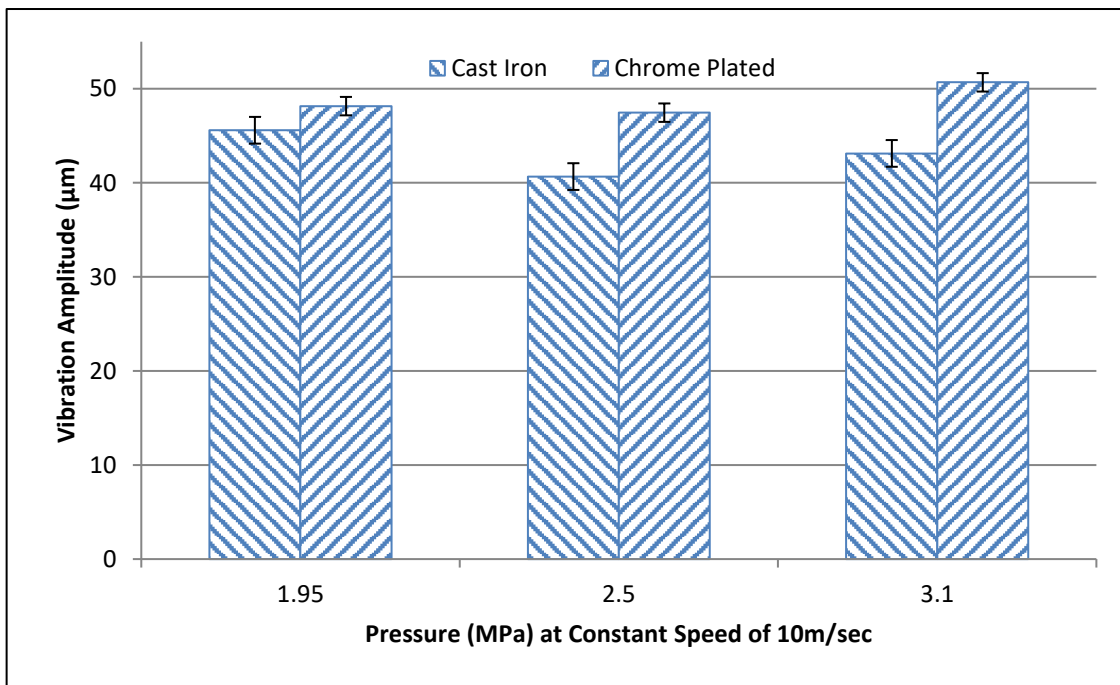


Figure 4.16: Vibration amplitude of cast iron and chromium plated cast iron against steel pin at constant speed of 10m/s

4.2.4. Temperature Rise

Continuous relative motion between two metals is the source of temperature and as the motion continues the temperature rises continuously. The rise in temperature was governed by the surface roughness of the materials in contact along with the mechanical properties of the materials of pin and disc. Experiments were conducted at varying distance travelled in the range of 1000–5000 m for different diameter of the disc with the pressure values as 1.95 MPa, 2.5 MPa and 3.1 MPa. Figure 4.17, 4.18 & 4.19 depicts the temperature rise at the interface of the tribopair and it varies between 4K and 9 K as measured by thermal image camera when lubricant was flowing continuously.

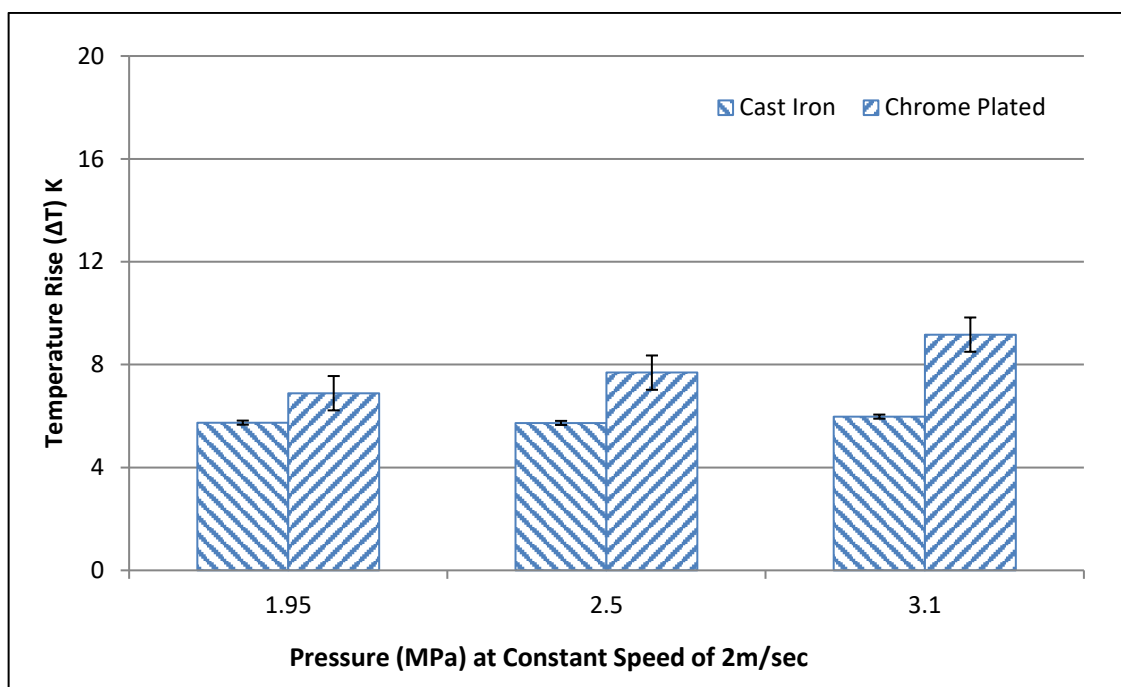


Figure 4.17: Temperature rise of cast iron and chromium plated cast iron against steel pin at constant speed of 2m/s

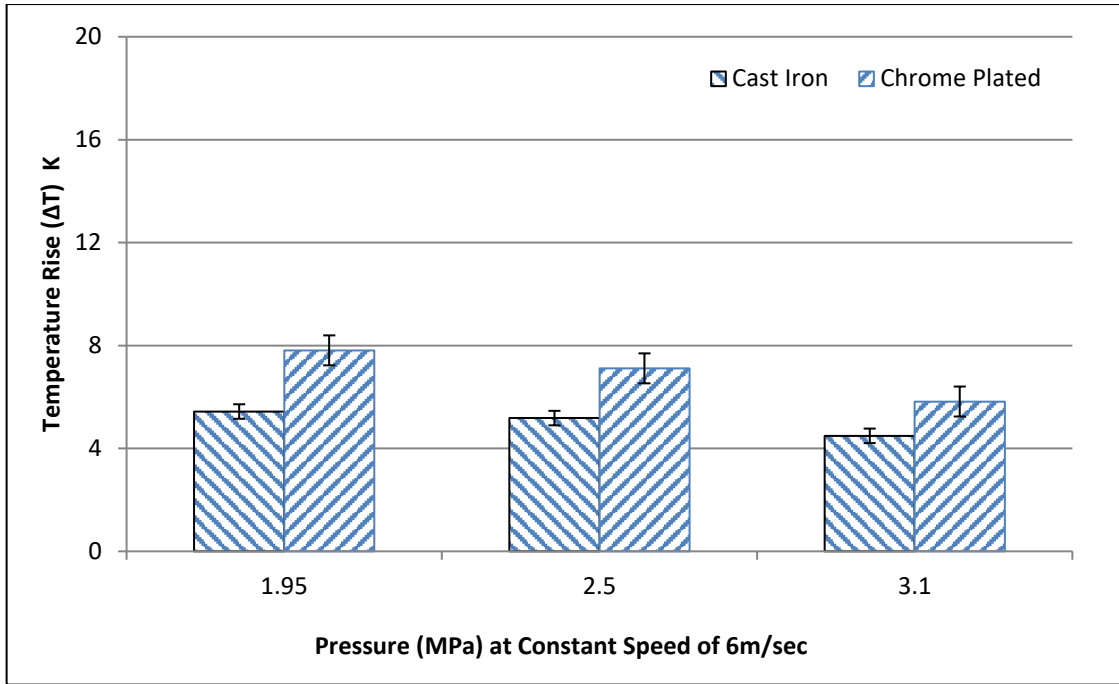


Figure 4.18: Temperature rise of cast iron and chromium plated cast iron against steel pin at constant speed of 6m/s

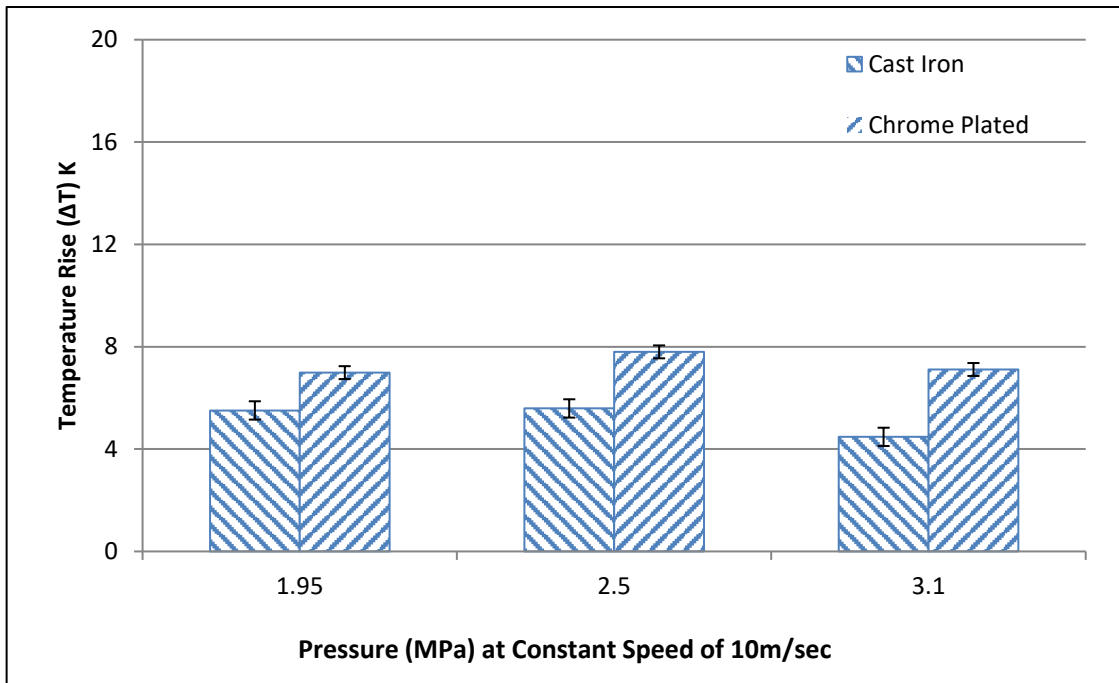


Figure 4.19: Temperature rise of cast iron and chromium plated cast iron against steel pin at constant speed of 10m/s

4.2.5. Sound

The rules of noise pollution, 2000, had set different acceptable limits depending upon the category i.e. day and night. For industries, it is 75 dB for the day and 70 dB for the night. Similarly, for residential areas, it is 55 dB for the day and 45 dB for the night. Figure 4.20, 4.21 & 4.22 shows the trend of sound as observed during the experimentation procedure. It was noted in the Figure 4.20, 4.21 & 4.22 that sound varies from 66.8 dB to 78 dB. High noise observed in the Chromium plated disc as compared to the cast iron disc. This was due to the property of cast iron of absorbing the energy or vibration experienced during the running conditions. At low speeds and for longer distance traversed it was ascertained that cast iron disc absorbed more energy and hence made less noise. The continuous flow of lubricant also acted as the medium of sound for the base material in motion with respect to pin material. The measuring instrument was the sound meter which was kept 0.25 m away from the pin and disc.

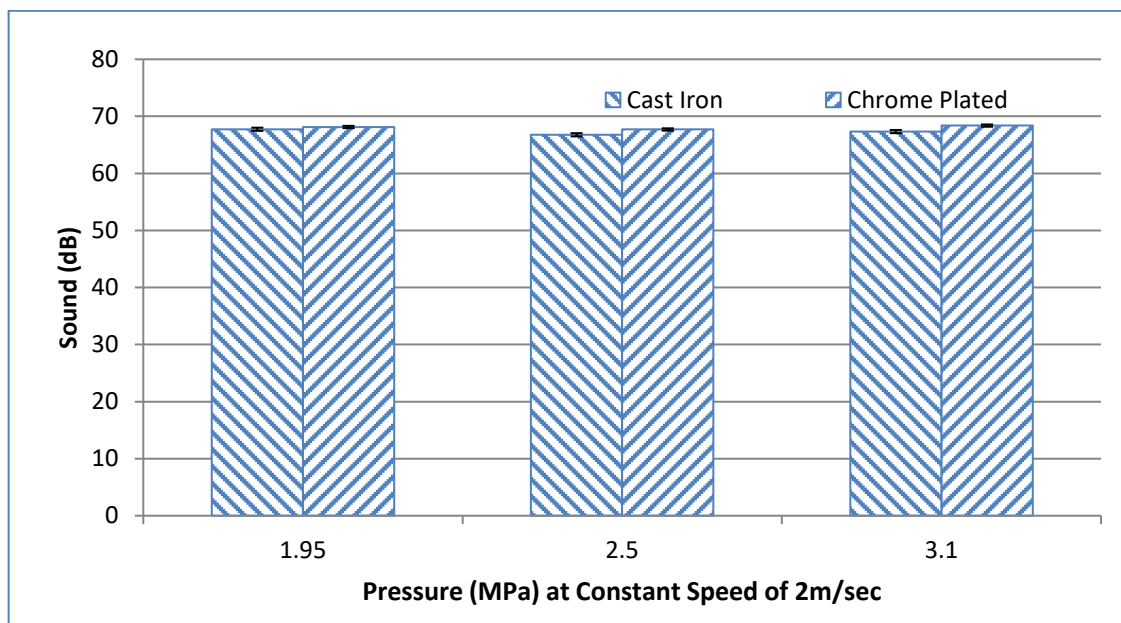


Figure 4.20: Sound of cast iron and chromium plated cast iron against steel pin at constant speed of 2m/s

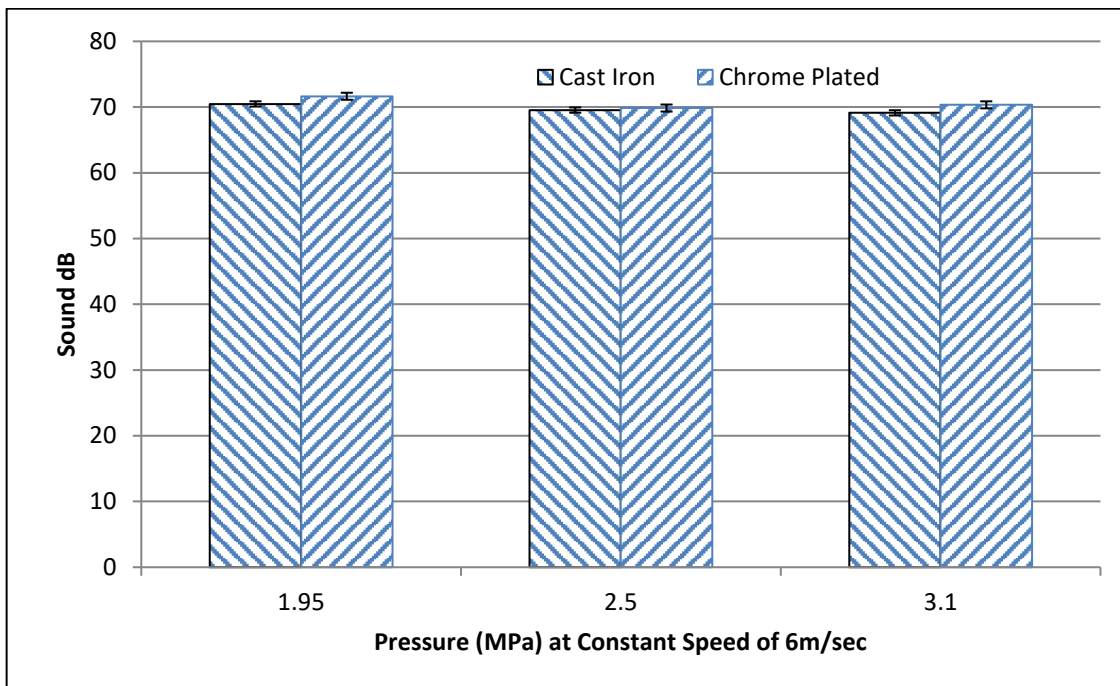


Figure 4.21: Sound of cast iron and chromium plated cast iron against steel pin at constant speed of 6m/s

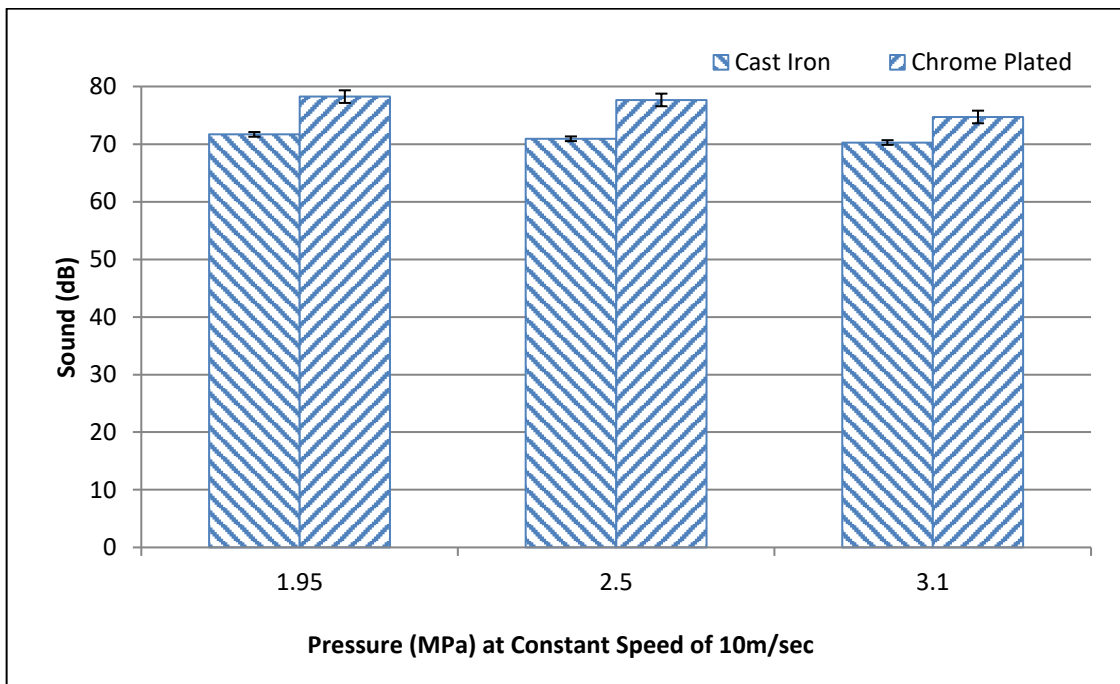


Figure 4.22: Sound of cast iron and chromium plated cast iron against steel pin at constant speed of 10m/s

4.3. Plain & Textured Cast Iron Disc vs Steel Pin

The specimens of the cast iron disc and laser textured cast iron disc of diameter 165 mm and thickness 8 mm were manufactured as depicted in the Figure 3.10, for the conduction of experimental investigation.

A cylindrical steel pin with diameter 8 mm and length 70 mm was considered for testing the circular discs made of cast iron and laser textured cast iron. The face of the circular pin was levelled and checked by rubbing it against a soft paper for removing the debris if any. Face flatness was checked with the help of ink impression on paper. The pin attained the surface roughness in the range 0.15 to 0.35 μm R.M.S. value. Surface roughness was measured by Talysurf; 3 readings along the radial direction at interval of 45° and 3 readings perpendicular to it from middle of the stroke of Talysurf. Pin was held rigidly 4 mm below the clamp for the test purpose on the disc to minimize bending and this distance was ignored while evaluating the tribological properties.

Generally, the lubricating oil (15W40) used in tropical regions was considered for the experimentation (Singh et al., 2016). Following are the characteristics determined in the laboratory at the temperature of 40°C and atmospheric pressure:

- (1) Kinematic viscosity of $160.32\text{ mm}^2/\text{s}$ as per ASTM D—445,
- (2) Density of 0.8744 g/cm^3 as per ASTM D—4052 and
- (3) Specific gravity of 0.8752 as per ASTM D—287.

4.3.1. Coefficient of Friction

Graphs of friction coefficient (μ) versus contact pressure (1.95 MPa – 3.1 MPa) with sliding speed 2 m/s, 6 m/s, and 10 m/s, are plotted in Figure 4.23, 4.24 & 4.25 respectively, for fully flooded lubrication conditions. A plain surface C. I. (cast iron) disc and a textured surface C. I. disc were taken for the determination of friction coefficient between discs and the Chrome steel pin. Better tribological parameters were obtained in case of textured surface C. I. disc in comparison to plain surface C.I. disc. Friction coefficient at the interface of the pin (Chrome steel) and plain surface C. I. disc was observed to lie between 0.021 - 0.041.

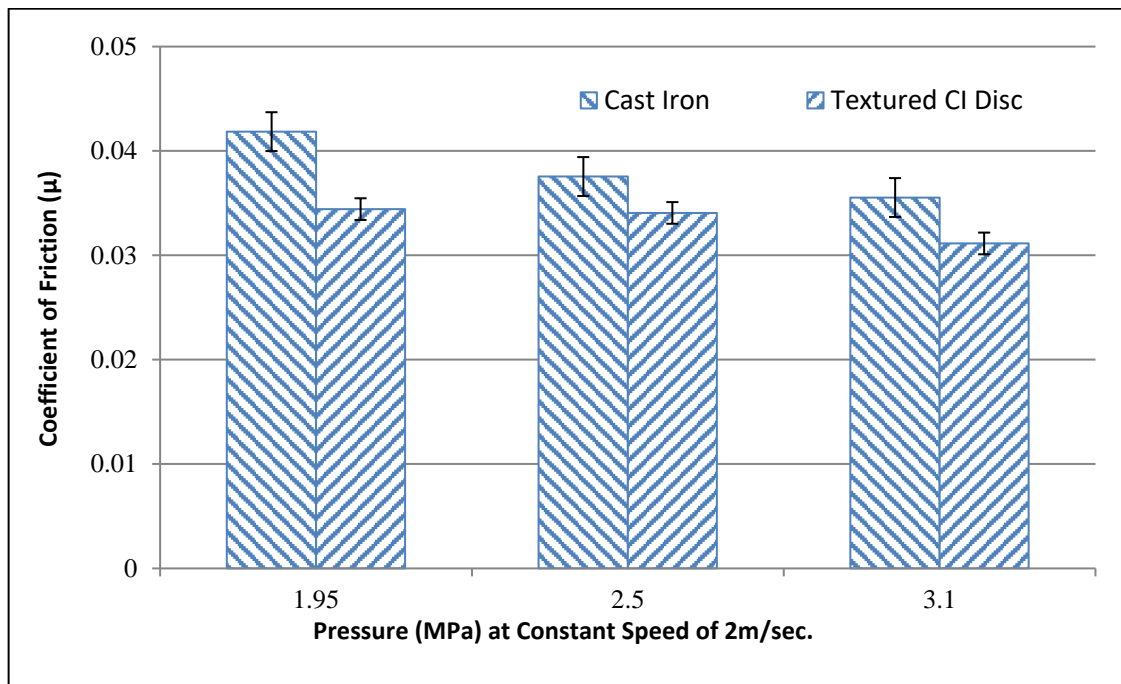


Figure 4.23: Coefficient of friction (μ) of plain cast iron and textured cast iron against steel pin at constant speed of 2m/s

It was seen that a plain surface C. I. disc has a maximum value of friction coefficient as 0.041. While, under similar conditions, the textured surface C. I. disc has a friction coefficient of 0.021 – 0.035. Also, the textured surface C. I. disc has a minimum friction coefficient. It was observed that the friction coefficient varies

within the range 0.021 to 0.041 in fully flooded conditions of lubrication developed by a continuous flow of lubricating oil on the disc. Also, it was ascertained that there was a continuous decrease in friction coefficient with an increase in load defined in terms of pressure.

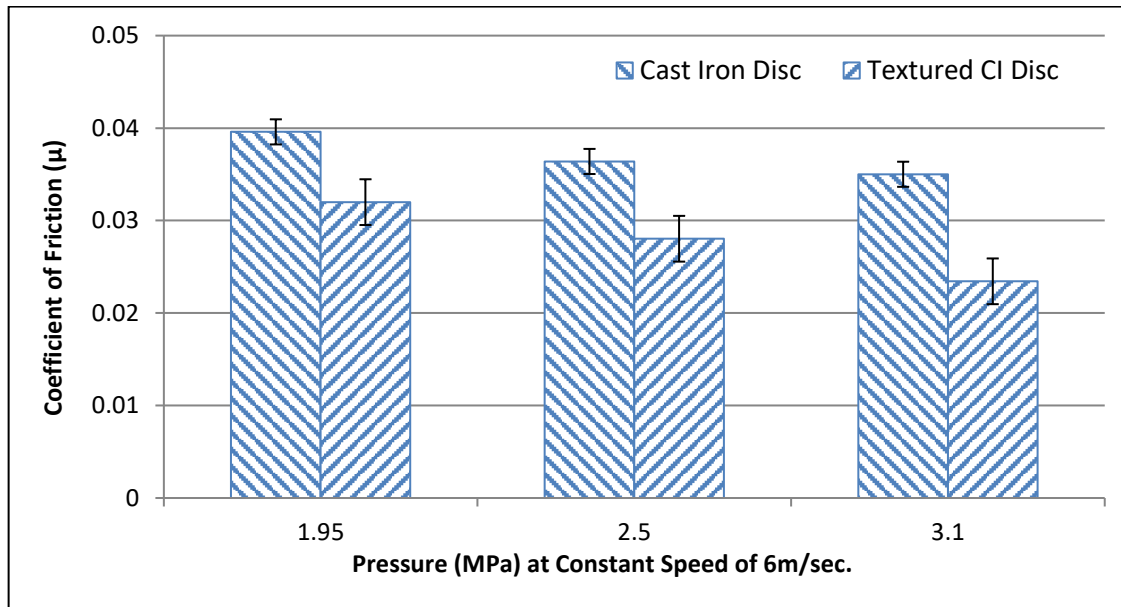


Figure 4.24: Coefficient of friction (μ) of plain cast iron and textured cast iron against steel pin at constant speed of 6m/s

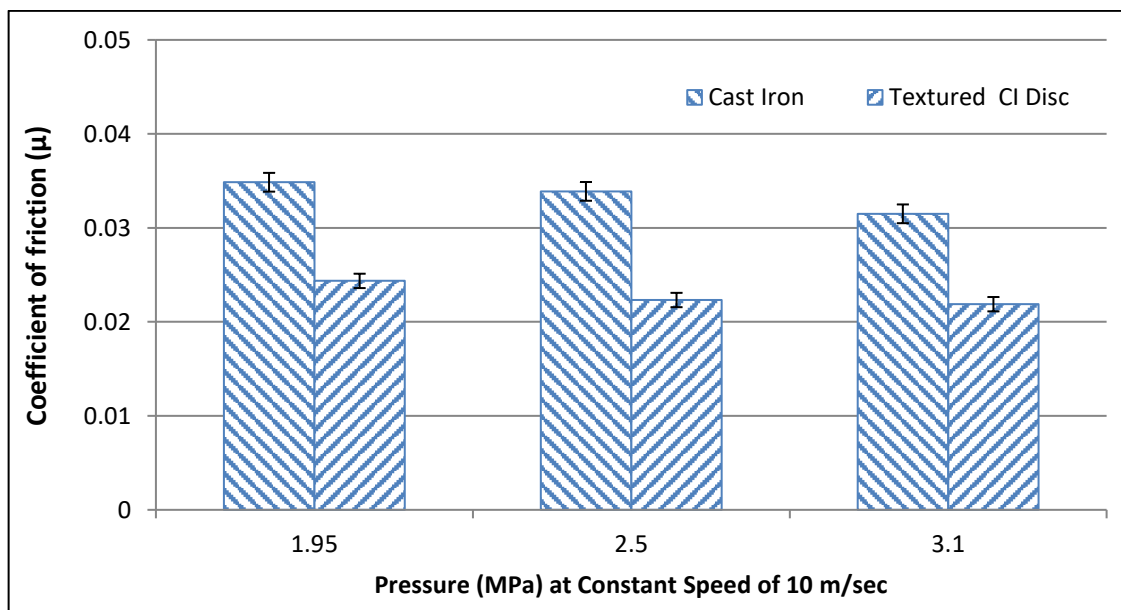


Figure 4.25: Coefficient of friction (μ) of plain cast iron and textured cast iron against steel pin at constant speed of 10m/s

4.3.2. Wear

Wear was measured by weight loss method i. e. reduction in weight of the pin. In Figure 4.26, 4.27 & 4.28, the trend of wear is shown by wear characteristics, at the initial stage, where wear growth is fast. It might be due to the breaking of asperities in the contact surface of the tribopair. Variation of wear with different pressures is shown in the graphs displayed in Figure 4.26, 4.27 & 4.28 for fully flooded lubrication. Wear decreases with increase in pressure. Which may be due to elasto-hydrodynamic lubrication up to 3.1 MPa.

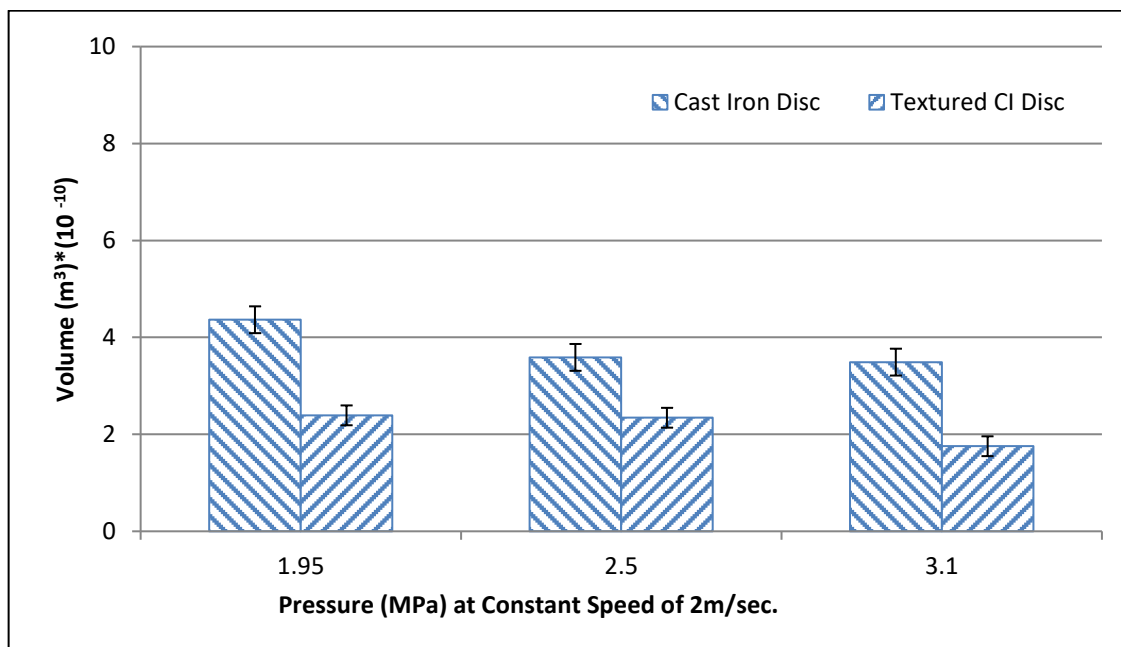


Figure 4.26: Wear of plain cast iron and textured cast iron against steel pin at constant speed of 2m/s

Wear pattern on pin material shows increase initially but later it decreases (Figure 4.26, 4.27 & 4.28). It might be due abrasion first followed by diffusion of surface debris. There exists a partial metal to metal contact between pin and discs. But because of the presence of a thin layer of lubricant at the interface, a continuous decrease in wear is observed. Also, reduction in wear is observed at the interface of

textured surface C.I. disc and chrome steel pin when fully flooded lubrication conditions were maintained. Overall wear values vary between $1.5 \times 10^{-10} \text{ m}^3$ and $8 \times 10^{-10} \text{ m}^3$. It is inferred that the wear values were less at the interface of textured surface C. I. disc and steel pin due to the hydrodynamic lubrication effect of oil trapped in circular textures.

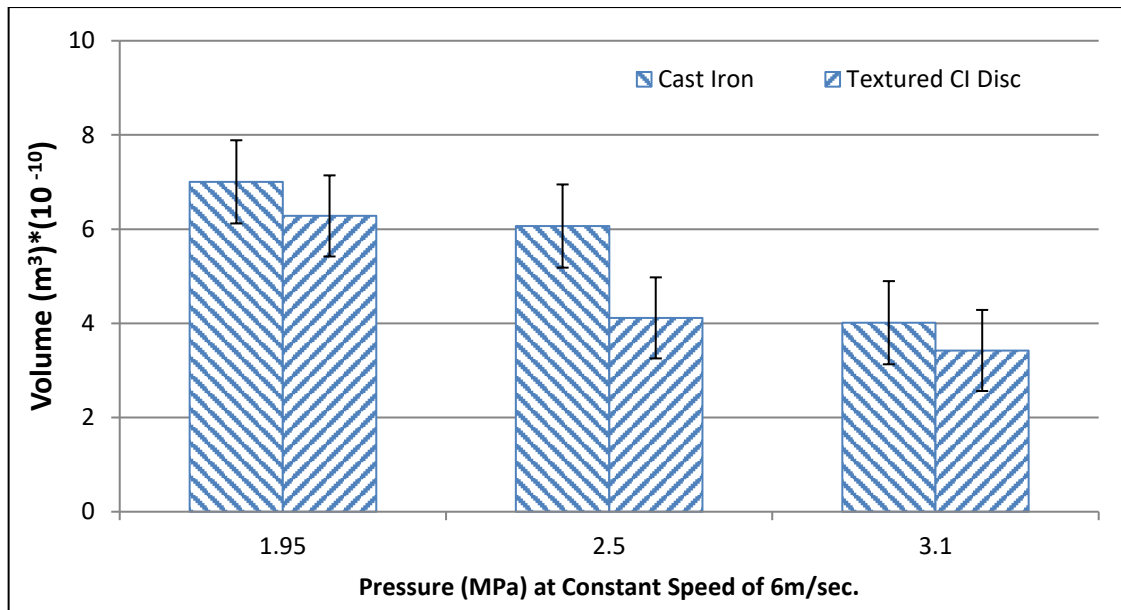


Figure 4.27: Wear of plain cast iron and textured cast iron against steel pin at constant speed of 6m/s

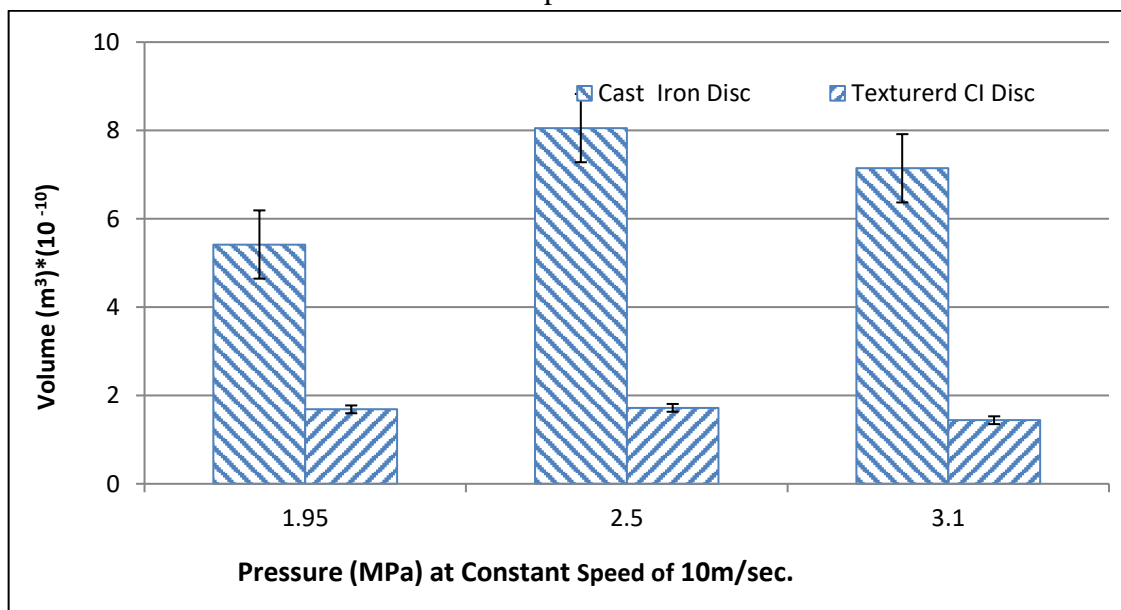


Figure 4.28: Wear of plain cast iron and textured cast iron against steel pin at constant speed of 10m/s

4.3.3. Vibrations Amplitude

Experiments were performed at different speeds and loads taken in terms of contact pressure. Speeds were taken between 1000 and 5000 rpm along with the different predetermined track diameter of rotation on disc with varying the pressure. At these different condition vibration amplitudes measured with the help of Vibro Expert Instrument and graphs which plotted as shown in Figure 4.29, 4.30 & 4.31. It was observed that the overall vibration amplitude varies between 38 μm to 48 μm . When the interface was formed by textured surface C.I. (Cast Iron) disc and pin (chrome steel), the vibration amplitude varies from 38 μm to 45 μm under fully flooded lubrication conditions. Similarly, when the interface was formed by plain surface C. I. disc and pin under fully flooded lubrication conditions, the vibration amplitude varied between 45 μm and 48 μm . Reduction in the amplitude of vibration was observed in the case of the interface formed by textured surface C. I. disc and pin, due to energy absorption by the lubricant oil trapped in the textured grooves.

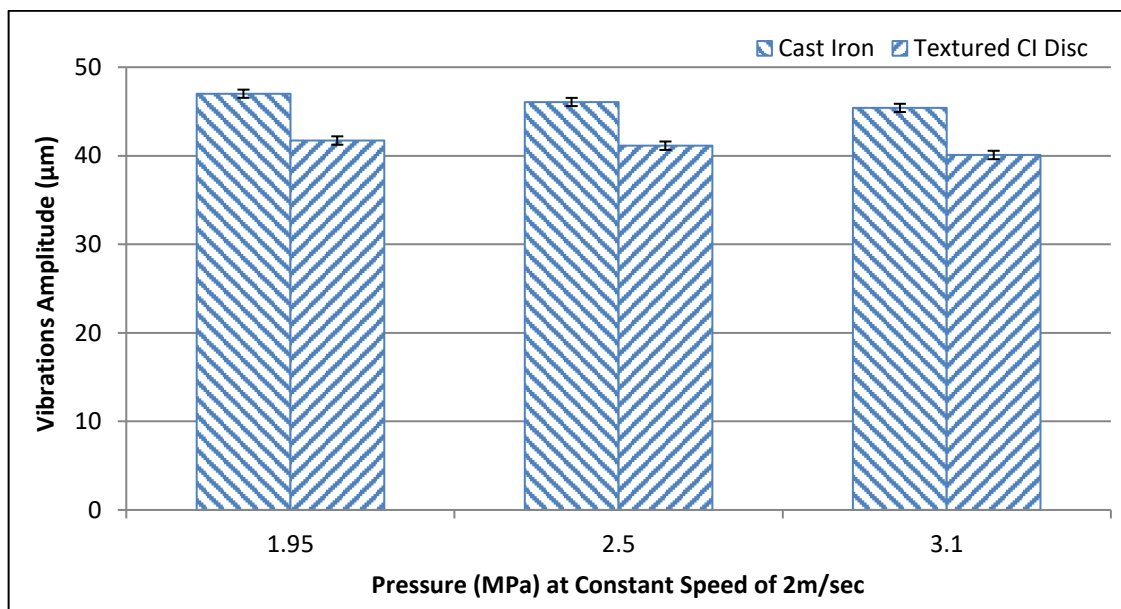


Figure 4.29: Vibration amplitude of plain cast iron and textured cast iron against steel pin at constant speed of 2m/s

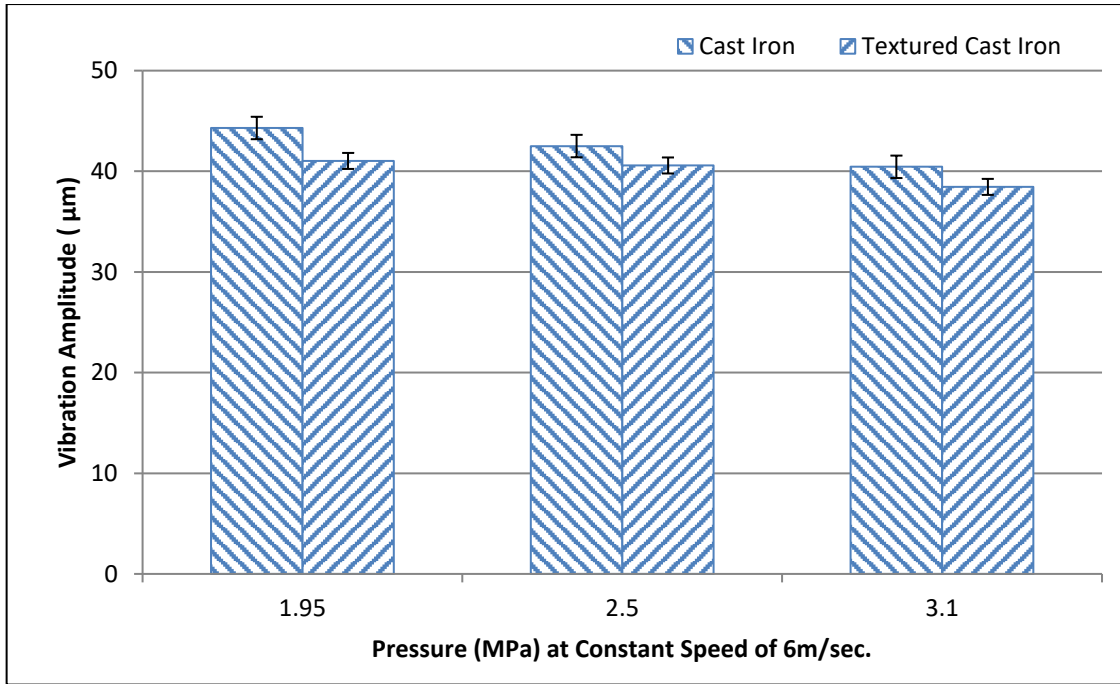


Figure 4.30: Vibration amplitude of plain cast iron and textured cast iron against steel pin at constant speed of 6m/s

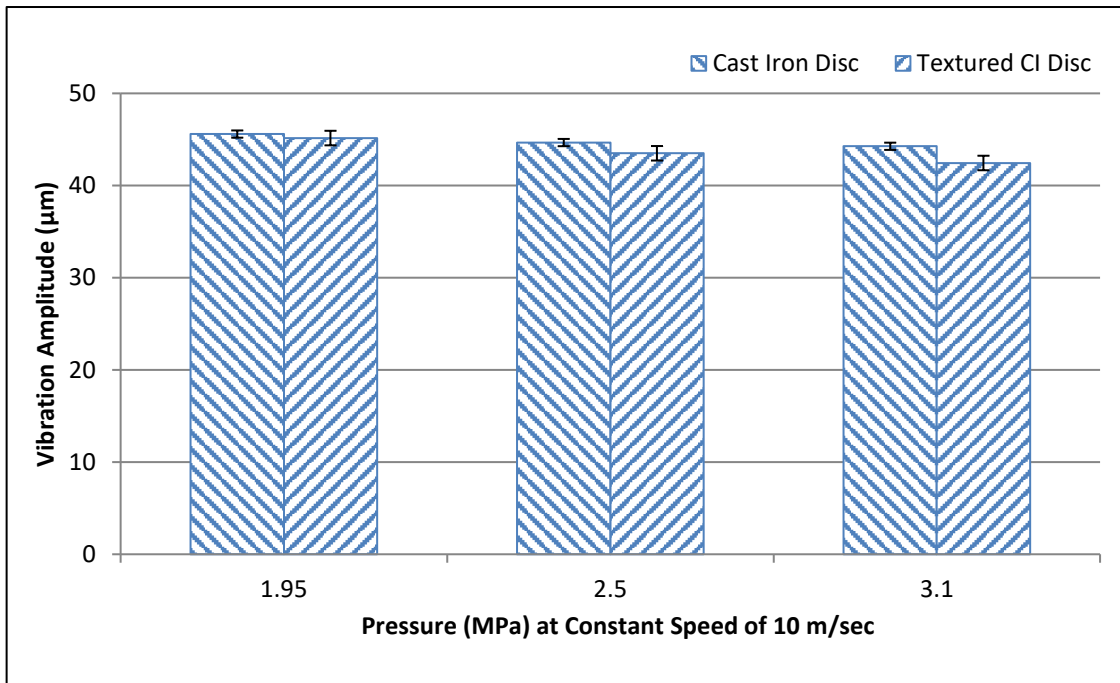


Figure 4.31: Vibration amplitude of plain cast iron and textured cast iron against steel pin at constant speed of 10m/s

4.3.4. Temperature Rise

There was very nominal temperature rise due to the relative motion between discs and pin. Though fully flooded lubrication conditions were maintained by the continuous flow of lubricating oil, metal to metal contact existed due to thin layer lubrication present at the contact area of the disc and pin. Also, temperature rise depends upon the roughness of the surfaces in contact and nature of the material along with the mechanical properties. Graphs between the rise in temperature at the interface of tribo - pairs formed by plain C.I. (Cast Iron) disc, textured surface C. I. disc with a pin (Chrome Steel) and pressure have been in shown Figure 4.32, 4.33 & 4.34. It was found that temperature rise varies in the range 4 K and 6 K. The marginal rise in temperature was observed which occurred due to a continuous flow of lubricating oil at the interface.

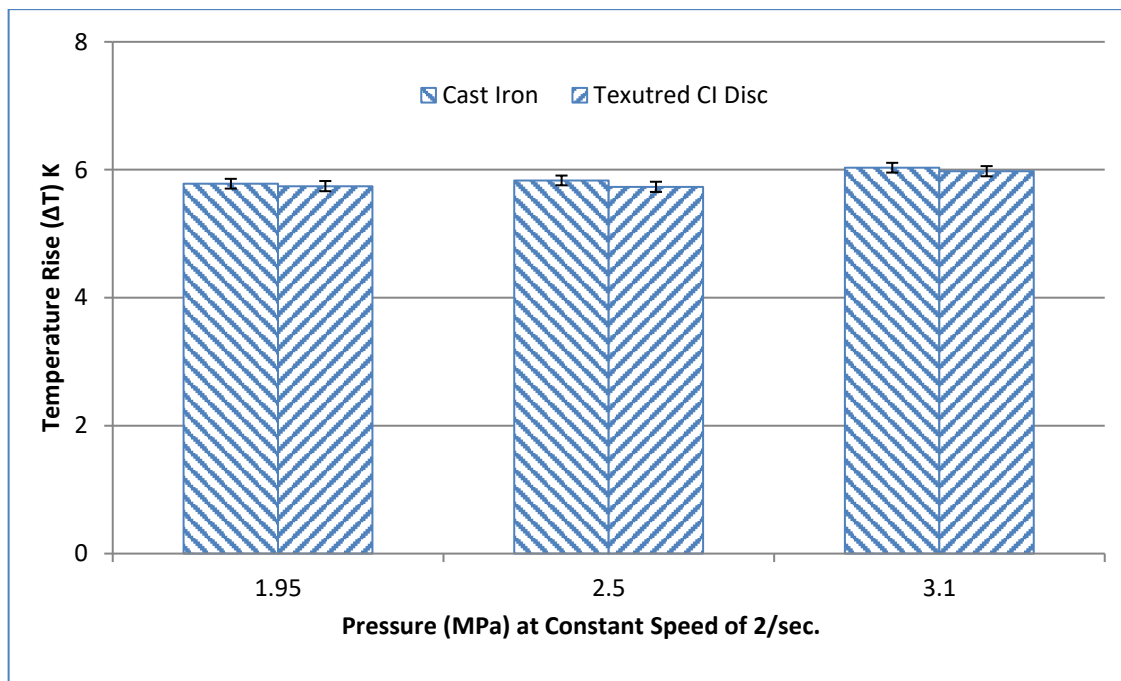


Figure 4.32: Temperature rise of plain cast iron and textured cast iron against steel pin at constant speed of 2m/s

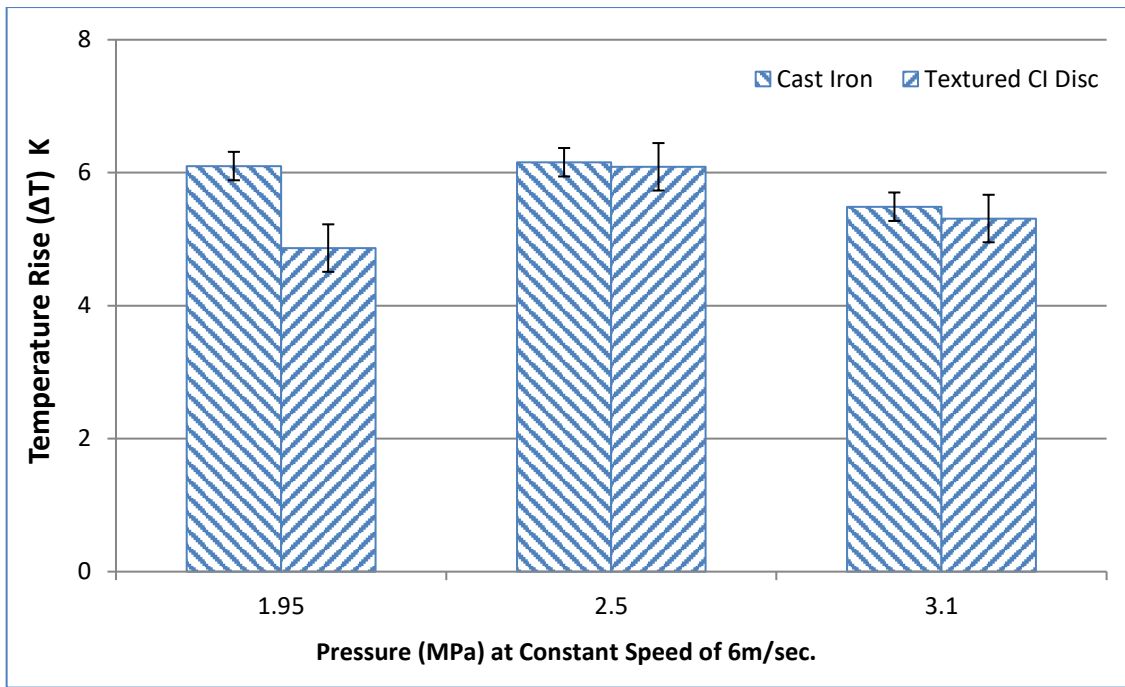


Figure 4.33: Temperature rise of plain cast iron and textured cast iron against steel pin at constant speed of 6m/s

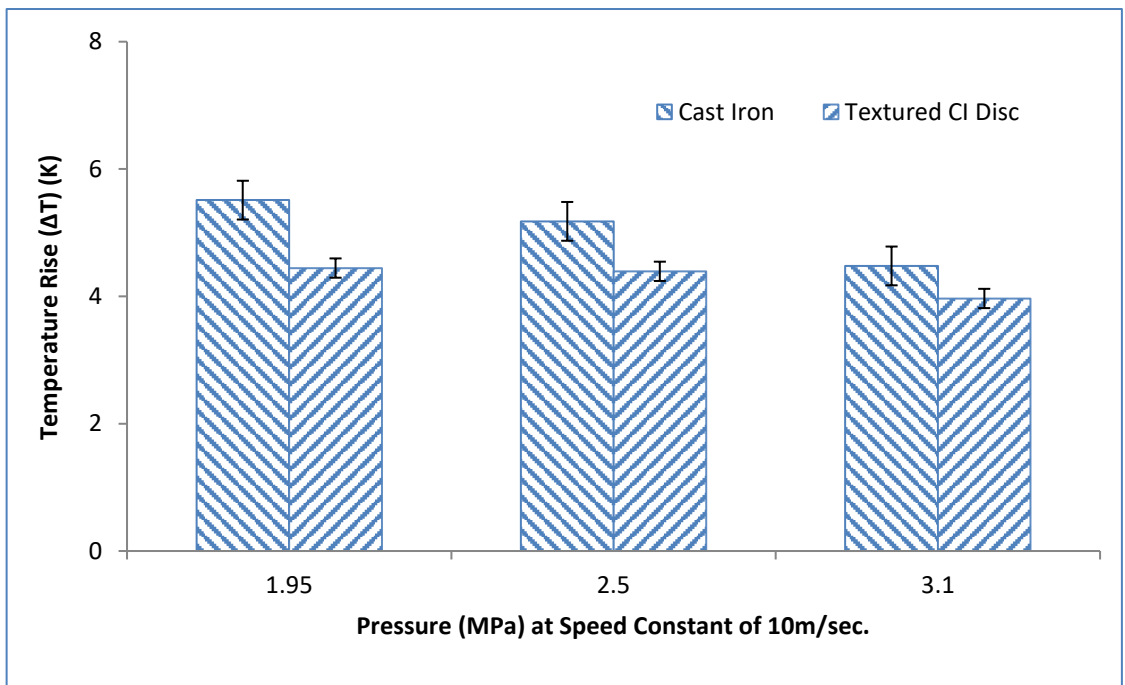


Figure 4.34: Temperature rise of plain cast iron and textured cast iron against steel pin at constant speed of 10m/s

4.3.5. Sound

The noise Pollution rules have been set acceptable at different noise limits as per its category of day or night. Noise pollution level limit for industries during daytime is 75 dB and during night time is 70 dB. Similarly, Noise pollution level limit for residential areas during daytime is 55 dB and during night time is 45 dB. The fully flooded lubrication conditions were maintained by the continuous flow of the lubricating oil. But due to pressure at the interface of pin and discs, a thin layer of lubricating oil exists in the contact area, which develops a possibility of metal to metal contact between the discs and pin, leading to the creation of sound. Also, sound was produced because of the relative motion of disc with respect to the pin. The sound was measured by the sound meter, kept 25 cm away from wear and friction test rig. It was observed that the sound level varies between 66 dB and 73 dB (Figure 4.35, 4.36 & 4.37). More noise level was observed in case of plain surface C. I. disc as compared with textured C. I. disc, in the presence of thin layer lubrication conditions.

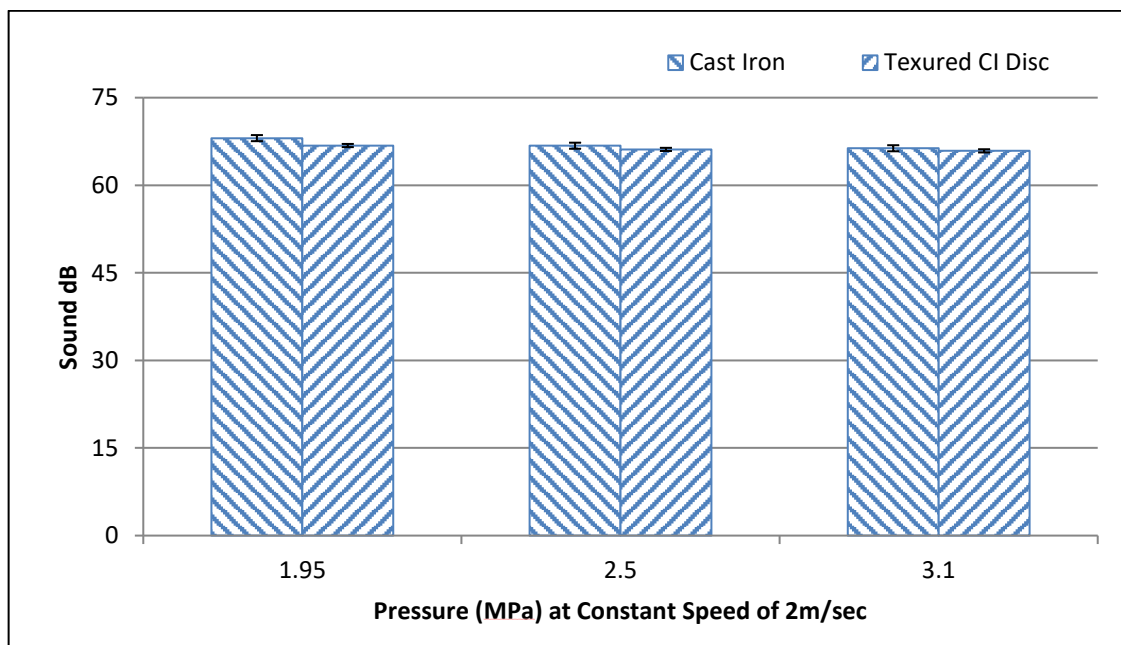


Figure 4.35: Sound of plain cast iron and textured cast iron against steel pin at constant speed of 2m/s

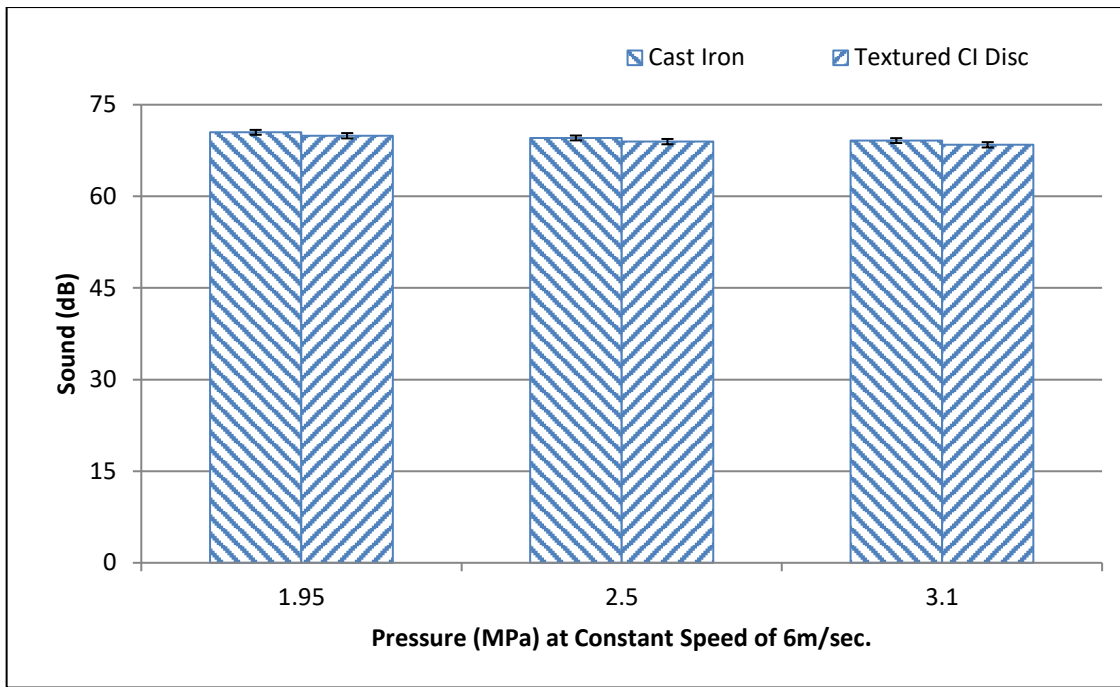


Figure 4.36: Sound of plain cast iron and textured cast iron against steel pin at constant speed of 6m/s

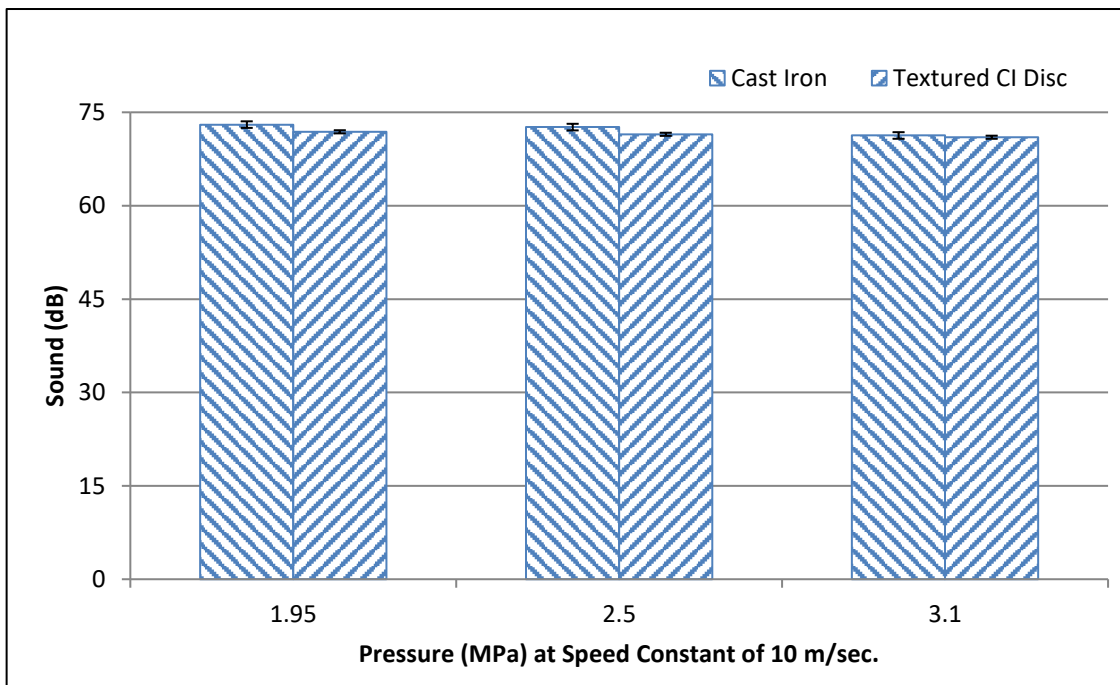


Figure 4.37: Sound of plain cast iron and textured cast iron against steel pin at constant speed of 10m/s

4.4. Engine

In Figure 4.38 to Figure 4.55 the term “D100T” stands for Diesel with textured Piston Rings, and “D100N” stands for Diesel with Non-textured Piston rings. Similarly, “B100T” stands for Biodiesel with textured Piston Rings, and “B100N” stands for Biodiesel with Non-textured Piston rings.

4.4.1. Brake Thermal Efficiency

Brake Thermal Efficiency of diesel engine piston ring without textures is lower than diesel engine piston ring with textures due to less friction in the rings. Similarly, Biodiesel fuel exhibit higher Brake Thermal Efficiency with textured piston rings. From Figure 4.40 it was found that Brake Thermal Efficiency for Diesel is higher than Biodiesel.

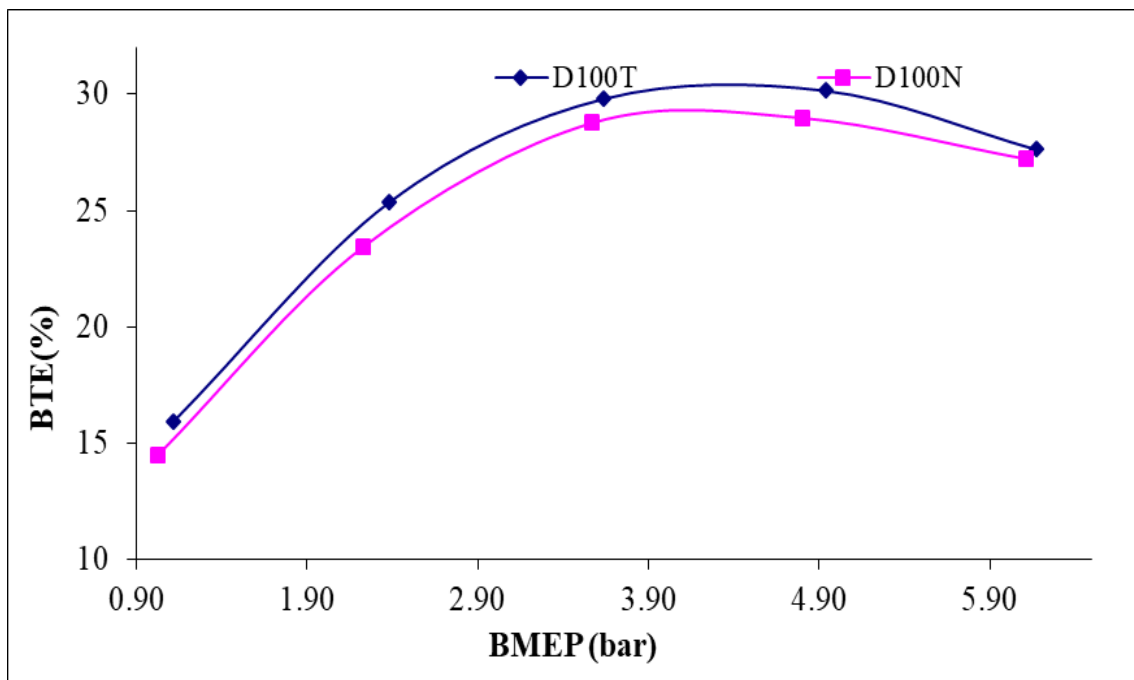


Figure 4.38: Variation of Brake Thermal Efficiency of Diesel as fuel with Textured and Non-textured Piston Ring

Maximum brake thermal efficiency achieved for diesel with textured piston ring was 30.17% at 80% of load and with non-textured piston ring was 28.99% at 80% of the load as shown in Figure 4.38.

Figure 4.39 shows that maximum brake thermal efficiency achieved for biodiesel with textured piston ring was 27.42% at 60% of load and with non-textured piston ring was 27.29% at 80% of load. The reason for lower brake thermal efficiency achieved with biodiesel is due to its lower calorific value which in turns requires more energy to produce higher BTE. Better lubrication reduces the mechanical losses at the interface of cylinder liner and piston rings, which enhances the efficiency of the engine.

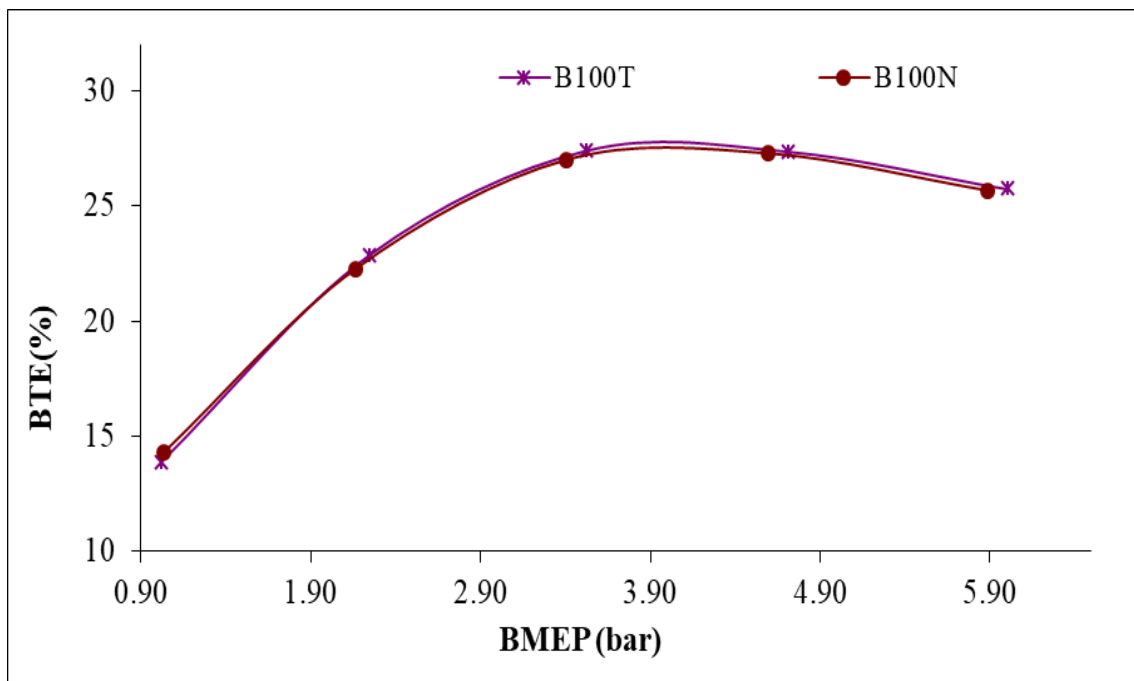


Figure 4.39: Variation of Brake Thermal Efficiency of Biodiesel as fuel with Textured and Non-textured Piston Ring

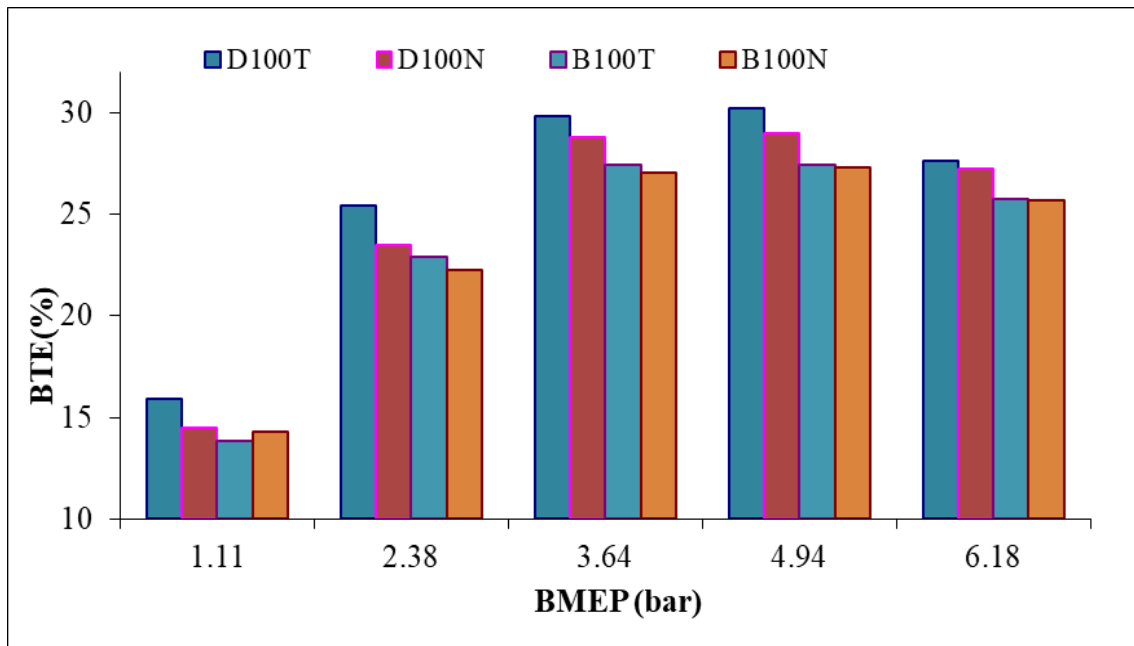


Figure 4.40: Combined variation of Brake Thermal Efficiency of both Diesel and Biodiesel as fuel with Textured and Non-textured Piston Ring

4.4.2. Brake Specific Fuel Consumption

Brake Specific Fuel Consumption (BSFC) is inversely proportional to Brake Thermal Efficiency. Therefore, as seen from Figure 4.41 Brake Specific Fuel Consumption of diesel is lower for textured piston rings. The reason is less friction for textured piston rings that decrease the fuel requirement and hence, lower fuel consumption. A similar trend is seen in Figure 4.42 for Biodiesel.

Minimum brake specific fuel consumption (BSFC) achieved for diesel with textured piston ring was 0.2824 kg/kW-hr at a load of 80% and with non-textured piston ring was 0.2939 kg/kW-hr at a load of 80% as shown in Figure 4.41. Minimum brake specific fuel consumption (BSFC) achieved for diesel with textured piston ring was 0.3311 kg/kW-hr at a load of 60% and with non-textured piston ring was 0.3327 kg/kW-hr at a load of 80% as shown in Figure 4.42.

The brake specific fuel consumption (BSFC) of Biodiesel without texturing is found to be higher. As, seen from Figure 4.43, due to more calorific value and lower

viscosity of diesel, less fuel consumption is observed. It is also attributed to effective lubrication causing reduction of interface friction with modified piston rings.

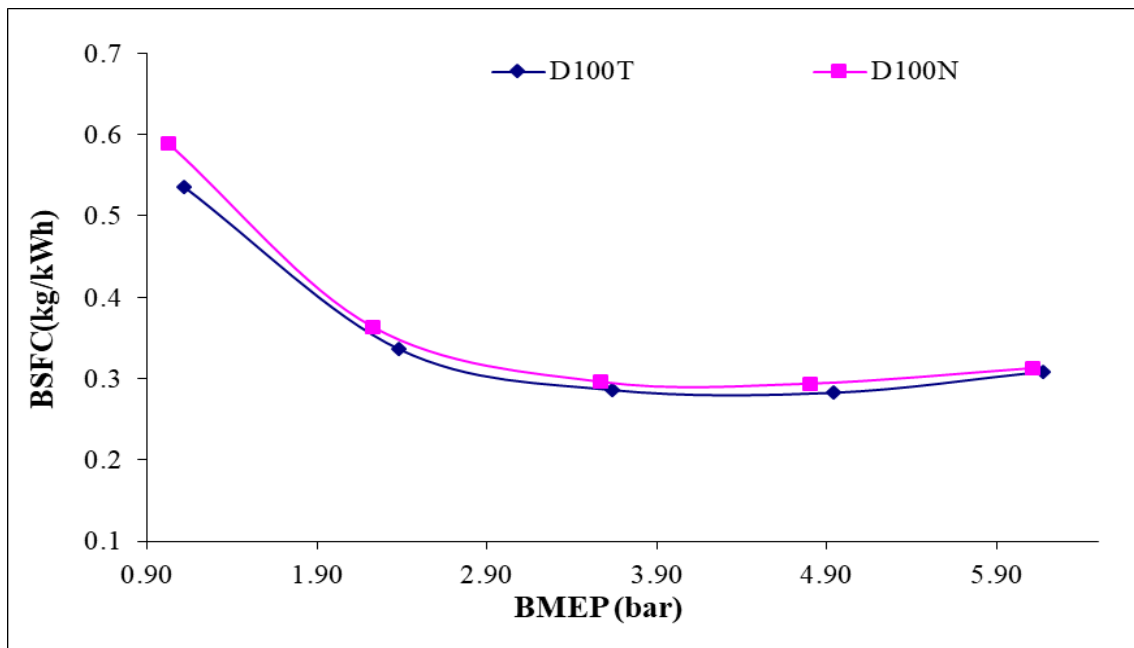


Figure 4.41: Variation of Brake Specific Fuel Consumption of Diesel as fuel with Textured and Non-textured Piston Ring

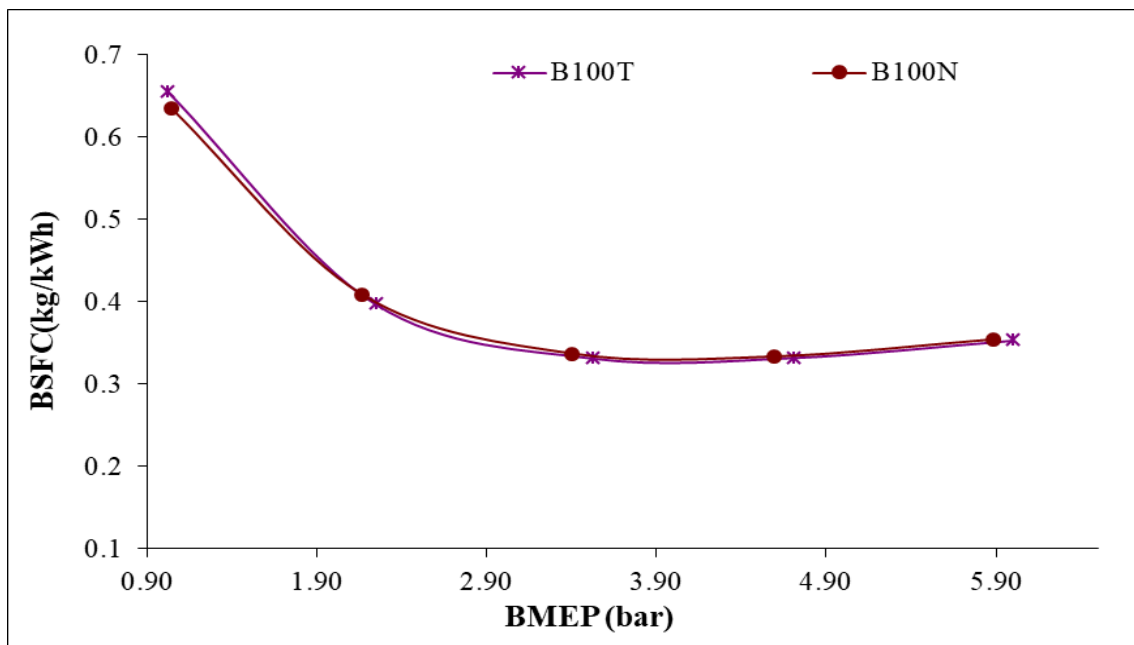


Figure 4.42: Variation of Brake Specific Fuel Consumption of Biodiesel as fuel with Textured and Non-textured Piston Ring

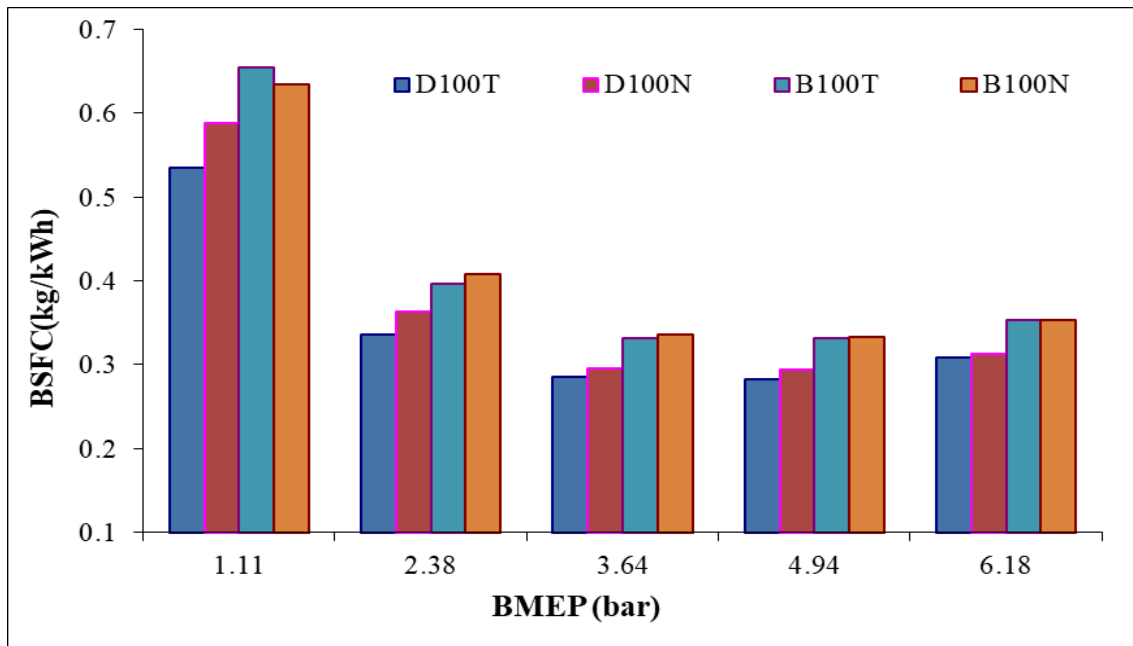


Figure 4.43: Combined variation of Brake Specific Fuel Consumption of both Diesel and Biodiesel as fuel with Textured and Non-textured Piston Ring

4.4.3. Carbon Monoxide

In CI engine overall air-fuel ratio remains very lean up to 60% load. Typically, the air-fuel ratio varies from 80:1 to about 20:1 during idling to about 60% load. However, it is found that CO emissions increased rapidly when engine has been operated from 80% load to full load. During these conditions overall air-fuel ratio varies from 40:1 to about 22:1. In these conditions due to combustion mechanism of CI engine local air-fuel ratio may be either overrich or overlean.

Figure 4.44 shows the CO emissions of diesel was lower with texturing in as comparison to that without texturing. Figure 4.45 shows the CO emissions of biodiesel was lower with texturing in as comparison to that without texturing.

From Figure 4.46 it is found that, CO emissions for Biodiesel as fuel is lower than diesel as fuel due to added oxygen in biodiesel. Therefore, CO emissions of diesel were higher than biodiesel.

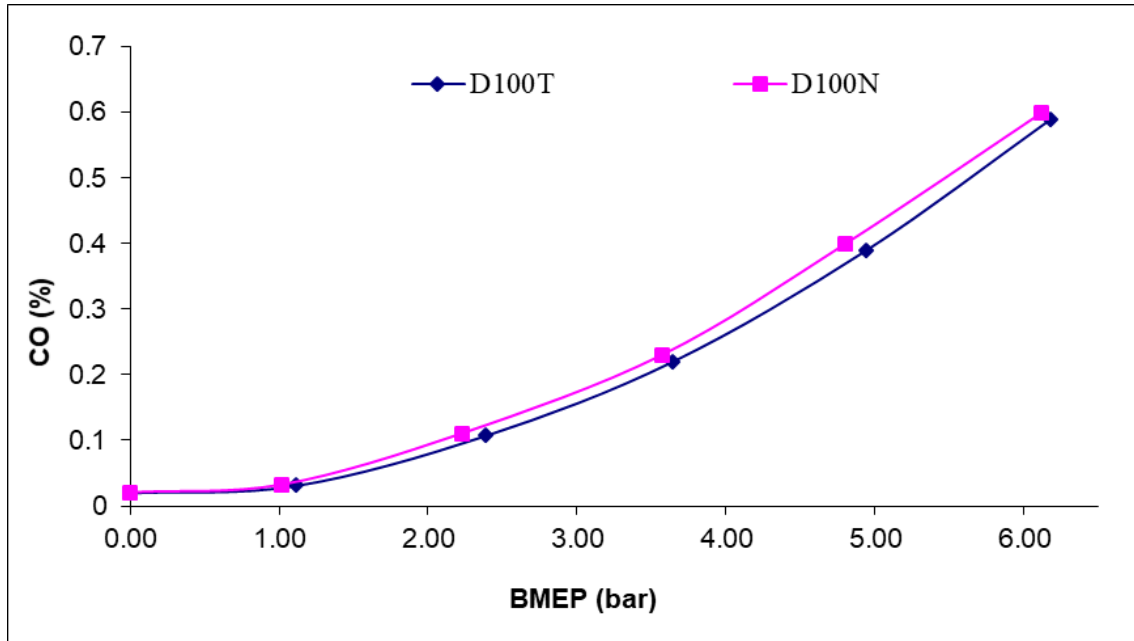


Figure 4.44: Variation of Carbon Monoxide emissions of Diesel as fuel with Textured and Non-textured Piston Ring

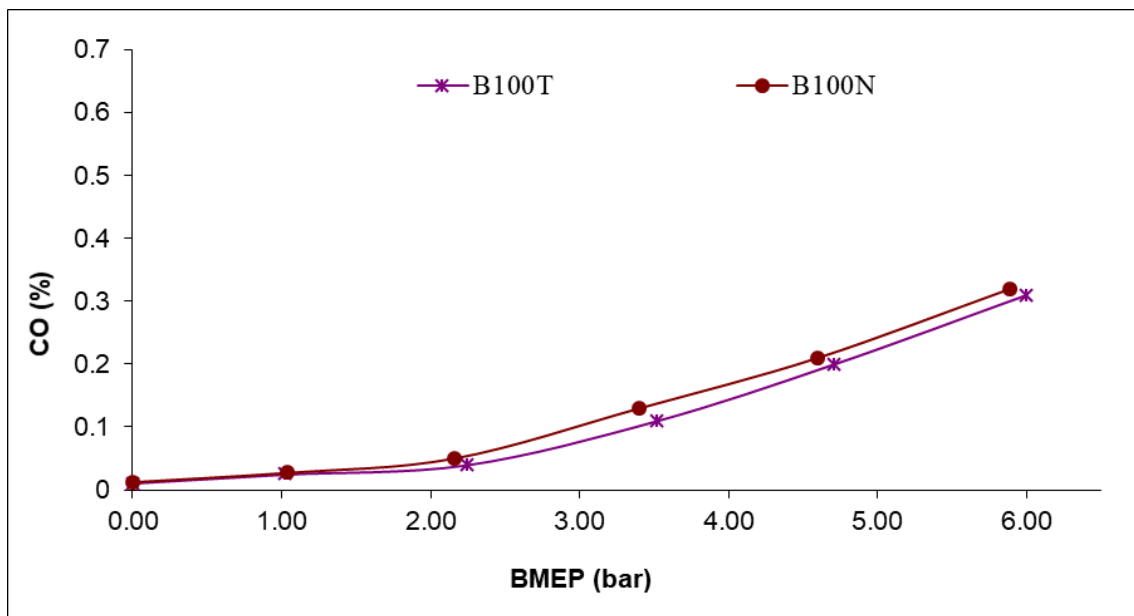


Figure 4.45: Variation of Carbon Monoxide emissions of Biodiesel as fuel with Textured and Non-textured Piston Ring

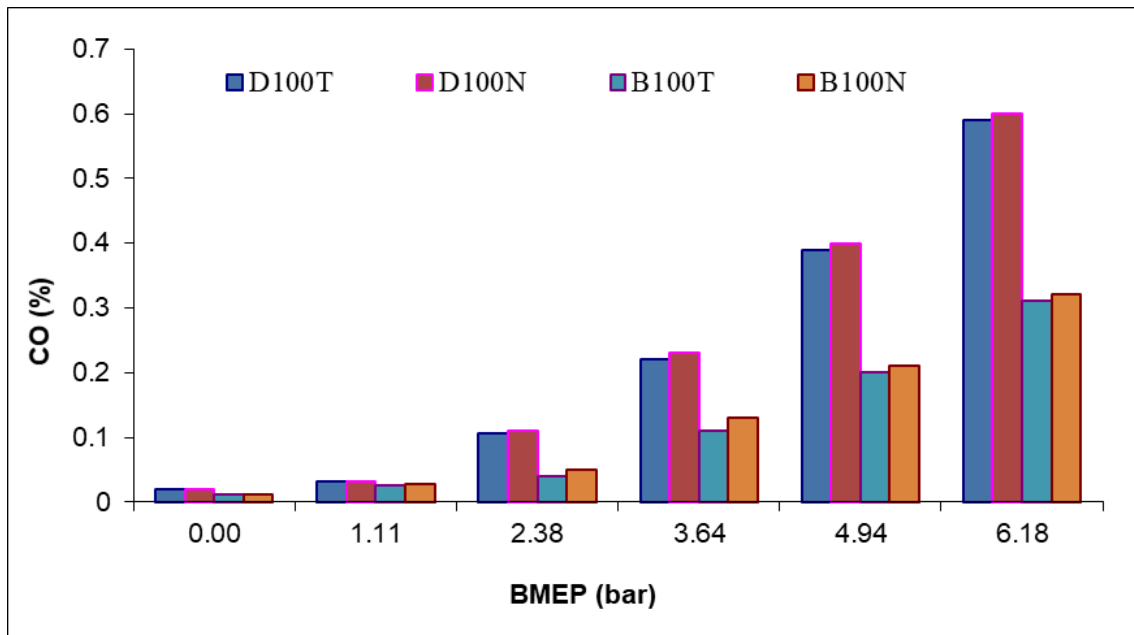


Figure 4.46: Combined variation of Carbon Monoxide emissions for both Diesel and Biodiesel as fuel with Textured and Non-textured Piston Ring

4.4.4. Hydrocarbon (HC)

The fuel used in this engine has higher molecular weight and less volatility. During uncontrolled and controlled combustion phase there can be locally overlean mixture, locally overrich mixture and some combustible mixture. Therefore, the Hydrocarbon (HC) formation is very-very complex phenomena in such cases. However, it is found that Hydrocarbon (HC) remains similar in both type of piston rings when diesel fuel is used as can be seen in Figure 4.47. Similarly, in figure 4.48 it is found that Hydrocarbon (HC) remains close for both type of piston rings when biodiesel fuel is used. But from figure 4.49 it quite clear that, the Hydrocarbon (HC) emissions are quite low for biodiesel in comparison to diesel as fuel.

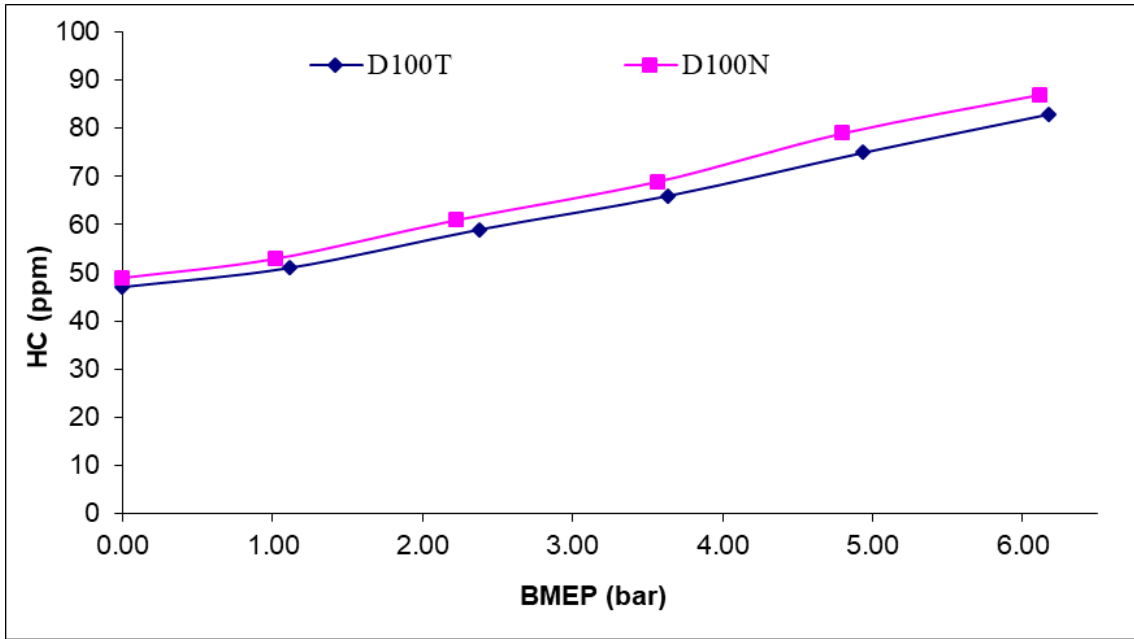


Figure 4.47: Variation of Hydrocarbon emissions for Diesel as fuel with Textured and Non-textured Piston Ring

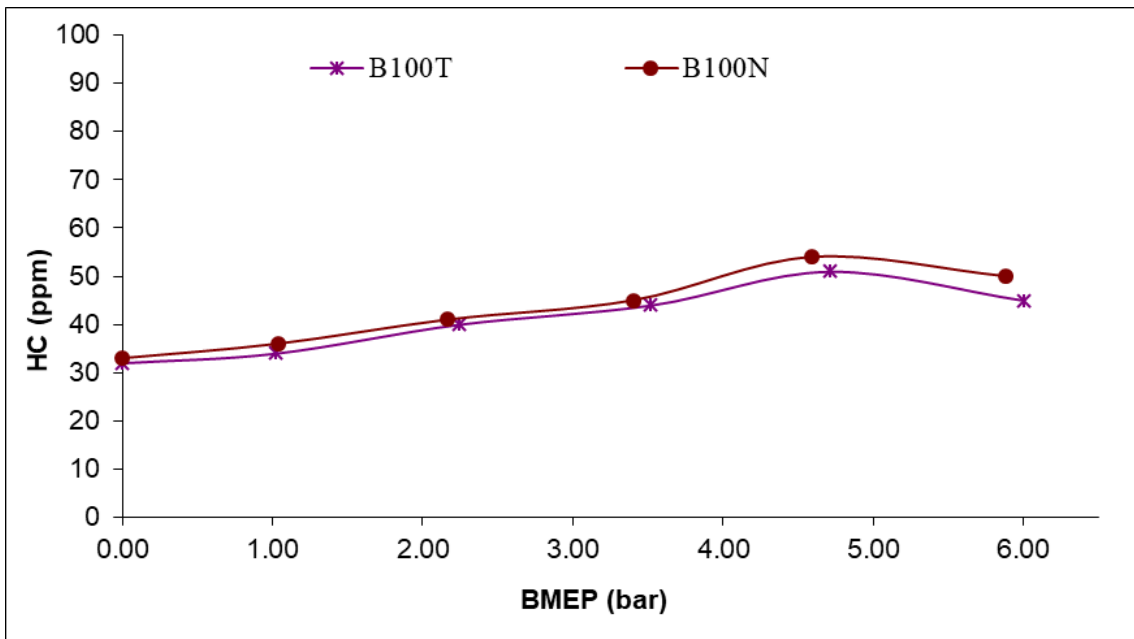


Figure 4.48: Variation of Hydrocarbon emissions for Biodiesel as fuel with Textured and Non-textured Piston Ring

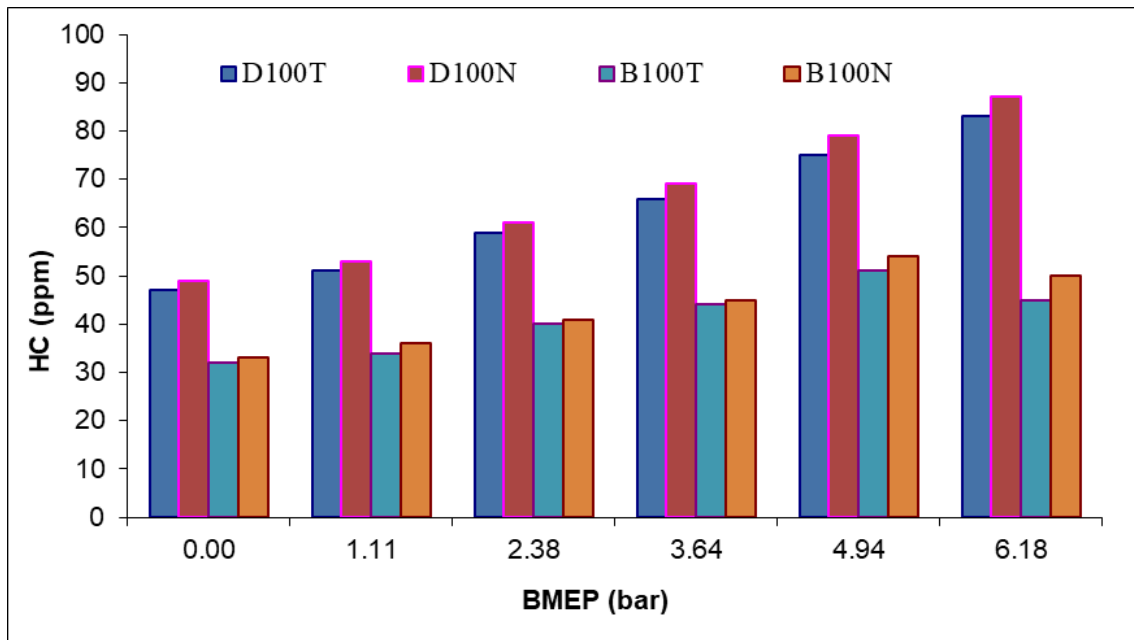


Figure 4.49: Combined variation of Hydrocarbon emissions for both Diesel and Biodiesel as fuel with Textured and Non-textured Piston Ring

4.4.5. Nitrogen Oxide

The variation of NO_x emission using diesel and biodiesel as a fuel is shown in Figure 4.50 and Figure 4.51 respectively. In CI engine load increases as the temperature increases. It is clearly evident from Figure 4.50 and Figure 4.51 that the NO_x emissions continuously go on increasing with increase of engine load and then decrease. The increase can be attributed to the fact that the chemical kinetics of the reaction leading to high heat release rate and thereby increasing the local temperature. This high temperature is translated into corresponding higher NO_x emissions. The principal source of NO_x emission is the oxidation of atmospheric N₂. However, if the fuel contains significant amount of nitrogen, the oxidation of fuel nitrogen-containing compounds is an additional source of NO_x emission.

Biodiesel may have little more amount of N_2 in the fuel itself compared to diesel which, can be noticed in Figure 4.52. Marginal decrease of NO_x at full load is may be due to higher rate of fuel evaporation at the combustion zone at higher loads.

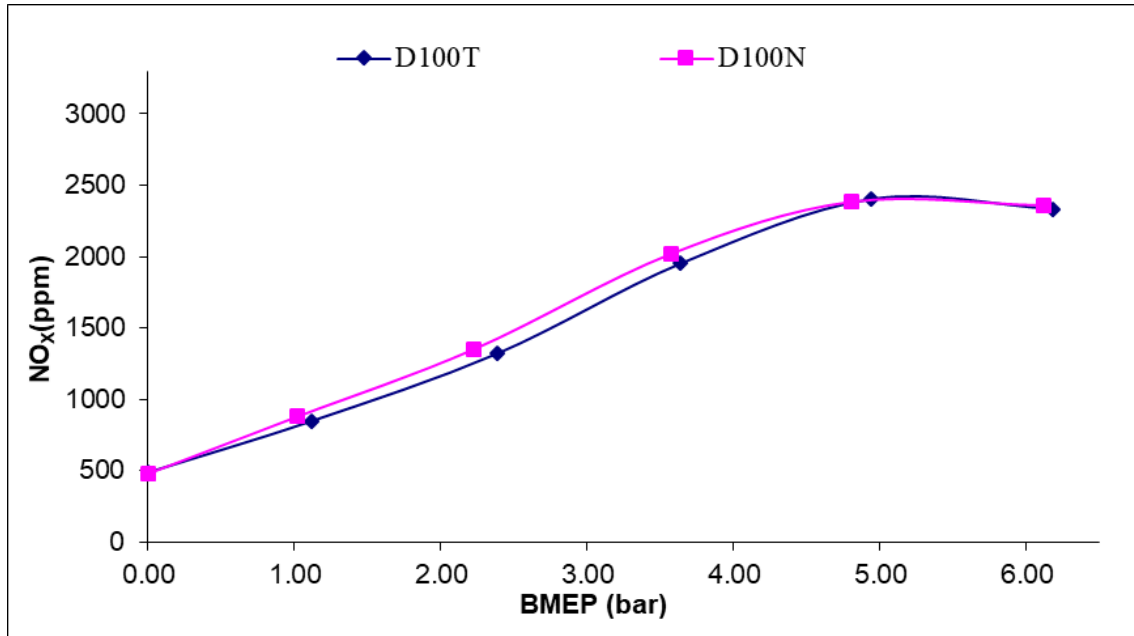


Figure 4.50: Variation of NO_x emissions for Diesel as fuel with Textured and Non-textured Piston Ring

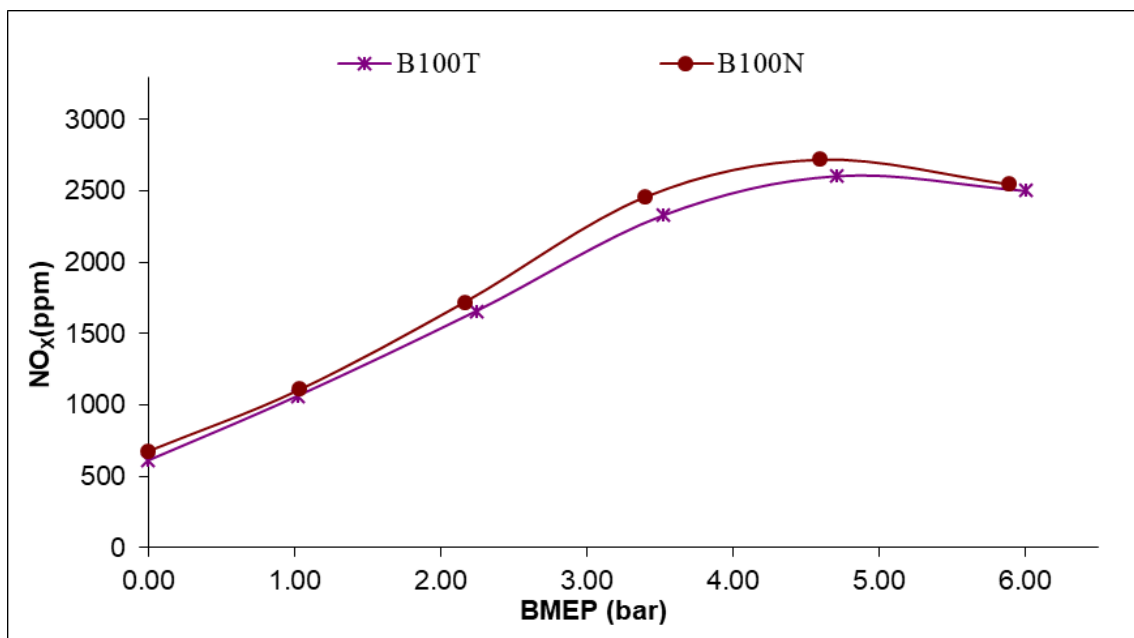


Figure 4.51: Variation of NO_x emissions for Biodiesel as fuel with Textured and Non-textured Piston Ring

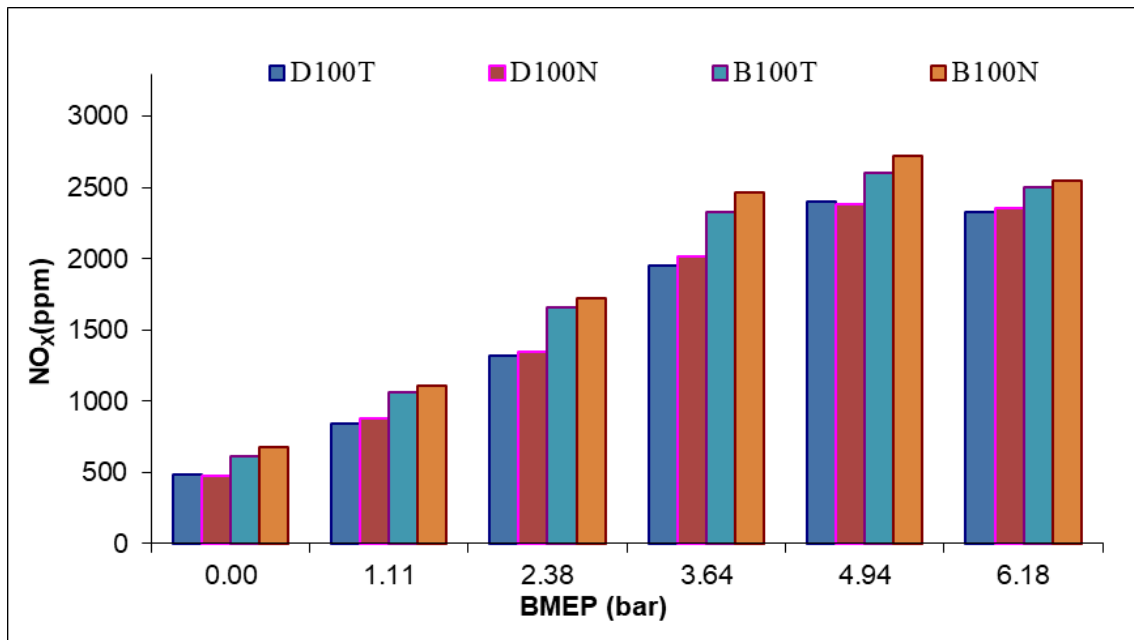


Figure 4.52: Combined variation of NO_x emissions for both Diesel and Biodiesel as fuel with Textured and Non-textured Piston Ring

4.4.6. Smoke Opacity

Smoke Opacity is the degree to which smoke blocks light, and the basis for measuring the amount of smoke coming from a diesel-powered vehicle. The variation of black smoke with both type of piston rings is shown in Figure 4.53 & Figure 4.54 for diesel and biodiesel as fuel respectively. Primarily, black smokes in CI engines consist of combustion generated carbonaceous material (soot). Sometimes some organic compounds are absorbed on an around soot particles. In most cases soot formation occurs in overrich zones due to lack of oxygen in these pockets. Smoke density increases at higher loads for both the fuels. This is due to rich mixture causing partial combustion of fuel droplets. From Figure 4.55 it can be clearly seen that smoke opacity for Biodiesel is lower than that of diesel due to better burning & hence lower waste products liberated. In the combustion process of different hydrocarbons, acetylene (C₂H₂) is formed as an intermediate. These acetylene molecules after simultaneous polymerisation and dehydration produce carbon particles, which are the

main constituent of the particulate. Since facility to measure fine carbon particles such as PM 2.5 and PM 10 was not available in house, so may be considered for future scope of study.

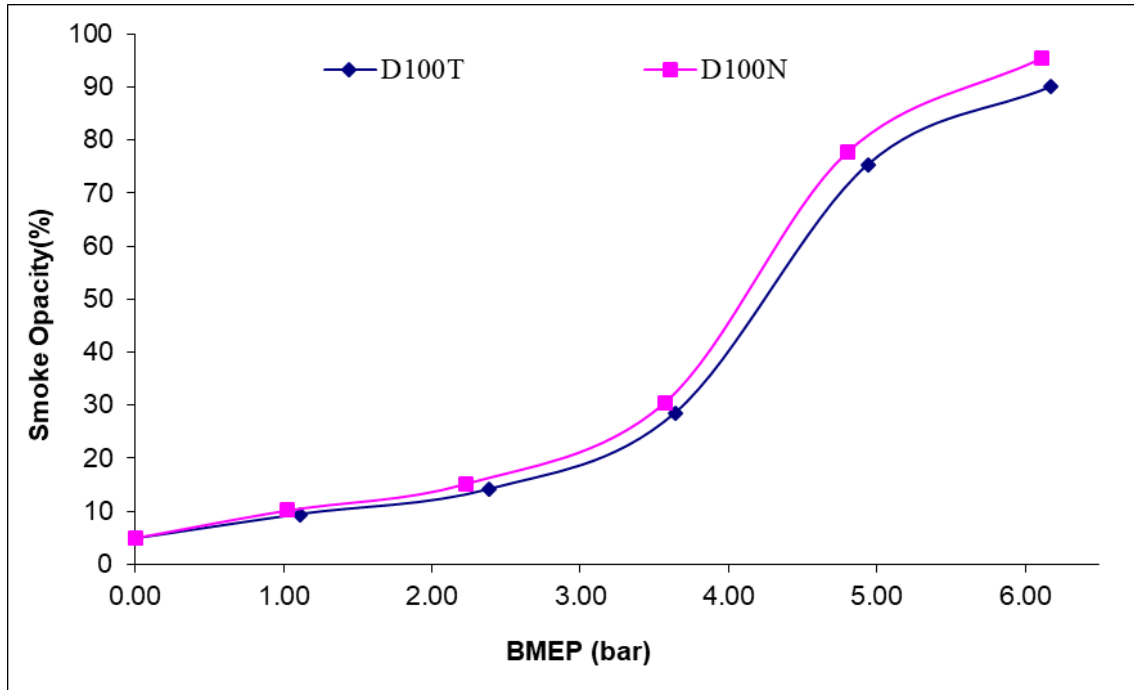


Figure 4.53: Combined variation of Smoke Opacity emissions for Diesel as fuel with Textured and Non-textured Piston Ring

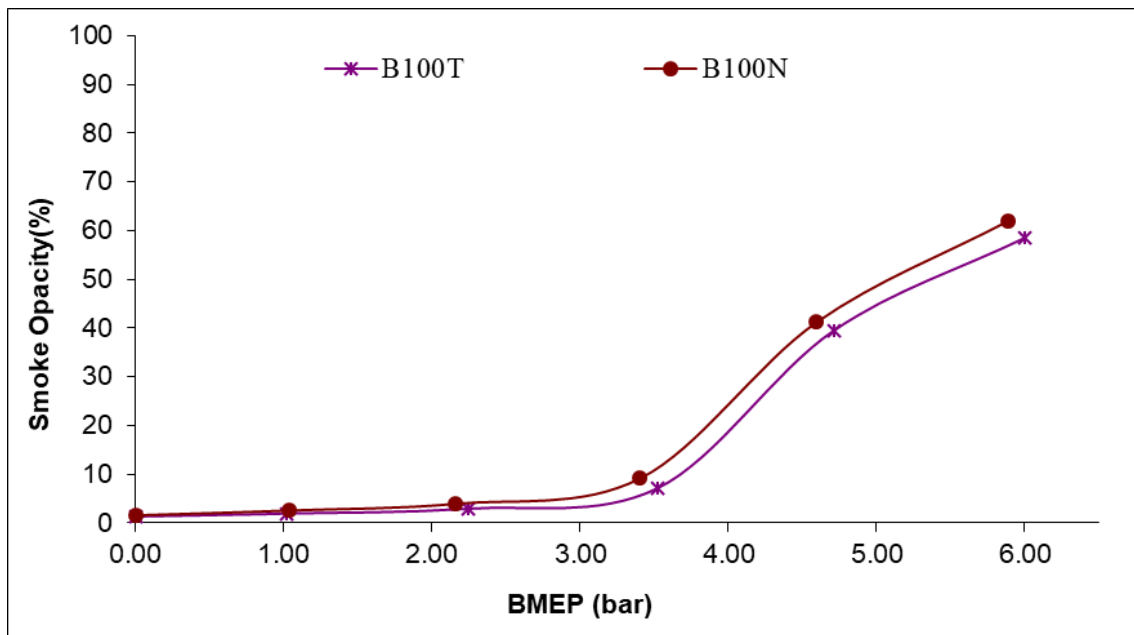


Figure 4.54: Combined variation of Smoke Opacity emissions for Biodiesel as fuel with Textured and Non-textured Piston Ring

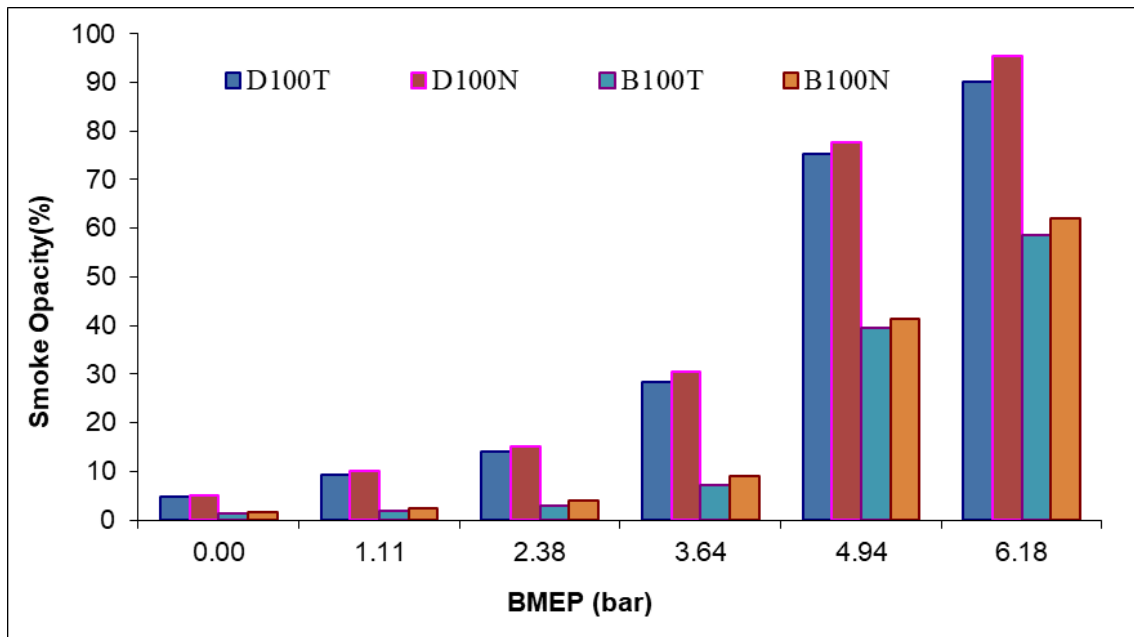


Figure 4.55: Combined variation of Smoke Opacity emissions for both Diesel and Biodiesel as fuel with Textured and Non-textured Piston Ring

Chapter 5

Conclusion and Future Scope of the work

5.1. Conclusions

In the present thesis work, attempts have been made to improve the performance of the diesel engine by using textured piston rings. The designing of the textured surface of the piston rings was considered and worked upon for the possible improvement in the engine performance. Two experiments were performed for deciding the design textures on piston rings.

The main conclusions drawn from all the experimentation drawn are given below:

- It has been observed that Chrome-plated cast iron disc significantly improved the coefficient of friction and the value 0.025 found to be at 3.1 MPa and 6 m s^{-1} relative velocity at the interface under the condition of fully flooded lubrication as compared with cast iron disc with chrome steel pin. In such condition, the lubricating oil helped in reducing the shear force which further reduced the coefficient of friction with the increase in speed. The chrome-plated cast iron disc had hard surface to reduce coefficient of friction at thin layer lubrication.
- Chrome-plated cast iron disc experienced less wearing due to the formation of a hard surface layer of chromium and the presence of thin layer mixed and elasto hydrodynamic lubrication in the contact area of the tribopair. The chrome-plated cast iron disc had hard surface to reduce wear rate at thin layer tribo lubrication.

- The amplitude of vibration was observed to be minimum at $40\ \mu\text{m}$ and maximum at $52\ \mu\text{m}$. The chromium plated cast iron disc had more amplitude of vibration in comparison to cast iron disc due to less energy absorption in the chrome-plated cast iron disc.
- The rise in temperature at the interface of the tribo—pair formed between the cast Iron, Chromium plated cast Iron discs and the steel pin was observed from 4 K to 9 K. The combination of Chrome-plated cast iron disc with steel pin showed more temperature rise when compared with cast iron disc and steel pin. This rise in temperature was negligible due to the condition of fully flooded lubrication.
- The experimental results show that sound varied between 66.8 dB to 78 dB. Chrome-plated cast iron disc owing to hard surface generated more noise while the cast iron disc generated less noise due to its property of absorption of energy and also the continuous flow of lubrication acted as the sound absorber leading to a quiet movement between the two surfaces in contact.
- It was observed that there was a significant improvement in friction coefficient at the interface formed by textured surface cast iron disc and pin of chrome steel, under the fully flooded lubrication condition. the lubricating oil trapped in surface textures helped to reduce shear force which in turn reduced the friction coefficient. Also, the friction coefficient continuously decreased with the increase in the contact pressure up to a certain limit and then remained steady at the minimum value of 0.021.
- Further, the textured surface cast iron disc showed less wear. It was due to the lubricating oil trapped in the textures which helped in reducing wear. These textures on the surface act as a cushion. Also, the presence of the oil pockets due to the textured surface of the disc reduces the contact area of the tribopair which in turn reduce the metal to the metal contact

area. The overall effect was to reduce wear significantly in case of tribopair formed by textured surface C. I. (cast iron) disc with Steel pin (chrome steel).

- The minimum and maximum vibration amplitude were observed in case of tribopair formed by textured surface C. I. (cast iron) disc with a pin (chrome steel) were 38 μm and 48 μm respectively. Plain surface C.I. disc has greater vibration amplitude in comparison to textured surface C.I. disc. It was due to lubrication and more metal to metal contact.
- The temperature rise at the contact area of the tribo - pair formed by (i) plain surface C.I. disc, and (ii) Textured surface C.I. disc, with steel pin, was observed between 4 K to 6 K. Negligible temperature rise was observed in case of the textured surface of C.I. disc as compared to the plain surface C.I. disc with the steel pin. Overall, it was observed that there was a negligible rise in temperature, due to fully flooded lubrication at the interface.
- The sound values recorded during the experiments were between 66 dB and 73 dB. The plain disc generated more noise as compared of textured surface for C.I. disc. Presence of oil in tiny pockets (Surface textures) and continuous flow of lubricating oil acted as a cushion and oil reservoir. Hence there was less metal to metal contact which helped in reduction of sound in case of the textured surface C.I. disc.
- Brake Thermal Efficiency of diesel engine piston ring without textures was lower than diesel engine piston ring as compared to textured due to less friction in the rings. Similarly, biodiesel fuel exhibit higher Brake Thermal Efficiency with textured piston rings. Maximum brake thermal efficiency achieved for diesel with textured piston ring was 30.17% and with non-textured piston ring was 28.99%. Also, the maximum brake thermal efficiency achieved for biodiesel with textured piston ring was 27.42% and with non-textured piston ring was 27.29%.

- Minimum brake specific fuel consumption (BSFC) achieved for diesel with textured piston ring was 0.2824 kg/kW-hr at a load of 80% and with non-textured piston ring was 0.2939 kg/kW-hr at a load of 60%. Minimum brake specific fuel consumption (BSFC) achieved for diesel with textured piston ring was 0.3311 kg/kW-hr at a load of 80% and with non-textured piston ring was 0.3327 kg/kW-hr at a load of 80%.
- The brake specific fuel consumption (BSFC) achieved for diesel with textured piston ring was lower as compared to non-textured piston ring for the entire range of applied load.
- CO emissions was measured for non-textured and textured piston ring using both diesel and biodiesel as fuel. It is found that CO emissions increased rapidly when engine has been operated from 80% load to full load. CO emissions for Biodiesel as fuel is lower than diesel at all the time.
- Hydrocarbon (HC) emissions was measured for non-textured and textured piston ring using both diesel and biodiesel as fuel. It is found that Hydrocarbon (HC) remains similar with both type of piston rings. But overall it is found that, the Hydrocarbon (HC) emissions are quite low for biodiesel in comparison to diesel as fuel.
- NO_x particles emissions were measured for non-textured and textured piston ring using both diesel and biodiesel as fuel. NO_x emissions continuously go on increasing with increase of engine load and then decrease at about full load. It was noticed that biodiesel releases a little more amount of N₂ in comparison to diesel fuel.
- Smoke Opacity was measured for non-textured and textured piston ring using both diesel and biodiesel as fuel. Smoke opacity increases at higher loads for both the fuels. Overall smoke opacity for biodiesel is lower than that of diesel.

5.2.Scope of Future Work

- This thesis work presents the insights about the tribological properties of the piston ring material along with design modifications and compared their properties with the conventional piston ring material and design. Other properties of the piston ring materials could be evaluated further for the fewer emissions of the CO, HC, NOx particles and Smoke Opacity.
- The effects of surface textures on the piston ring have found to improve the performance of the four-stroke diesel engine. However, further study on the effects of different surface texture shapes and sizes could be conducted to inspect their effects.
- The use of thermal image camera in real situation at the combustion chamber of IC Engine is beyond limitations. Therefore, may be taken care in future and incorporated in future scope of this study.
- Since facility to measure fine carbon particles such as PM 2.5 and PM 10 was not available in house, so may be considered for future scope of study.

References

1. Amini, S., Hosseinabadi, N.H. and Sajjady, S.A. (2016), "Experimental study on effect of micro textured surfaces generated by ultrasonic vibration assisted face turning on friction and wear performance", *Applied Surface Science*, Vol. 390, pp. 633-648.
2. Anderson A E, "Friction and Wear of Automotive Brakes", *ASM Handbook*, Materials Park, OH, p.569–577 (1992).
3. Bhushan Bharat, "Modern Tribology hand book", John Wiley & Sons, New York, (2013).
4. Bijwe J, Gupta M K, Parida T and Trivedi P, "Design and development of advanced polymer composites as high performance tribo-materials based on blends of PEK and ABPBI", *Wear*, 342–3 65–76, (2015).
5. Bijwe, J, Gupta, M K, Parida, T and Trivedi, P, "Design and development of advanced polymer composites as high performance tribo-materials based on blends of PEK and ABPBI", *Wear*, Vols 342/343, pp. 65-76 (2015).
6. Breur B, Bill K H, "Brake Technology Handbook", SAE International, Pennsylvania, Warrendale, PA, (2008).
7. Chaudhari T and Sutaria B, "Investigation of friction characteristics in segmented piston ring liner assembly of IC engine," *Perspect. Sci.*, vol. 8, pp. 599–602, (2016).
8. Childs T H C and Sabbagh F, "Boundary-lubricated wear of cast irons to simulate automotive piston ring wear rates," *Wear*, vol. 134, no. 1, pp. 81–97, (1989).
9. Childs T H C and Sabbagh F, "Boundary-lubricated wear of cast irons to simulate automotive piston ring wear rates", *Wear*, 134 81–97, (1989).
10. Cho, M. (2016), "Friction and wear of a hybrid surface texturing of polyphenylene sulfide-filled micro pores", *Wear*, Vol 346, pp. 158-167.
11. Da Silva, L.R.R. and Costa, H.L. (2017), "Tribological behavior of gray cast iron textured by maskless electrochemical texturing", *Wear*, Vols 376/377, pp. 1601-1610.
12. Demirbas A, "Progress and recent trends in biodiesel fuels," *Energy Convers. Manag.*, vol. 50, no. 1, pp. 14–34, (2009).
13. Djoufack M H, May U, Repphun G, Brögelmann T and Bobzin K, "Wear behaviour of hydrogenated DLC in a pinon- disc model test under lubrication with different diesel fuel types", *Tribol. Int.* 92 12–20 (2015).
14. Djoufack, M.H., Maya, U., Repphun, G., Brögelmann, T. And Bobzin, K. (2015), "Wear behaviour of hydrogenated DLC in a pin-on-disc model test under lubrication with different diesel fuel types", *Tribology International*, Vol. 92, pp. 12-20.
15. Dowson D, "History of Tribology", Longman Group Limited, New York, (1979).
16. Dunn, A., Wlodarczyk, K.L., Carstensen, J.V., Hansen, E.B., Gabzdyl, J., Harrison, P.M., Shephard, J.D. and Hand, D.P., "Laser surface texturing for high friction contacts", *Applied Surface Science*, Vol. 357, pp. 2313-2319 (2015).

17. Etsion, I. and Sher, E. (2009), "Improving fuel efficiency with laser surface textured piston rings", *Tribology International*, Vol. 42No. 4, pp. 542-547.
18. Ezugwu E O, Da Silva R B, Bonney J, Machado A R, "Evaluation of performance of CBN tools when turning Ti6Al4V alloy with high pressure coolant supplies", *Int. J. Mach. Tools Manuf.*, 45 (9) 1009–1014 (2005).
19. Ezugwu E O, Wang Z M, "Titanium alloys and their machinability—a review", *J. Mater. Process. Technol.*, 68, 262–274 (1997).
20. Gachot, C., Rosenkranz, A., Hsu, S.M. and Costa, H.L. (2017), "A critical assessment of surface texturing for friction and wear improvement", *Wear*, Vols 372/373, pp. 21-41.
21. Gara L, Zou Q, Sangeorzan B P, Barber G C, McCormick H E and Mekari M H, "Wear measurement of the cylinder liner of a single cylinder diesel engine using a replication method", *Wear*, 268 558–64 (2010).
22. Gara L, Zou Q, Sangeorzan B P, Barber G C, McCormick H E, and Mekari M H, "Wear measurement of the cylinder liner of a single cylinder diesel engine using a replication method," *Wear*, vol. 268, no. 3–4, pp. 558–564, (2010).
23. Ghanshyam C, Bagchi S, Kapur P., "Optimization of spray parameters in the fabrication of SnO₂ layers using electrostatic assisted deposition technique", *J. Electrostat.*, 71 (71), 68–76 (2013).
24. Grabon W, Koszela W, Pawlus P and Ochwat S, "Improving tribological behaviour of piston ring–cylinder liner frictional pair by liner surface texturing", *Tribol. Int.*, 61 102–08, (2013).
25. Grabon W, Pawlus P and Sep J, "Tribological characteristics of one-process and two-process cylinder liner honed surfaces under reciprocating sliding conditions", *Tribol. Int.*, 43 1882–92, (2010).
26. Grabon,W., Pawlus, P., Wos, S., Koszela,W. and Wieczorowski, M. (2017), "Effects of honed cylinder liner surface texture on tribological properties of piston ring-liner assembly in short time tests", *Tribology International*,Vol. 113, pp. 137-148.
27. Gunda R K, Narala S K R, "Tribological studies to analyze the effect of solid lubricant particle size on friction and wear behaviour of Ti-6Al-4V alloy", *Surf. Coat. Technol.* 308, 203–212 (2016).
28. Hazar H, "Characterization of MoN coatings for pistons in a diesel engine," *Mater. Des.*, vol. 31, no. 1, pp. 624–627, (2010).
29. Hu, J. and Xu, H. (2016), "Friction and wear behavior analysis of the stainless steel surface fabricated by laser texturing underwater", *Tribology International*, Vol. 102, pp. 371-377.
30. Hwu C J and Weng C, "Elastohydrodynamic lubrication of piston rings", *Wear*, 150 203–15, (1991).
31. Iliuc Ivan, "Tribology of thin layers", *Tribology series four*, Elsevier, New York, (1980).
32. Jia B, Mikalsen R, Smallbone A, and Roskilly A P, "A study and comparison of frictional losses in free-piston engine and crankshaft engines," *Appl. Therm. Eng.*, vol. 140, pp. 217–224, (2018).
33. Johansson S, Nilsson P H, Ohlsson R and Rosén B G, "Experimental friction evaluation of cylinder liner/piston ring contact" *Wear*, 271 625–33, (2011).

34. Johansson S, Nilsson P H, Ohlsson R, and Rosén B G, “Experimental friction evaluation of cylinder liner/piston ring contact,” *Wear*, vol. 271, no. 3–4, pp. 625–633, (2011).
35. Jones, K. and Schmid, S.R. (2016), “Experimental investigation of laser texturing and its effect on friction and lubrication”, *Procedia Manufacturing*, Vol. 5, pp. 568-577.
36. Kapsiz M, Durat M and Ferit F, “Friction and wear studies between cylinder liner and piston ring pair using Taguchi design method”, *Adv. Eng. Soft.*, 42 595–603 (2011).
37. Khusainov A S and Glushchenko A A, “Increasing Wear Resistance of Internal Combustion Engines Cylinders with Work Friction Surface Metal Coating,” *Procedia Eng.*, vol. 206, pp. 1618–1622, (2017).
38. Kim E S, Kim S M, and Lee Y Z, “The effect of plateau honing on the friction and wear of cylinder liners,” *Wear*, vol. 400–401, no. September 2016, pp. 207–212, (2018).
39. Kim, B., Chae, Y.H. and Choi, H.S. (2014), “Effects of surface texturing on the frictional behavior of cast iron surfaces”, *Tribology International*, Vol. 70, pp. 128-135.
40. Lal, R. and Singh, R.C. (2018), “Experimental comparative study of chrome steel pin with and without chrome plated cast iron disc in situ fully flooded interface lubrication”, *Surface Topography, Metrology and Properties*, Vol. 6.
41. Law S E, “Agricultural electrostatic spray application a review of significant research and development during the 20th century”, *J. Electrostat.*, 51-52, 25–42 (2001).
42. Lenauer C, Tomastik C, Wopelka T, and Jech M, “Piston ring wear and cylinder liner tribofilm in tribotests with lubricants artificially altered with ethanol combustion products,” *Tribol. Int.*, vol. 82, no. PB, pp. 415–422, (2015).
43. Li S W, Wang Y P, Wang Y, Kui H L, Zhou R B, “An electrostatic atomization to save fuel and reduce emissions”, *Automot. Eng.*, 23,283–286 (2001).
44. Li, K., Yao, Z., Hu, Y. and Gu, W. (2014), “Friction and wear performance of laser peen textured surface under starved lubrication”, *Tribology International*, Vol. 77, pp. 97-105.
45. Liu X, Xu W J, Sun J, “Experimental research on the dry electrostatic cooling assisted machining for hardened steel”, *Adv. Mater. Res.*, 189–193, 3026–3030 (2011).
46. Luo, K.Y., Wang, C.Y., Li, Y.M., Luo, M., Huang, S., Hua, X.J. and Lu, J.Z. (2014), “Effects of laser shock peening and groove spacing on the wear behavior of non-smooth surface fabricated by laser surface texturing”, *Applied Surface Science*, Vol. 313, pp. 600-606.
47. Marksberry P W, Jawahir I S, “A comprehensive tool-wear/tool-life performance model in the evaluation of NDM (near dry machining) for sustainable manufacturing”, *Int. J. Mach. Tools Manuf.*, 48, 878–886 (2008).
48. Marques A, Narala S K R, Machado A R, Gunda R K, Josyula S K, Da Silva R B, Da Silva M B, “Performance assessment of MSQL: minimum quantity solid lubricant during turning of Inconel 718”, *J. Eng. Manuf. B*, 1–16, (2015).
49. McCarthy P, Rasul M G, and Moazzem S, “Analysis and comparison of performance and emissions of an internal combustion engine fuelled with petroleum diesel and different bio-diesels,” *Fuel*, vol. 90, no. 6, pp. 2147–2157, (2011).

50. Meng, R., Deng, J., Liu, Y., Duan, R. and Zhang, G. (2018), "Improving tribological performance of cemented carbides by combining laser surface texturing and W-S-C solid lubricant coating", *International Journal of Refractory Metals & Hard Materials*, Vol. 72, pp. 163-171.
51. Mezghani S, Demircia I, Zahouani H and Mansori M El, "The effect of groove texture patterns on piston-ring pack friction", *Precis. Eng.*, 36 210–7, (2012).
52. Michalski J and Woś P, "The effect of cylinder liner surface topography on abrasive wear of piston–cylinder assembly in combustion engine", *Wear*, 271 582–89, (2011).
53. Mo, J.L., Wanga, Z.G., Chen, G.X., Shao, T.M., Zhu, M.H. and Zhou, Z.R. (2013), "The effect of groove-textured surface on friction and wear and friction-induced vibration and noise", *Wear*, Vol. 301 Nos 1/2, pp. 671-681.
54. Moore S L, "Piston ring lubrication in a two-stroke diesel engine", *Wear*, 72 353–69, (1981).
55. Mukhopadhyay D, Banerjee S, Narala S K R, "Investigate to study the application of solid lubricant in turning AISI 1040 steel", *Trans. ASME*, 129, 520–526 (2007).
56. Muthiah S, Singh R C, Pathak B D and Dhar A, "Mechanical properties of thermoelectric n-type magnesium silicide synthesized employing in situ spark plasma reaction sintering", *Mater. Res. Express* 4 075507, (2017).
57. Muthiah, S., Singh, R.C., Pathak, B.D. and Dhar, A. (2017), "Mechanical properties of thermoelectric n – type magnesium silicide synthesized employing in situ spark plasma reaction sintering", *Materials Research Express*, Vol.4No. 7, pp.075507
58. Narala S K R, Nouari Mohammed, Yang Minyang, "Development of electrostatic solid lubrication system for improvement in machining process performance", *Int. J. Mach. Tools Manuf.*, 50 789–797 (2010).
59. Nautiyal P C, Singhal S and Sharma J P, "Friction and wear processes in piston rings", *Tribol. Int.*, 16 43–9, (1983).
60. Olander P, Hollman P and Jacobson S, "Piston ring and cylinder liner wear aggravation caused by transition to greener ship transports–comparison of samples from test rig and field", *Wear*, 302 1345–50 (2013).
61. Olofinjana, B., Lorenzo-Martin, C., Ajayi, O.O. and Ajayi, E.O. (2015), "Effect of laser surface texturing (LST) on tribochemical films dynamics and friction and wear performance", *Wear*, Vols 332/333, pp. 1225-1230.
62. Pandey R K, Tandon N and Singh A K, "Fuel saving in IC engine by surface texturing of piston rings", *Nat. Conf. on Recent Advancements in Mech. Engg. (NCRAME-2013)*, (Itanagar, Arunachal Pradesh, India: NERIST) pp 1–4 (2013).
63. Pandey, R.K., Tandon, N. and Singh, A.K. (2013), "Fuel saving in IC engine by surface texturing of piston rings", *National Conference on Recent Advancements in Mechanical Engineering (NCRAME-2013)*.
64. Pawlus P, "Effects of honed cylinder surface topography on the wear of piston-piston ring-cylinder assemblies under artificially increased dustiness conditions", *Tribol. Int.*, 26 49–55, (1993).

65. Picken D J and Hassaan H A, "A method for estimating overhaul life of internal combustion engines including engines operating on biogas and methane", *J. Agric. Eng. Res.* 28 139–47 (1983).
66. Priest M and Taylor C, "Automobile engine tribology — approaching the surface," *Wear*, vol. 241, no. 2, pp. 193–203, Jul. 2000.
67. Priest M, Dowson D, and Taylor C, "Predictive wear modelling of lubricated piston rings in a diesel engine," *Wear*, vol. 231, no. 1, pp. 89–101, (1999).
68. Qu, Z., Wei, K., He, Q., He, R., Pei, Y., Wang, S. and Fang, D. (2018), "High temperature fracture toughness and residual stress in thermal barrier coatings evaluated by an in-situ indentation method", *Ceramics International*, Vol. 44 No. 7, pp. 7926-7929.
69. Rana, R., Walia, R.S. and Lata, S. (2018), "Development and investigation of hybrid electric discharge machining electrode process", *Materials Today Proceedings*, Vol. 5 No. 2, pp. 3936-3942.
70. Reddy N S K, Yang M, "Development of an electro static lubrication system for drilling of SCM 440 steel", *J. Eng. Manuf.*, 224 (2), 217–224 (2010).
71. Reddy P U M, Reddy N S K, "Investigation on wear behavior of electrostatic micro-solid lubricant coatings under dry sliding conditions", *ASME Proceedings Design and Manufacturing IMECE2012–87201*, pp. 2105–2110 (2012).
72. Riahi A R, Alpas A T, "Wear map for grey cast iron", *Wear*, 255, 401–409 (2003).
73. Ryk, G. and Etsion, I. (2006), "Testing piston rings with partial laser surface texturing for friction reduction", *Wear*, Vol. 261 Nos 7/8, pp. 792-796.
74. Sahoo R R, Biswas Sanjay, "Deformation and friction of MoS₂ particles in liquid suspensions used to lubricate sliding contact", *Thin Solid Films*, 518, 5995–6005 (2010).
75. Sanders P, Xu N, Dalka T M, Maricq M M, "Air borne brake wear debris size distributions, composition, and a comparison of dynamometer and vehicle tests", *Environ. Sci. Technol.*, 374060–4069 (2003).
76. Scott D, Smith A I, Tait J and Tremain G R, "Materials and metallurgical aspects of piston ring scuffing—a literature survey", *Wear*, 33 293–315, (1975).
77. Scott D, Smith A, Tait J, and Tremain G, "Materials and metallurgical aspects of piston ring scuffing - A literature survey," *Wear*, vol. 33, no. 2, pp. 293–315, (1975).
78. Sharma V K, Singh R C and Chaudhary R, "Effect of fly ash particles with aluminium melt on the wear of aluminium metal matrix composites", *Int. J. Adv. Res.*, 20 1318–23 (2017).
79. Sharma, K.V., Singh, R.C. and Chaudhary, R. (2017), "Effect of flyash particles with aluminium melt on the wear of aluminium metal matrix composites", *Engineering Science and Technology, an International Journal*, Vol. 20 No. 4, pp. 1318 -1323.
80. Shinkarenko A, Kligerman Y, and Etsion I, "The effect of elastomer surface texturing in soft elasto-hydrodynamic lubrication," *Tribol. Lett.*, vol. 36, no. 2, pp. 95–103, (2009).
81. Shokrani A, Dhokia V, Newman S T, "Environmentally conscious machining of difficult-to-machine materials with regard to cutting fluids", *Int. J. Mach. Tools, Manuf.* 57,83–101 (2012).

82. Singh R C, Pandey R K, Lal Roop, Ranganath M S and Maji S, “Tribological performance analysis of textured steel surfaces under lubricating conditions”, *Surf. Topogr.: Metrol. Prop.*, 4 034005, (2016).
83. Singh, R.C., Pandey, R.K., Rooplal, R. and MS and Maji, S. (2016), “Tribological performance analysis of textured steel surfaces under lubricating conditions”, *Surface Topography, Metrology and Properties*, Vol. 4.
84. Srivastava D K, Agarwal A K and Kumar J, “Effect of liner surface properties on wear and friction in a non-firing engine simulator”, *Mater. Des.*, 28 1632–40 (2007).
85. Straffelini G, *Friction and Wear – Methodologies for Designing and Control*, Springer Verlag, The Netherlands, (2015).
86. Straffelini G, Maines L., “The relationship between wear of semi metallic friction materials and pearlitic castiron in dry sliding”, *Wear*, 307, 75–80 (2013).
87. Sudeep U, Pandey R K and Tandon N, “Effects of surface texturing on friction and vibration behaviours of sliding lubricated concentrated point contacts under linear reciprocating motion”, *Tribol. Int.*, 62 198–207 (2013).
88. Sudeep, U., Pandey, R.K. and Tandon, N. (2013), “Effects of surface texturing on friction and vibration behaviors of sliding lubricated concentrated point contacts under linear reciprocating motion”, *Tribology International*, Vol. 62, pp. 198-207.
89. Taie, I., Al-Shahrani, A., Qari, N., Fihri, A., Al-Obaid, W. and Alabedi, G. (2018), “High temperature corrosion resistant coatings for gas flare systems”, *Ceramics International*, Vol. 44 No. 5, pp. 5124-5130.
90. Tiwari S, Bijwe J and Panier S “Gamma radiation treatment of carbon fabric to improve the fiber–matrix adhesion and tribo-performance of composites”, *Wear*, 271 2184–92 (2011).
91. Truhan J J, Qu J and Blau P J, “A rig test to measure friction and wear of heavy duty diesel engine piston rings and cylinder liners using realistic lubricants”, *Tribol. Int.*, 38 211–8, (2005).
92. Truhan J J, Qu J and Blau P J, “The effect of lubricating oil condition on the friction and wear of piston ring and cylinder liner materials in a reciprocating bench test”, *Wear*, 259 1048–55, (2005).
93. Van Kuilenburg, J., Masen, M.A., Groenendijk, M.N.W., Bana, V., and Van der Heide, E. (2012), “An experimental study on the relation between surface texture and tactile friction”, *Tribology International*, Vol. 48, pp. 15-21.
94. Velkavrh I, Ausserer F, Klien S, Voyer J, Ristow A, Brenner J, Forêt P and Diem A, “The influence of temperature on friction and wear of un-lubricated steel/steel contacts in different gaseous atmospheres”, *Tribol. Int.*, 98 155–71 (2016).
95. Vladescu, S.-C., Olver, A.V., Pegg, I.G. and Reddyhoff, T. (2016), “Combined friction and wear reduction in a reciprocating contact through laser surface texturing”, *Wear*, Vol. 358-359, pp. 51-61.
96. Wakuri Y, Hamatake T, Soejima M and Kitahara T, “Piston ring friction in internal combustion engines” *Tribol. Int.* 25 299–308, (1992).

97. Wos, S., Koszela, W. and Pawlus, P. (2017), "The effect of both surfaces textured on improvement of tribological properties of sliding elements", *Tribology International*, Vol. 113, pp. 182-188.
98. Wos, S., Koszela, W., Pawlus, P., Drabik, J. and Rogos, E. (2018), "Effects of surface texturing and kind of lubricant on the coefficient of friction at ambient and elevated temperatures", *Tribology International*, Vol. 117, pp. 174-179.
99. Xing, Y., Deng, J., Wua, Z. and Wu, F. (2017), "High friction and low wear properties of laser-textured ceramic surface under dry friction", *Optics and Laser Technology*, Vol. 93, pp. 24-32.
100. Yamaguchi, K., Takada, Y., Tsukuda, Y., Ota, M., Egashira, K. and Morita, T. (2016), "Friction characteristics of textured surface created by electrical discharge machining under lubrication", *Procedia CIRP*, Vol. 42, pp. 662 -667.
101. Yamakiri H, Sasaki S, Kurita T, and Kasashima N, "Effects of laser surface texturing on friction behavior of silicon nitride under lubrication with water," *Tribol. Int.*, vol. 44, no. 5, pp. 579–584, (2011).
102. Zenebe Segu, D. and Hwang, P. (2015), "Friction control by multi-shape textured surface under pin-on-disc test", *Tribology International*, Vol. 91, pp. 111-117.

Appendix - I

A1: Specifications of Lubricating Oil (15W40)

Table A1.1: Properties and Specifications of Lubricating Oil (15W40)

S. No.	Property	Details
1	Grade	SAE 15W-40
2	Ash, Sulfated, mass%, ASTM D874	0.5
3	Density @ 15.6 C, g/ml, ASTM D4052	0.866
4	Kinematic Viscosity @ 100 C, mm ² /s, ASTM D445	14.6
5	Kinematic Viscosity @ 40 C, mm ² /s, ASTM D445	107
6	Flash Point, Cleveland Open Cup, °C, ASTM D92	230
7	Pour Point, °C, ASTM D97	-39
8	Total Base Number, mgKOH/g, ASTM D2896	6
9	Viscosity Index, ASTM D2270	141

Appendix - II

A2: Specifications of Pin on Disc Tribometer

Table A2.1: Pin on Disc tribometer specifications

Parameter	Value	
Disc speed	Range (rpm)	200-2000
	Sensor	Drive output
	Least count (rpm)	1
Load Parameters	Range (N)	0-200
	Specification	20 Kg Beam type load cell
	Least count (N)	0.1
Machine Parameters	Range (mm)	2
	Sensors specs	LVDT, make: Syscon
	Least count (μm)	0.1
	Wear Track Diameter (mm)	150-50

A Brief Biographical Sketch

Roop Lal

Roop Lal is presently working as Assistant Professor in Mechanical Engineering Department, Delhi Technological University (Formerly Delhi College of Engineering), Delhi. He obtained his Masters degrees from Motilal Nehru Regional Engineering College (now Motilal Nehru National Institute of Technology, Allahabad, U.P.). He has 17-years of experience in aviation sector and over 20 years of experience in teaching engineering graduate and post-graduate students. He has taught various subjects like Machine Design, Strength of Materials, Engineering Mechanics, Theory of Machines, Engineering Graphics and Machine Drawing. Apart from teaching, he has also reviewed engineering books. He has many publications at various international journals and conferences. His current research area involves I.C. Engines and Tribology. He is lifetime Associate Member of Institution of Engineers (India).

Curriculum Vitae

PERSONAL INFORMATION:

First Name	ROOP LAL
Address	Type-5, Flat-14, Delhi Technological University, Shahbad, Daulatpur, Bawana Road, Delhi - 110042
Mobile	+91-9868389007
Website	www.rooplalrana.com
E-mail	rooplalrana@dce.ac.in ; rooplalrana@gmail.com
Nationality	Indian
Date of birth	15 th Mar 1963
Marital Status	Married

Work Experience:

Working at the post of Assistant Professor at Assistant Professor in Mechanical Engineering Department, Delhi Technological University (Formerly Delhi College of Engineering), Delhi since 2009.

EDUCATION AND TRAINING:

Title of Qualification	Doctor of Philosophy (Ph.D.)
Date (from - to)	Pursuing (2014-2019)
Name of University	Delhi Technological University, Delhi

Title of Qualification	Masters of Engineering (M.E.)
Specialization	Design of Process Machines
Year of Passing	1994
Name of University	Motilal Nehru Regional Engineering College, Allahabad (Motilal Nehru National Institute of Technology)

Title of Qualification	AMIE
Specialization	Mechanical Engineering
Year of Passing	1990
Name of University	Institution of Engineers (India)

Selected Publications:

1. **Roop Lal** and R C Singh, “Experimental comparative study of chrome steel pin with and without chrome plated cast iron disc in situ fully flooded interface lubrication”, Surface Topography: Metrology and Properties, IOP Publishing, Vol. 6, 2018, 035001. **(SCI Indexed, Impact No.: 2.074)**
2. **Roop Lal** and R C Singh, “Investigations of tribodynamic characteristics of chrome steel pin against plain and textured surface cast iron discs in lubricated conditions”, World Journal of Engineering, Vol. 16 No. 4, 2019, pp. 560-568. **(SCOPUS & ESCI Indexed, Impact No.: 0.46)**
3. R C Singh, R K Pandey, **Roop Lal**, M S Ranganath and S Maji, “Tribological performance analysis of textured steel surfaces under lubricating conditions” Surface Topography: Metrology and Properties, IOP Publishing, Vol. 4 (2016) 034005. **(SCI Indexed, Impact No.: 2.074)**
4. **Roop Lal** and R C Singh, “*Experimental Study of Performance Parameters of Newly Commissioned I.C. Engine*”, International Journal of advanced Production and Industrial Engineering. IJAPIE, ISSN: 2455-8419; ISSUE 2018, VOL. 3(4).
5. R. C. Singh, **Roop Lal**, Ranganath M S and Rajiv Chaudhary, “*Failure of Piston in IC Engines: A Review*”, International Journal of Modern Engineering Research (IJMER), Vol. 4, Issue 9, Sept. 2014, Page 1 -10, ISSN: 2249-6645.
6. **Roop Lal** and R. C. Singh, “*Reduction of Specific Fuel Consumption in CI Engine by using modified surface of Piston Rings*”, International Conference of Advance Research and Innovation (ICARI), New Delhi, India, 20 January 2019, ISBN 978-93-5346-324-3.
7. **Roop Lal** and R. C. Singh, “*A study of Tribological behavior at point of contact of cylinder liner and piston rings in a diesel engine*”, International Conference of Advance Research and Innovation (ICARI), New Delhi, India, 20 January 2019, ISBN 978-93-5346-324-3.
8. **Roop Lal** and R C Singh, “*Experimental Study of Performance Parameters of Newly Commissioned I.C. Engine*”, International Conference on Advanced Production and Industrial Engineering (ICAPIE-2018), Delhi, India, 5-6 October 2018.

9. R. C. Singh, R. K. Pandey, **Roop Lal** and S Maji, “*Experimental Studies for the Tribological Performances of Textured Steel Surfaces under Fully Flooded and Starved Lubricated Conditions*”, A Book on Automation in Manufacturing (AIM-2015), Page 51-62, TEQIP-II Sponsored Two Week Faculty Development Program, 04-15 May 2015.
10. **Roop Lal**, R C Singh, Ranganath M S, Rajiv Chaudhary, Gaurav Shukla, “*Tribological Analysis of Etched Mild Steel Surfaces*” “International Conference of Advance Research and Innovation (ICARI-2015), New Delhi, India, 31 January 2015. ISBN 978-93-5156-3280.
11. **Roop Lal**, R C Singh, Ranganath M.S., Rajiv Chaudhary, Ankit Kumar Saxena, “*Investigation of Wear Behavior of Aluminium Alloy and Comparison with Pure Aluminium*” “International Conference of Advance Research and Innovation (ICARI-2015), New Delhi, India, 31 January 2015. ISBN 978-93-5156-3280.
12. **Roop Lal** and R C Singh, “*A Study on Mild Steel and Chromium Coated Mild Steel Using Pin-On-Disc Method For Noise Pollution*”, National Conference on Recent Trends in Engineering, Science and Management, Shri Ram College of Engineering and Management, Palwal, Haryana, 18-19 April 2017. ISBN: 978-93-86238-21-4.